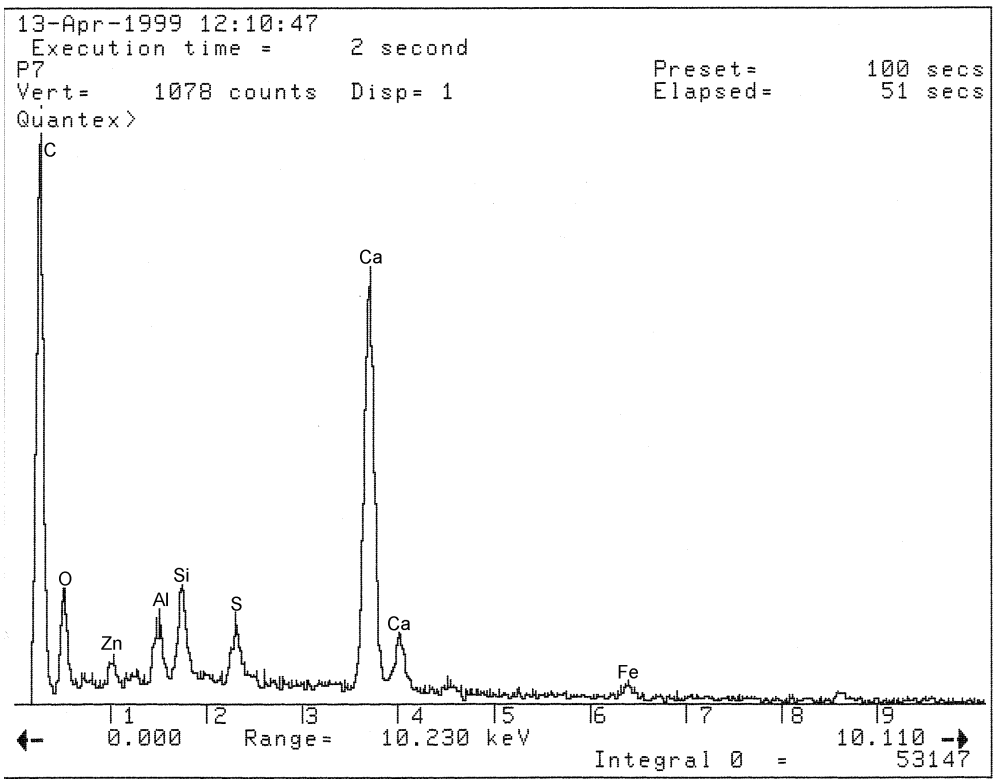

Figure 4-83. EDX spectrum taken at location P7 in the Piñon Pine filter cake nodule shown in Figure 4-76.

4.7 TRANSPORT REACTOR DEVELOPMENT UNIT

The Transport Reactor Development Unit (TRDU) is located at the University of North Dakota's Energy & Environmental Research Center (EERC), and was built under Southern Company Services, Inc. Contract No. C-92-000276.[15] Kellogg Brown & Root designed and procured the reactor and provided on-site personnel for start-up and during operation. The Electric Power Research Institute (EPRI) was involved in establishing the program and operating objectives with the EERC project team. The 200-lb/hr coal-limestone feed TRDU was built to augment studies performed with the Transport Reactor Test Unit in Houston and to provide support for the 3400-lb/hr feed rate Wilsonville transport reactor at the PSDF. Research at the TRDU also indirectly supports the Foster Wheeler advanced pressurized fluid-bed combustor, also located at the PSDF, and the Clean Coal IV Piñon Pine IGCC Power Project. Research at the TRDU is sponsored by the U.S. Department of Energy (DOE) Federal Energy Technology Center (FETC), under Contract DE-FC21-93MC30097. The TRDU has an exit gas temperature of up to 980 °C (1800 °F), a gas flow rate of 300 scfm, and an operating pressure of 120-150 psig.

The hot gas filter vessel (HGFV) is designed to handle all of the TRDU gas flow at its nominal operating conditions. This vessel has a 1.22 m inner diameter and is 4.7 m long with a refractory inside diameter of 71 cm (28 in.) and a shroud diameter of 61 cm (24 in.). Filter vessel design capabilities include operation at elevated temperatures (to 950 C) and pressures (up to 11.4 bar), with the initial test program operating in the 540 - 650 C range. The HGFV

can operate with filter face velocities in the range of 1.25 to 5.1 cm/s. Nineteen 1-meter long candles were used in the initial tests, but 1.5-meter candles can be installed.[16]

Michael Swanson of the University of North Dakota's Energy and Environmental Research Center provided nine samples from operation of the TRDU for analysis under this task. These samples are identified in Tables 4-28 and 4-29. Some of these samples were analyzed completely, while only limited analyses were performed on others. The physical and chemical analyses performed on these samples are summarized in Tables 4-30 and 4-31. Size distributions of these samples are presented in Figures 4-84 through 4-90. (Size distributions measured for ID # 4324 and 4325 are presented in section *5.7 Estimating Filter Vessel Inertial Collection from Size Distribution Data*.) Representative scanning electron micrographs of the majority of these samples are shown in Figures 4-91 through 4-97.

Table 4-28
Identification of TRDU Samples

ID #	run mode	run	sample location	dates and sampling times
4176*	combustion /gasification	P047	filter hopper	4/96
4199	gasification	P050	filter hopper	1/14/97
4324	gasification	P051	filter hopper	2/25/97 @ 12:00 to 2/27/97 @ 00:15
4325	gasification	P051	filter cake	2/28/97 @ EOT (end of test)
4326	gasification	P056	filter hopper	2/22/98 @ 08:00 to 16:15
4327	gasification	P056	filter hopper	2/25/98 @ 06:40 to 10:00
4328	gasification	P057	filter hopper	4/4/98 @ 14:00 to 18:00
4329	gasification	P057	filter hopper	4/7/98 @ 08:50 to 12:00
4330	combustion	P058	filter hopper	5/5/98 @ 17:00 to 5/8/98 @ 09:50

* contaminated sample

Table 4-29
Additional Identification of TRDU Samples

ID #	fuel source	% wt. Plum Run dolomite added
4324	Wyodak coal	5
4325	Wyodak coal	5
4326	Wyodak coal	5
4327	Illinois #6 coal	17
4328	SUFCo coal	5
4329	SUFCo coal	5
4330	petroleum coke	20

Table 4-30
Physical Characteristics of TRDU Samples

quantity ID #	4176	4199	4324	4325	4326	4327	4328	4329	4330
uncompacted bulk porosity, %	72.0	89.3	90.7	88.8	88.1	83.0	88.5	87.4	38.4
mass median diameter, µm	60	2.4	4.23	3.63	8.28	22.6	24.6	18.6	162
specific surface area, m^2/g	51	105.3	99.8	48.6	134	18.2	68	32.5	3.8
true density, g/cm^3	2.60	2.26	2.32	2.38	--	2.36	--	2.21	2.69
drag-equivalent diameter, µm	2.77	0.72	0.556	0.708	--	--	--	--	--
specific gas flow resistance, in H_2O·min·ft/lb*	2.8	8.5	9.1	9.5	--	--	--	--	--
tensile strength, N/m^2	2.8	5.7	--	--	--	--	--	--	--

* calculated for a filter cake porosity assumed to equal the uncompacted bulk porosity

Table 4-31
Chemical Composition of TRDU Samples, % wt.

constituent ID #	4176	4199	4324	4325	4327	4329	4330
Li_2O	0.01	0.01	0.01	0.01	0.01	0.02	<0.01
Na_2O	0.63	0.90	1.0	0.95	0.60	2.3	0.15
K_2O	0.12	0.18	0.12	0.18	0.89	0.62	0.09
MgO	5.2	11.0	13.4	12.5	16.4	8.1	4.4
CaO	11.2	44.0	40.4	42.2	26.3	18.5	7.2
Fe_2O_3	1.9	9.0	7.0	8.0	9.5	4.2	0.67
Al_2O_3	22.9	15.1	14.9	14.4	7.2	10.4	0.80
SiO_2	54.8	12.9	11.0	12.2	19.3	51.1	79.6
TiO_2	0.8	1.7	3.0	2.7	0.66	0.98	0.08
P_2O_5	0.55	1.0	0.76	0.96	0.13	0.27	0.04
SO_3	0.96	1.9	9.1	4.5	17.3	4.3	3.5
LOI	4.3	54.2	46.0	48.7	38.0	51.4	1.9
soluble $SO_4^{=}$	--	0.98	--	--	--	--	--
Equilibrium pH*	--	10.87	--	--	--	--	--

* dimensionless

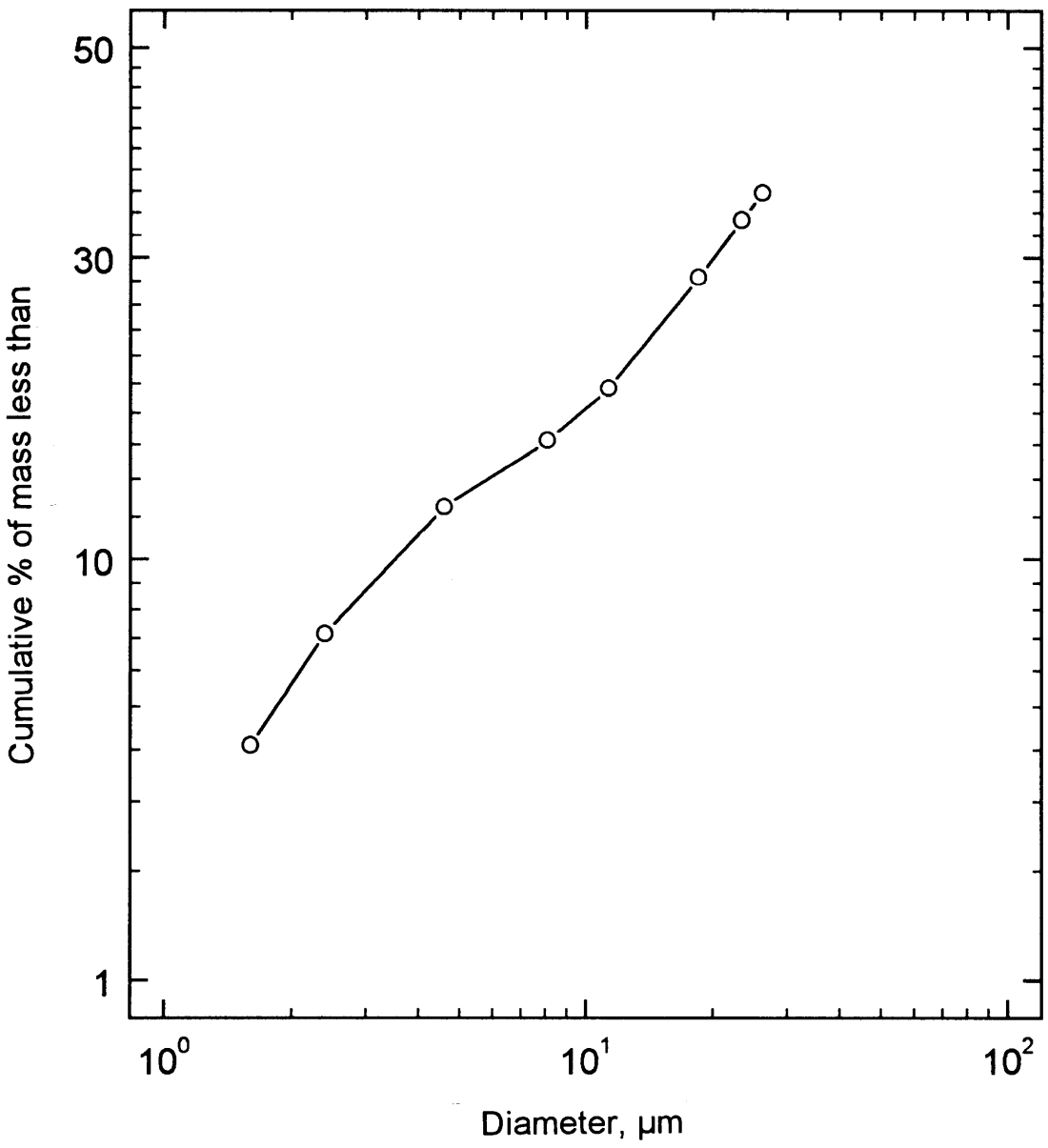

Figure 4-84. Cumulative size distribution of hopper ash from the UNDEERC TRDU (ID # 4176) measured with a Bahco aerodynamic classifier.

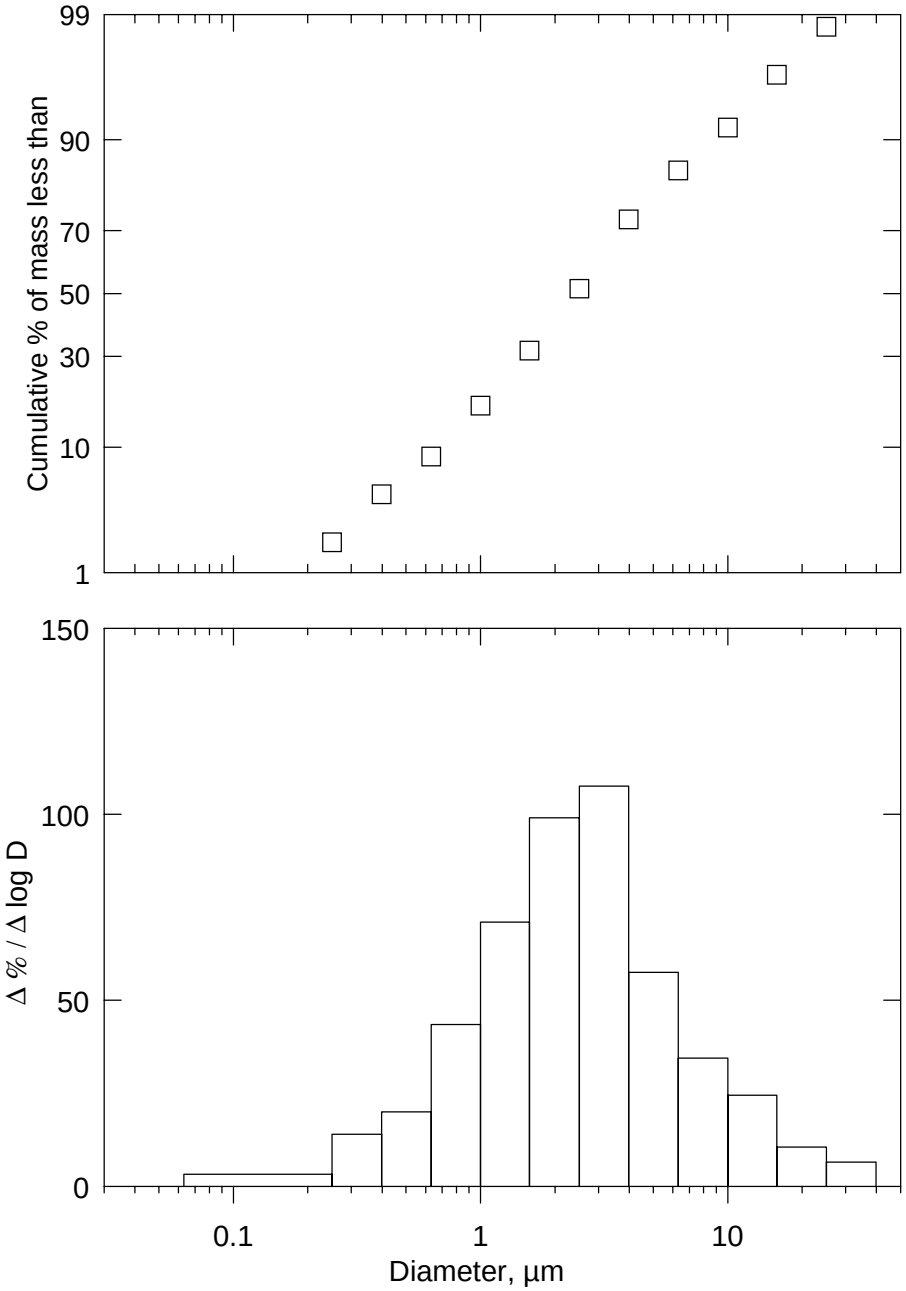

Figure 4-85. Cumulative and differential size distribution data measured for UNDEERC TRDU PO50 filter vessel ash (ID # 4199) measured with a Shimadzu SA-CP4 Centrifugal Particle Size Analyzer. The MMD of this distribution is 2.4 µm, and its geometric standard deviation is 2.6. The D_{16} of this distribution is 0.93 µm, and its D_{84} is 6.1 µm. (This size distribution data includes the assumption that the sample contains no particles smaller than 0.063 µm.)

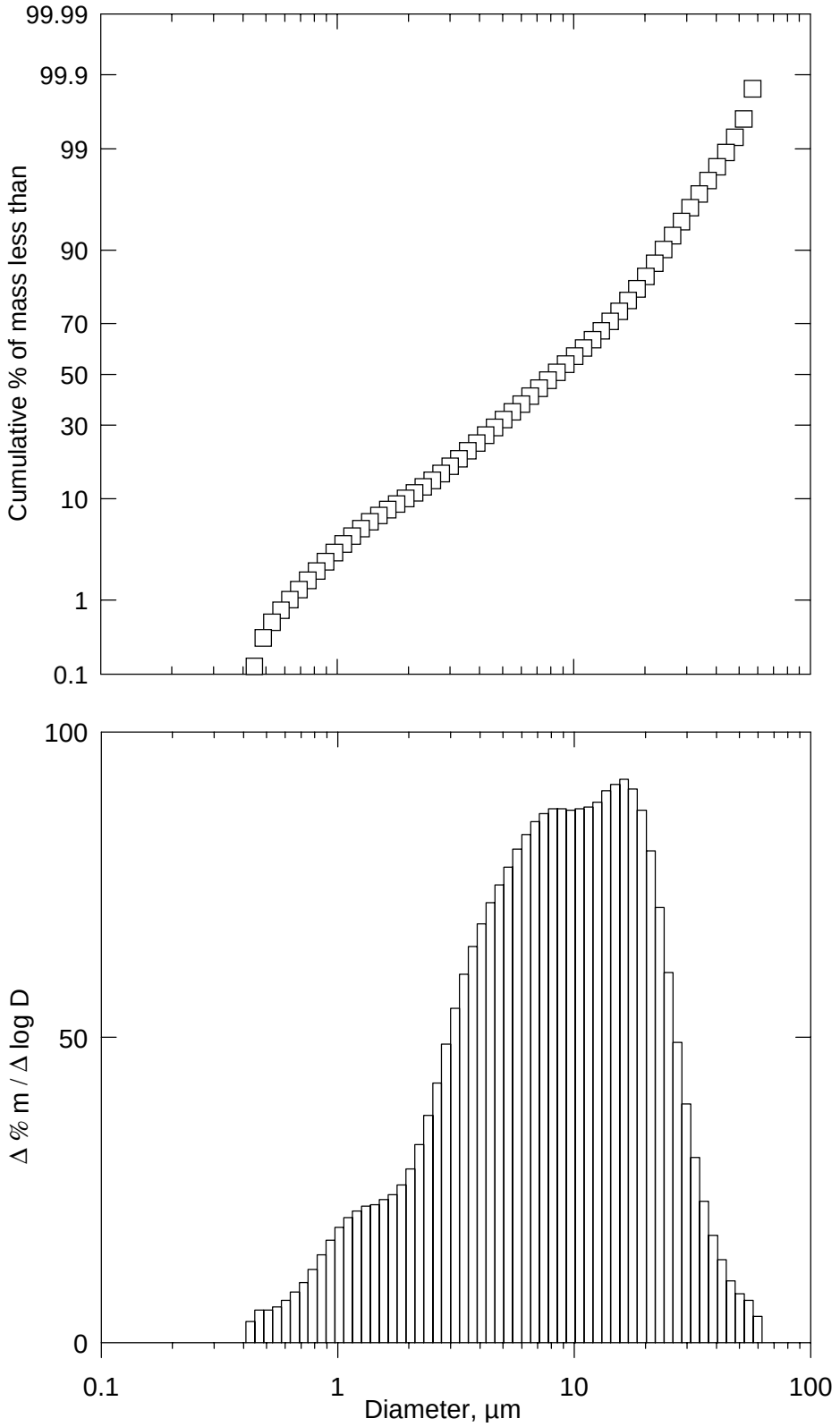

Figure 4-86. Cumulative and differential size distribution data for P056 filter hopper char (ID # 4326) measured with a Leeds and Northrup Microtrac Particle Size Analyzer.

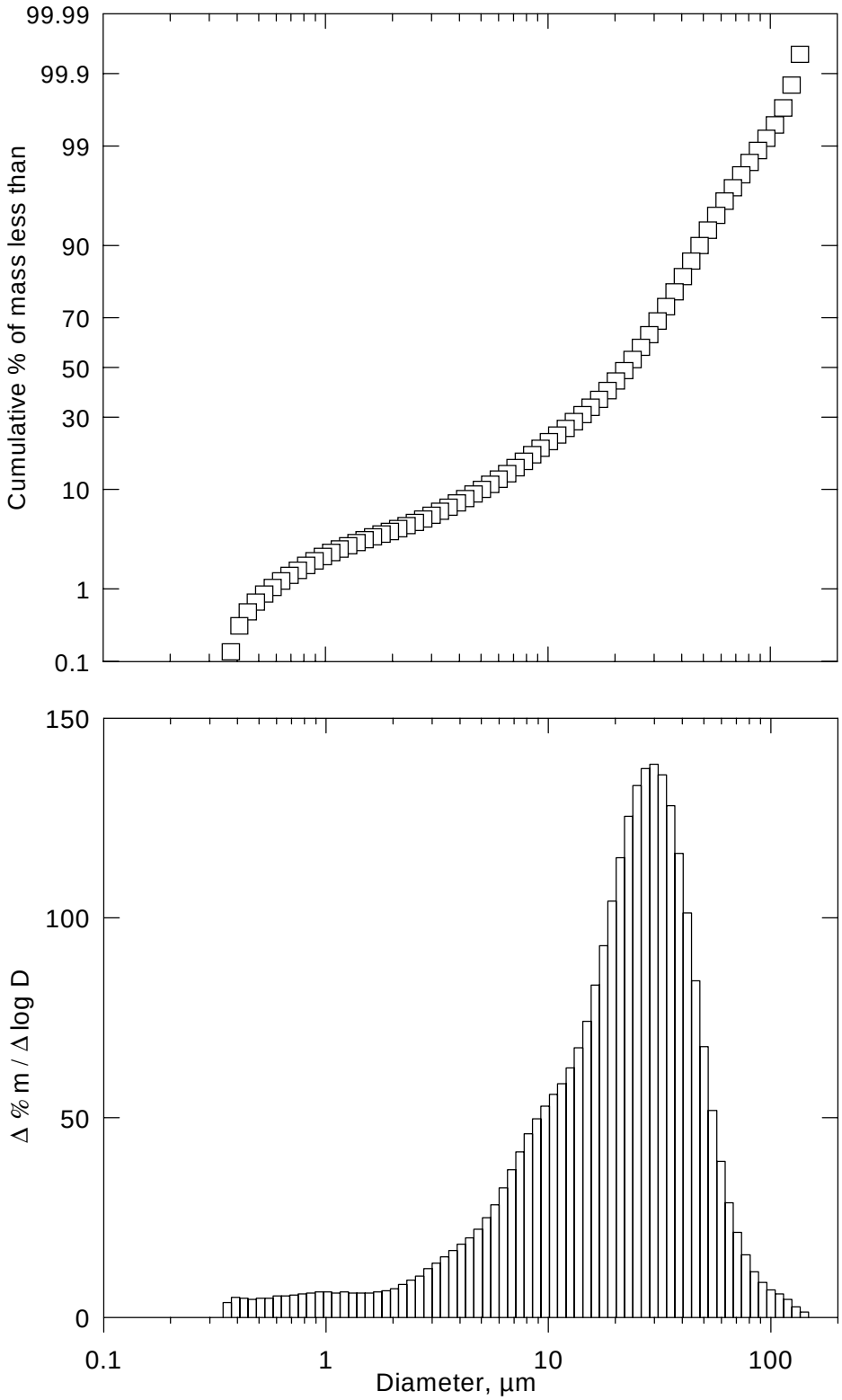

Figure 4-87. Cumulative and differential size distribution data for P056 filter hopper char (ID # 4327) measured with a Leeds and Northrup Microtrac Particle Size Analyzer.

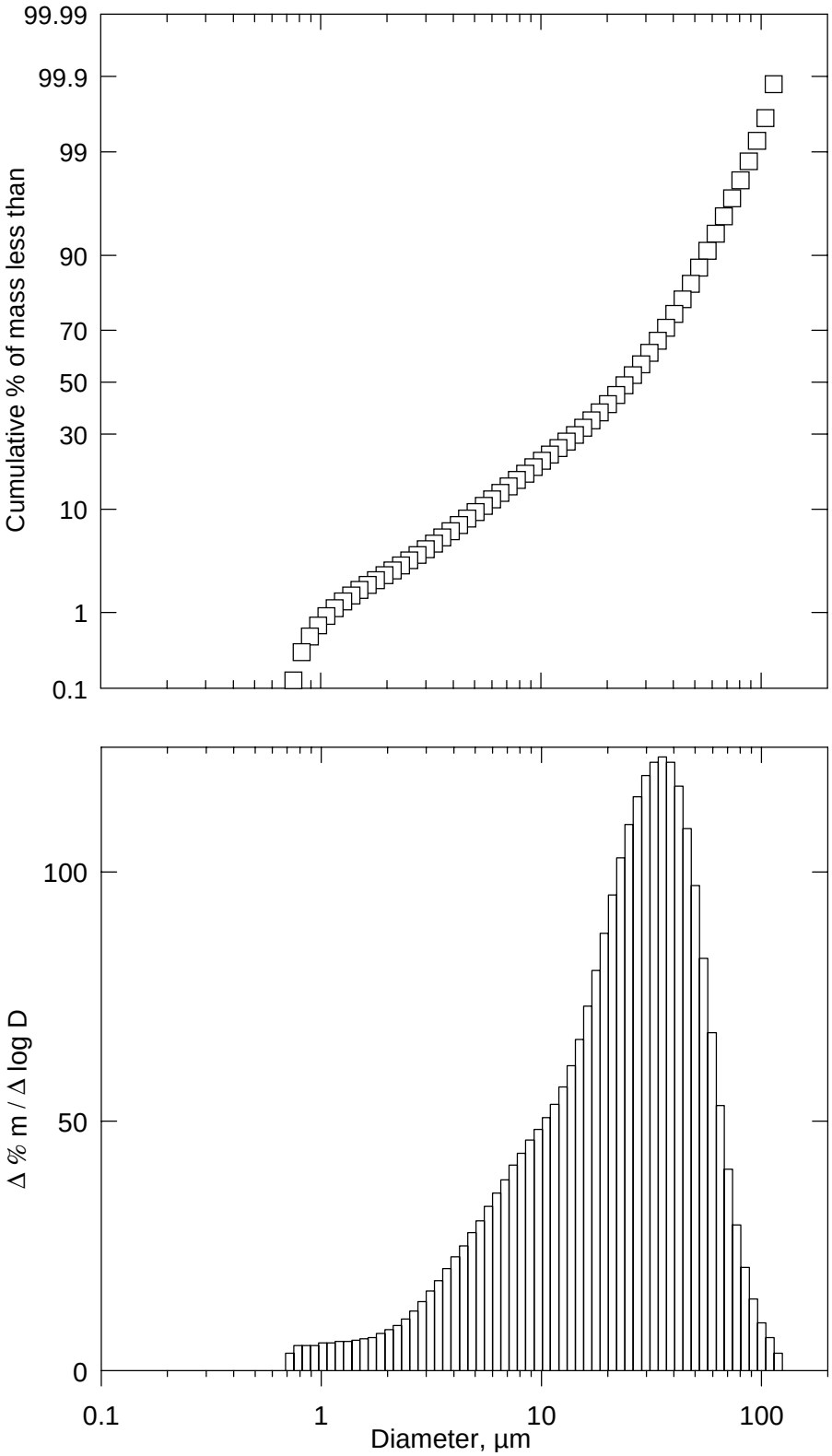

Figure 4-88. Cumulative and differential size distribution data for P057 filter hopper char (ID # 4328) measured with a Leeds and Northrup Microtrac Particle Size Analyzer.

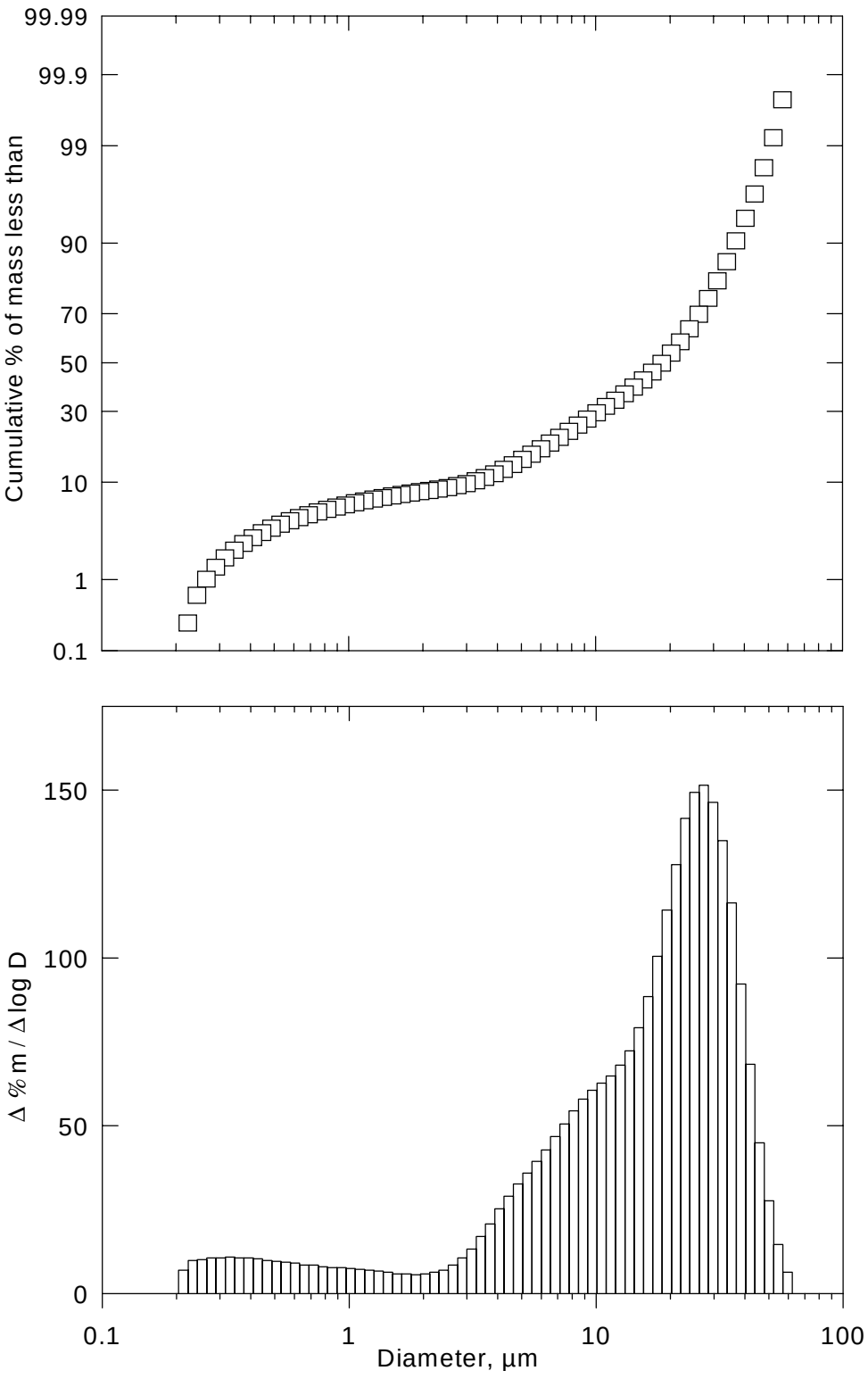

Figure 4-89. Cumulative and differential size distribution data for P057 filter hopper char (ID # 4329) measured with a Leeds and Northrup Microtrac Particle Size Analyzer.

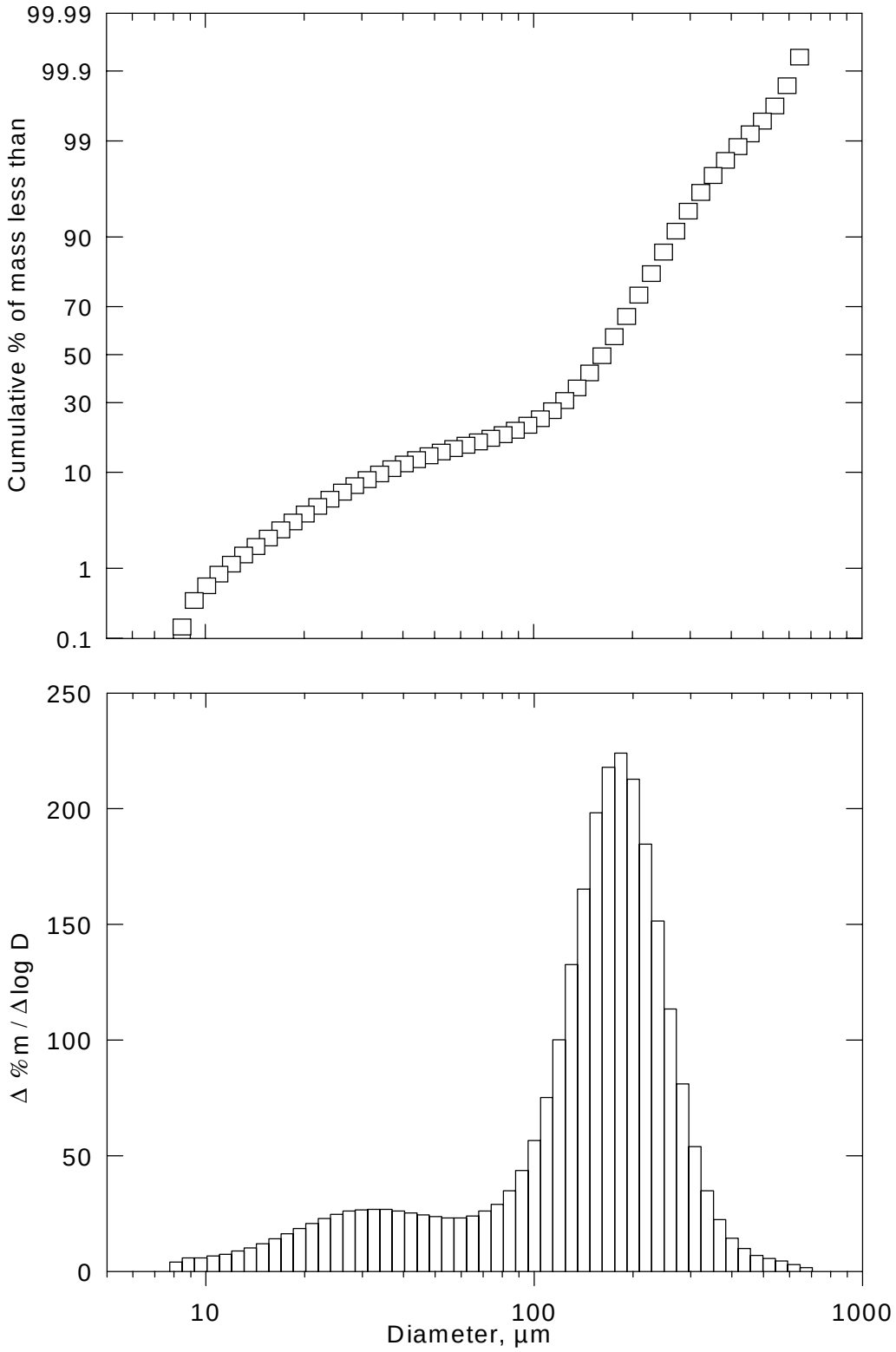

Figure 4-90. Cumulative and differential size distribution data for P058 filter hopper ash (ID # 4330) measured with a Leeds and Northrup Microtrac Particle Size Analyzer.

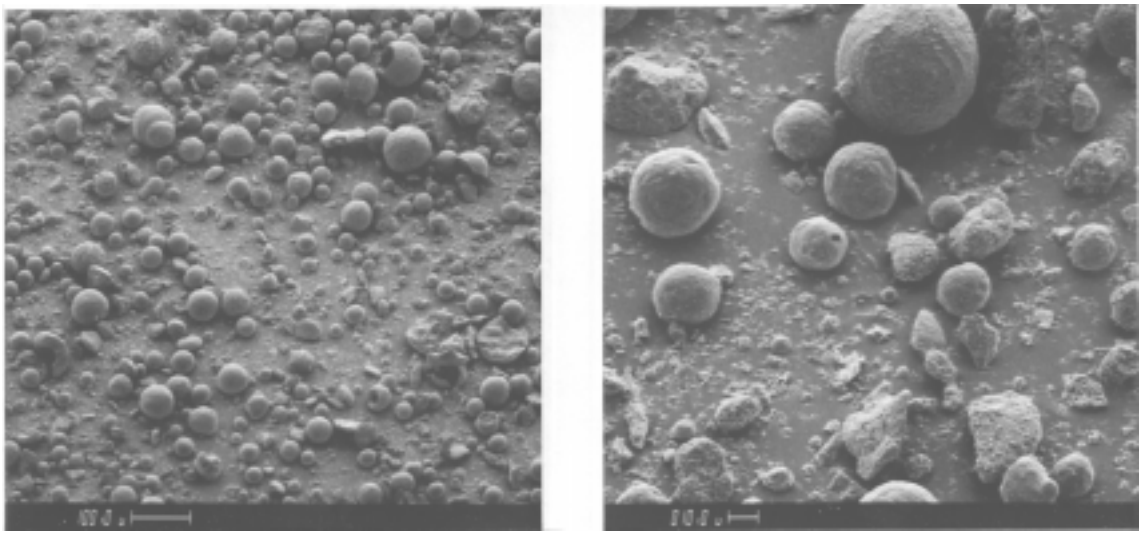

a b

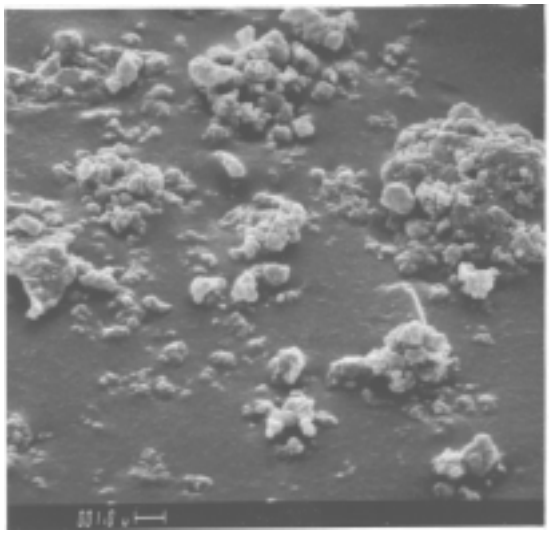

c

Figure 4-91. Micrographs of hopper ash from the UNDEERC TRDU (ID # 4176) taken at a) 100X, b) 500X, and c) 5000X.

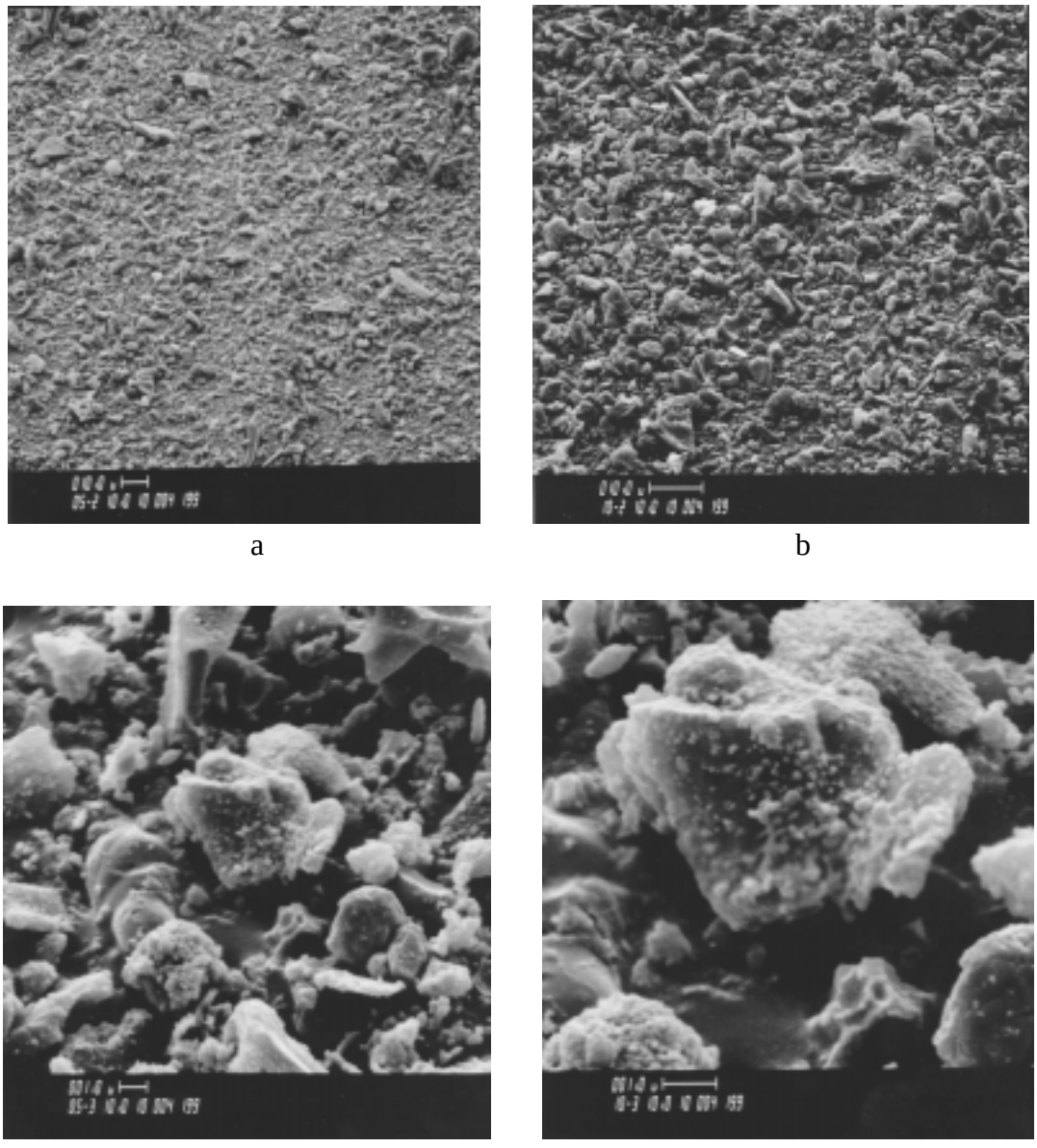

Figure 4-92. Representative scanning electron micrographs of UNDEERC TRDU PO50 filter vessel char (ID # 4199) taken at a) 500X, b) 1000X, c) 5000X and d) 10,000X.

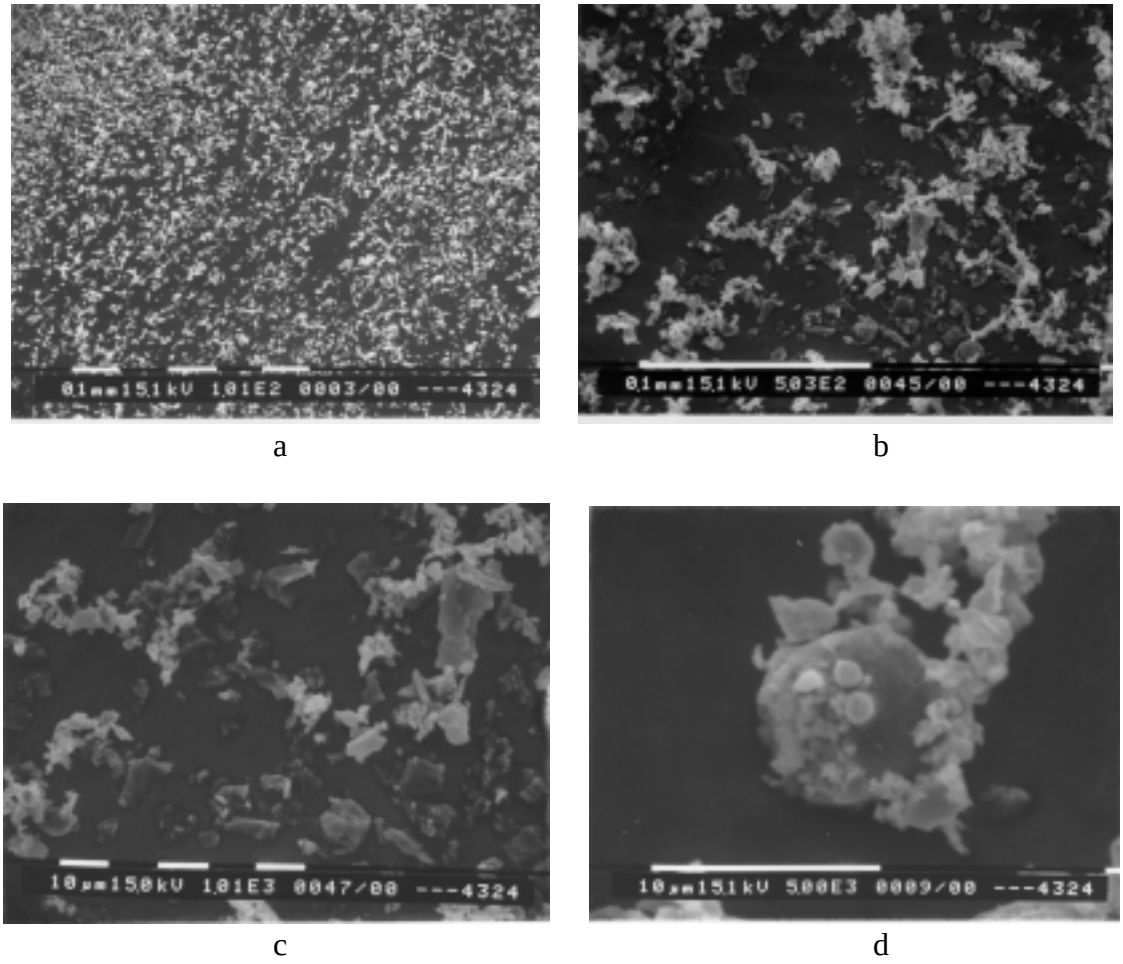

a b

c d

Figure 4-93. Representative Scanning Electron Micrographs of P051 filter hopper char (ID # 4324) taken at magnifications of a) 100x, b) 500x, c) 1000x, and d) 5000x.

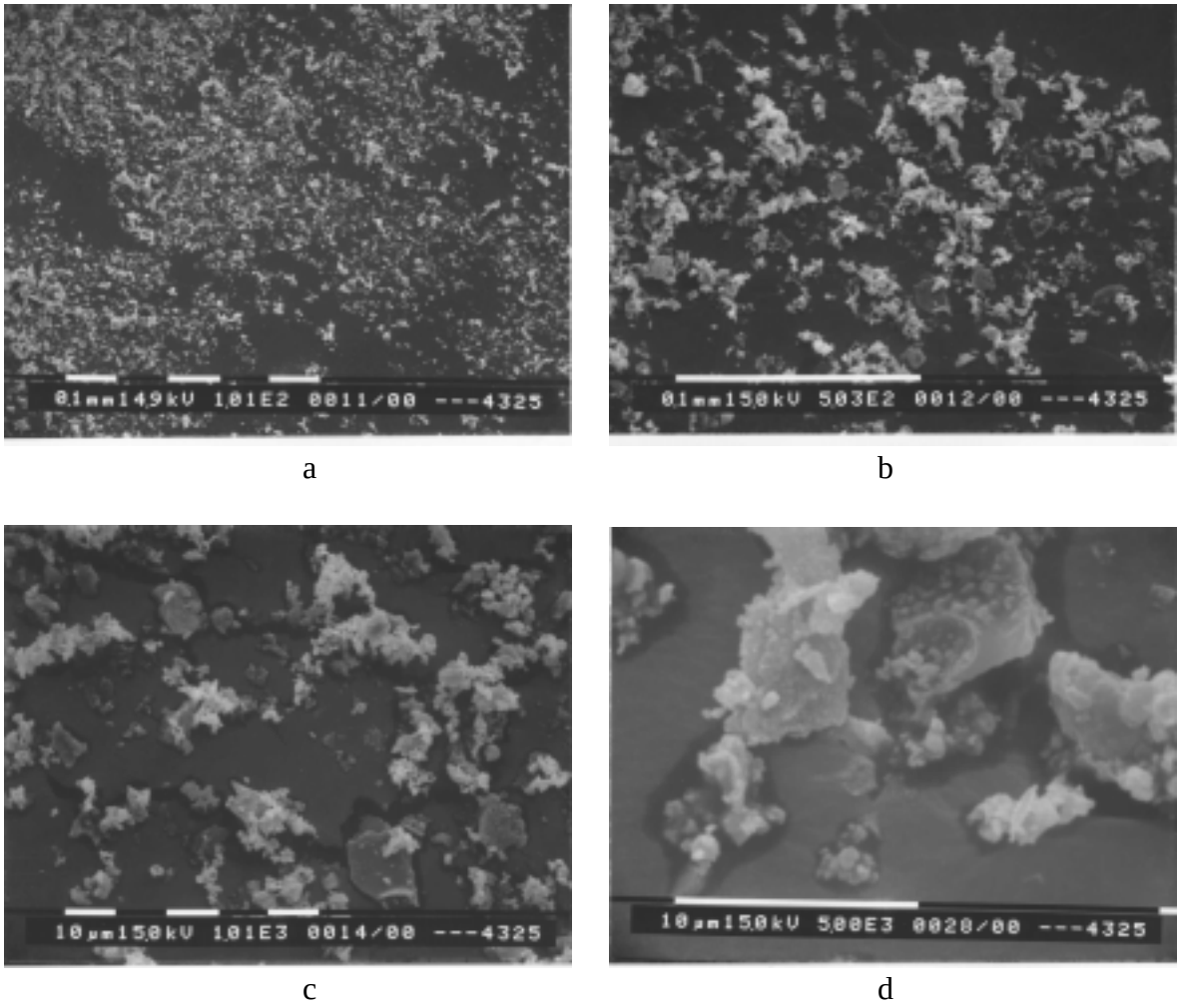

a b

c d

Figure 4-94. Representative Scanning Electron Micrographs of P051 filter cake char (ID # 4325) taken at magnifications of a) 100x, b) 500x, c) 1000x, and d) 5000x.

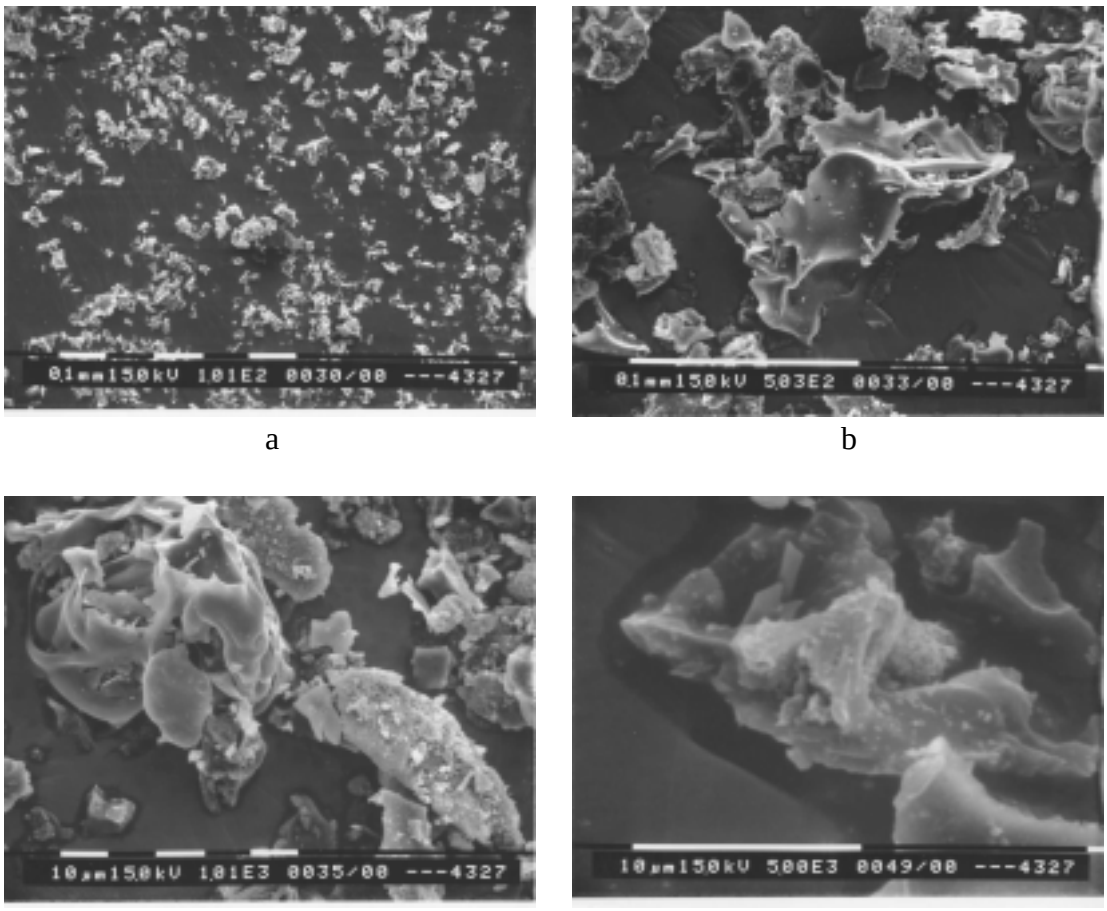

a b

c d

Figure 4-95. Representative Scanning Electron Micrographs of P056 filter hopper char (ID # 4327) taken at magnifications of a) 100x, b) 500x, c) 1000x, and d) 5000x.

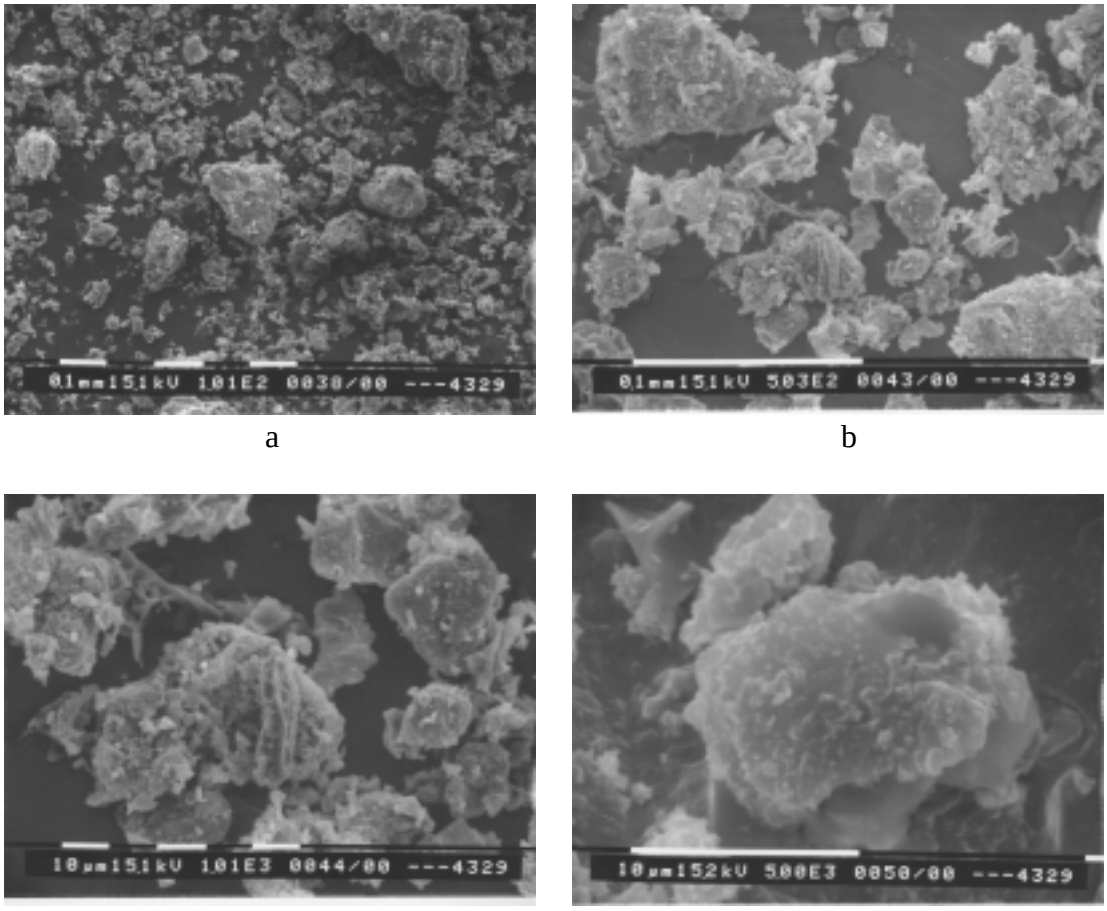

a b

c d

Figure 4-96. Representative Scanning Electron Micrographs of P057 filter hopper char (ID # 4329) taken at magnifications of a) 100x, b) 500x, c) 1000x, and d) 5000x.

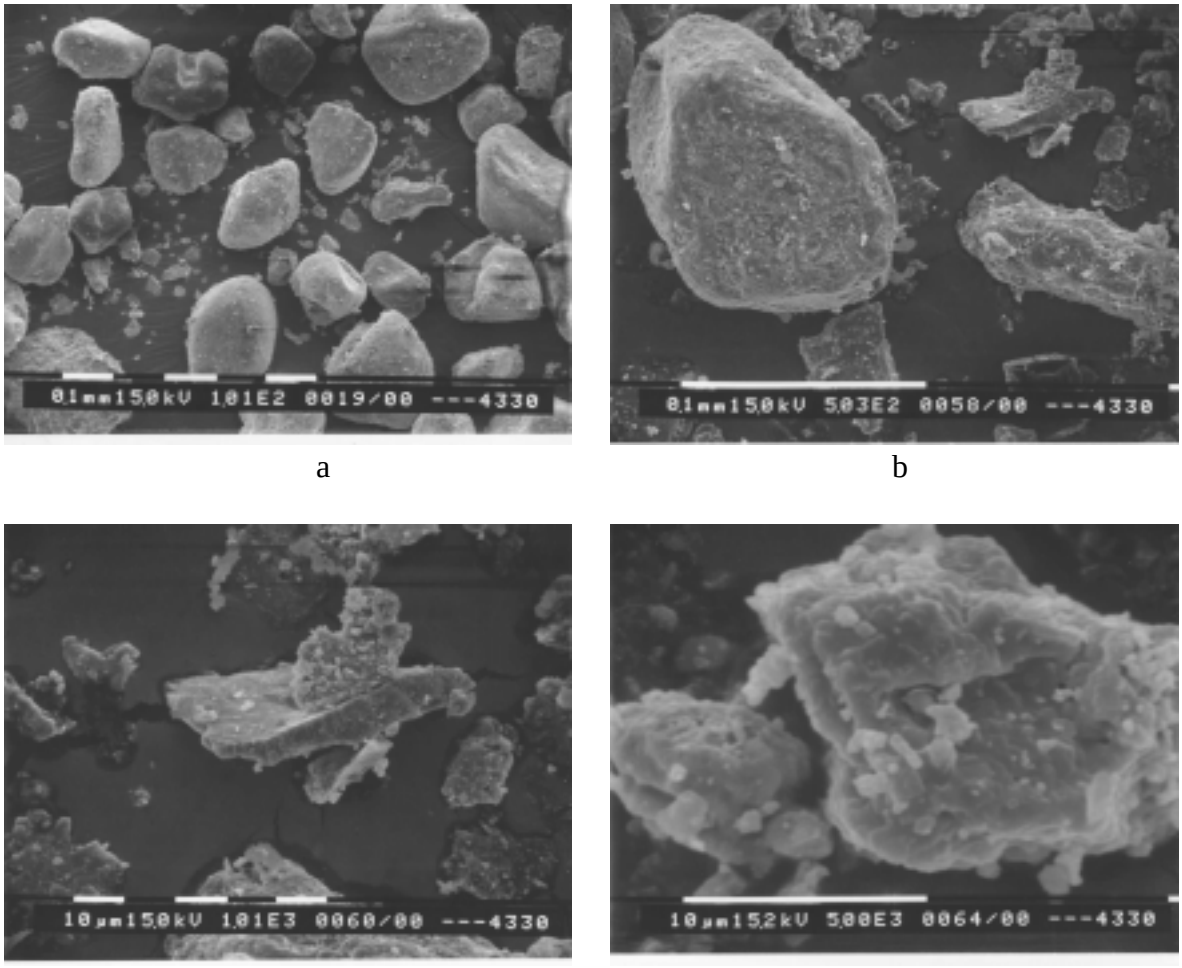

a b

c d

Figure 4-97. Representative Scanning Electron Micrographs of P058 filter hopper ash (ID # 4330) taken at magnifications of a) 100x, b) 500x, c) 1000x, and d) 5000x.

The analyses performed on the run P047 hopper ash from April 1996 (ID # 4176), in combination with observations made in handling the sample and micrographs of the sample ash particles (Figure 4-91), indicated that this sample has a high bulk density and has a very coarse size distribution. Although these characteristics were unexpected, they agree with quantitative evaluations that were performed. Because of the coarse size of this ash, a Bahco aerodynamic classifier was used to measure its size distribution. This procedure physically separates the ash into nine portions, depending on particle size. All nine fractions were about the same color gray, except the coarsest fraction (> 26 μm), which contained a fairly high percentage of large black particles. The size distribution of this TRDU ash is presented in Figure 4-84. The specific surface area of this ash is quite high, although ashes with coarse size distributions generally have relatively low specific surface areas. The uncompacted bulk porosity and tensile strength of this ash indicate it is free flowing and has little cohesive strength, as would be expected for such a coarse size distribution. As with most other ashes with coarse size distributions, this ash exhibited a large drag-equivalent diameter and a low specific gas-flow resistance.

After the analyses of this ash were completed, limited information describing the conditions under which it was produced was received. Apparently the material in the TRDU standpipe overflowed causing some relatively large particles to enter the filter vessel. Although these particles may not have reached the filter cake, they did eventually collect in the filter hopper from which the ash sample that was analyzed was obtained. The micrographs in Figure 4-91 clearly show large, spherical particles present in this sample. Because the presence of a high proportion of relatively large particles in an ash sample will significantly alter its bulk characteristics, the results of analyses of the UNDEERC TRDU ash sample (ID # 4176) probably do not accurately reflect the characteristics of TRDU filter cake ash. More representative TRDU ash samples were subsequently received for analysis.

Seven of the remaining eight samples from the TRDU (ID #'s 4199 and 4324 - 4329) were obtained from runs performed in gasification mode. Sample ID # 4330 was generated during combustion mode. As would be expected, the combustion sample (ID # 4330) differs in every respect from the gasification samples. Its physical properties show that it is coarser, much less cohesive, and has much less specific surface area than the char samples. Its chemistry also is quite different than those of the char samples. With the exception of sample ID # 4325, all of these samples were obtained from the HGFV hopper. Sample # 4199 is relatively fine (Figure 4-85), has a high uncompacted bulk porosity, and is dark black. Representative scanning electron micrographs of this sample can be viewed in Figure 4-92. Additionally, the sample has a relatively high specific surface area, a low drag-equivalent diameter, and a high uncompacted bulk porosity (Table 4-30). The specific gas flow resistance of this sample (calculated from drag-equivalent diameter and the assumption that filter cake porosity equals uncompacted bulk porosity) is not abnormally high. However, as with several other gasification samples that have been evaluated, the specific gas flow resistance of this sample could be much higher than the calculated value if the actual filter cake porosity is much lower than the measured uncompacted bulk porosity value of 89 %. The tensile strength of this sample (5.7 N/m^2) is low to moderate, indicating that this ash may tend to reentrain after being dislodged by back pulsing.

Some distinctions and comparisons can also be made among the char samples (generated during runs P050, P051, P056, and P057). The least cohesive char is ID # 4327 (based on its uncompacted bulk porosity), and it is also the second coarsest of the chars. Also in agreement with sample # 4327 being the second coarsest of these chars, its specific surface area is lower than the other char samples analyzed. The char samples generated in run P050 and P051 (ID #'s 4199, 4324 and 4325) are significantly finer than the chars generated in run P056 or run P057. These differences correlate with the uncompacted bulk porosities and specific surface areas of the chars from run P051, which are higher than the values measured for run P056 and run P057. Background information describing these runs and the samples submitted for analysis was provided by Michael Swanson. (Because no background information was provided for sample ID # 4199, the following discussion of the effects of process parameters on sample characteristics does not include this sample.) The sample information data sheets provided by Mr. Swanson are presented in Appendix B. There were two primary differences between runs P051 and P056:

1. There was no recirculation of dipleg solids during run P051, while dipleg solids were recirculated during all of run P056. This recirculation could have resulted in more carryover of coarse particles to the filter vessel.
2. The second difference between these two runs was the fuels used. Wyodak coal was used throughout run P051 and for the first part of run P056. The second part of run P056 was fueled with Illinois #6 coal. (Bituminous coal from the SUFCo mine was used in run P057.)

The differences in the fuels may be responsible for the measured differences in the size distributions and other characteristics of the chars produced in these runs. The MMD of sample # 4326 falls between the finer chars generated in run P051 and the coarser chars generated in run P056. (Wyodak coal was used during the first part of run P056, when sample 4326 was generated. Illinois #6 coal was used in the latter part of run P056 when sample 4327 was generated.) The high surface areas of sample ID #s 4324, 4325, 4328, and 4329 indicate that the fuel used affects the specific surface area of the resultant char. Specifically, the Wyodak and SUFCo coals produced chars with up to seven times the specific surface area of the chars produced from Illinois #6 coal. Because the proportion of added Plum Run dolomite corresponding to these samples (Table 4-29) was not varied unless the fuel source was changed, the effects that changes in the relative amounts of this sorbent added to the process cannot be fully resolved from these data. The higher SO_3 content of sample # 4327, as compared to the SO_3 contents of samples 4324, 4325, and 4329, correlates with the higher proportion of dolomite added during the final portion of run P056.

The characteristics of the char collected from the hopper during run P051 (ID # 4324) can be compared with the char collected from the filter cake on the candles after the run (ID # 4325). As has been observed in other filter vessels, the hopper material is coarser than the filter cake material; however, there is relatively little difference between the MMD's of these two samples. Although the relative fineness of these two samples would suggest that the filter cake char (ID # 4325) would exhibit a higher specific surface area and a smaller drag-equivalent diameter, this is not the case. The larger specific surface area of the char from the hopper compared with the value measured for the filter cake material agrees with the

difference in the drag-equivalent diameters of these two samples. These data suggest that the coarsest particles in the hopper char sample are more irregularly shaped (rougher and less spherical) than the particles in the filter cake sample. This type of behavior has been observed before (with some AFBC ash particles).

As was done for samples from Piñon Pine and Karhula, the size distributions of the two char samples from run P051 were compared to estimate the degree of settling in the filter vessel prior to formation of the filter cake. (This type of comparison should be valid if TRDU operation during the period when the hopper sample was obtained is comparable to the period of operation when the filter cake sample was formed. Because these two samples were reported to have been generated during steady state operation, this should be the case.) This comparison, which is presented in detail in the section *Estimating Filter Vessel Inertial Collection from Size Distribution Data*, implies that during run P051 about 33 % of the mass of the entrained particles entering the filter vessel settled out prior to reaching the filter cake surface.

4.8 HERMAN RESEARCH PTY LTD.

Three samples were received from Dr. Danh Huynh of Herman Research Pty Ltd. that were collected from the hot gas filter in the pressurized gasification test rig at Mulgrave, Australia. These samples are identified in Table 4-32, and represent gasification runs made with three different Latrobe Valley brown coals. Gasification was generally carried out at about 900 kPa (130 psi) and about 900 °C. Although the filter was operated at this same pressure, the temperature in the filter was around 400 °C. Dr. Huyhn also supplied some additional information about the gasification facility which is included in the interactive data bank. The results of physical and chemical analyses of the three HRL gasification particulate samples are included in Tables 4-33 and 4-34. Complete size distributions measured for these samples are given in Figures 4-98 through 4-100 and representative scanning electron micrographs are presented in Figures 4-101 through 4-103.

Table 4-32
Identification of HRL Gasification Chars Received for Analysis

ID #	Source	Brief description
4195	Herman Research Pty Ltd.	Mulgrave test rig: Morwell coal
4196	Herman Research Pty Ltd.	Mulgrave test rig: Loy Yang coal
4197	Herman Research Pty Ltd.	Mulgrave test rig: Yallourn coal

Table 4-33
Physical Characteristics of Herman Research Pty Ltd.
Gasification Particulate Samples

quantity ID #	4195	4196	4197
specific surface area, m^2/g	491	560	429
mass median diameter, µm	7.3	3.6	7.2
uncompacted bulk porosity, %	87	88	90
drag-equivalent diameter, µm	0.91	0.77	0.71
specific gas-flow resistance, in $H_2O \cdot min \cdot ft/lb$*	12.2	10.7	8.4
true particle density, g/cm^3	1.91	1.96	1.98

* specific gas-flow resistances were calculated for filter cake porosities equal to the uncompacted bulk porosity of the sample

Table 4-34
Chemical Characteristics of Herman Research Pty Ltd. Gasification Particulate Samples, % wt.

constituent ID #	4195	4196	4197
Li_2O	0.08	0.11	0.13
Na_2O	1.4	5.8	1.4
K_2O	0.31	1.3	0.36
MgO	20.9	21.3	22.3
CaO	38.8	16.0	16.9
Fe_2O_3	15.1	11.7	39.3
Al_2O_3	6.2	15.0	5.1
SiO_2	2.9	14.6	1.9
TiO_2	0.22	1.9	0.45
P_2O_5	0.11	0.15	0.22
SO_3	11.1	14.0	12.7
LOI	88.3	93.8	89.5
soluble $SO_4^{=}$	0.65	< 0.47	0.43
Equilibrium pH*	10.2	9.4	9.8

* dimensionless.

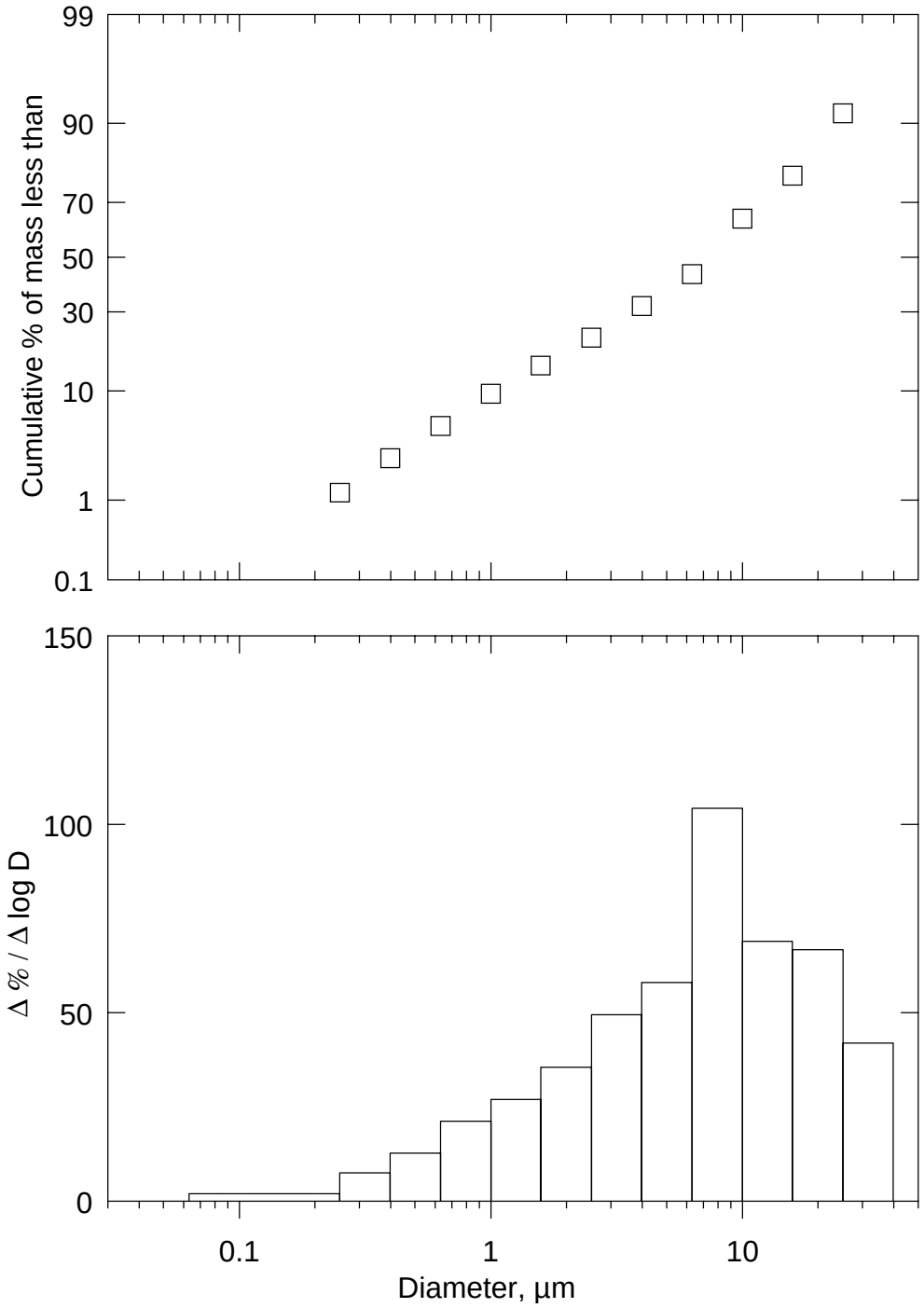

Figure 4-98. Cumulative and differential size distribution data measured for Herman Research Pty Ltd. Mulgrave test rig (Morwell coal) gasification particulate (ID # 4195) measured with a Shimadzu SA-CP4 Centrifugal Particle Size Analyzer. The MMD of this distribution is 7.3 µm, and its geometric standard deviation is 3.4. (This size distribution data includes the assumption that the sample contains no particles smaller than 0.063 µm.)

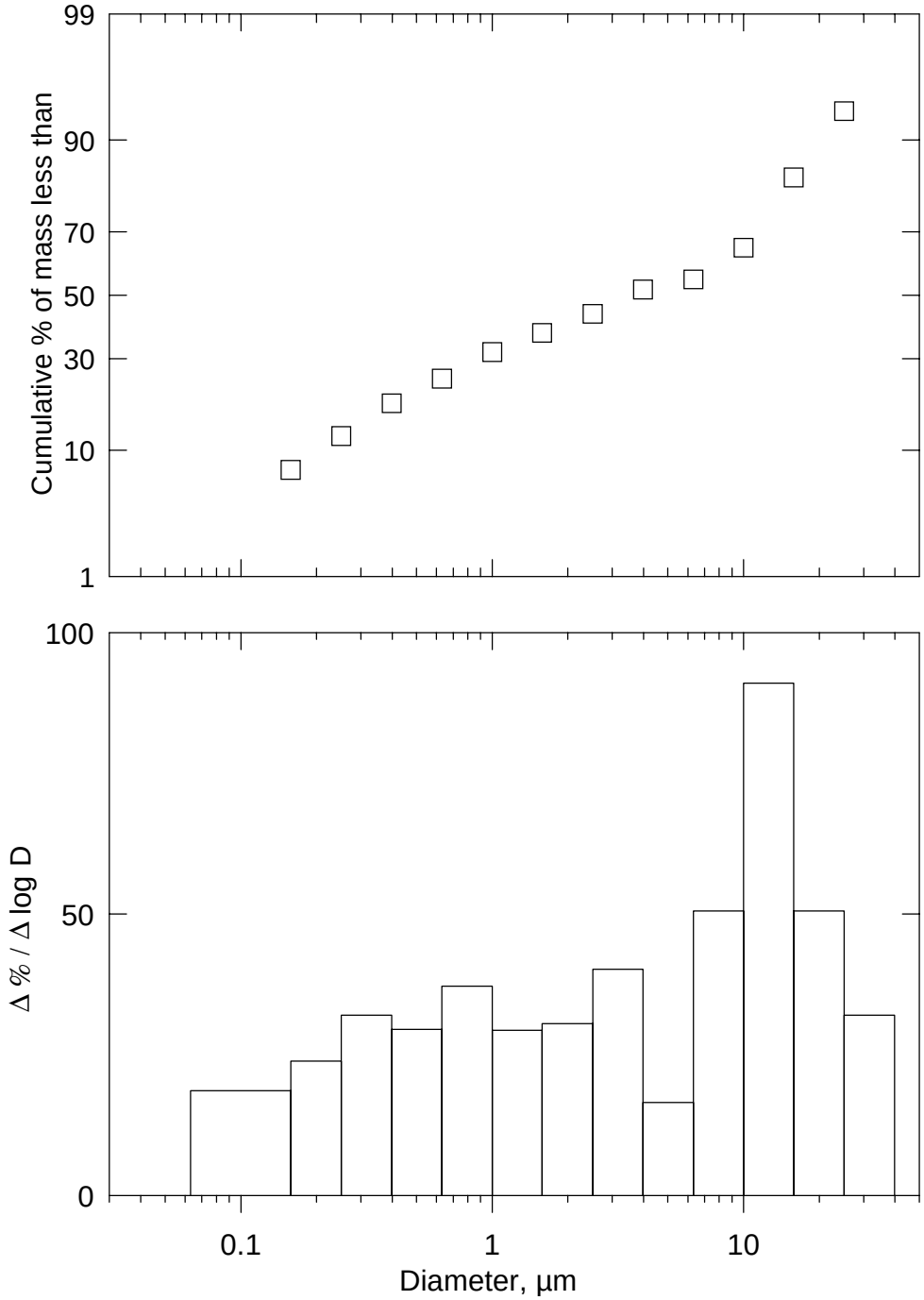

Figure 4-99. Cumulative and differential size distribution data measured for Herman Research Pty Ltd. Mulgrave test rig (Loy Yang coal) gasification particulate (ID # 4196) measured with a Shimadzu SA-CP4 Centrifugal Particle Size Analyzer. The MMD of this distribution is 3.6 µm, and its geometric standard deviation is 7.0. (This size distribution data includes the assumption that the sample contains no particles smaller than 0.063 µm.)

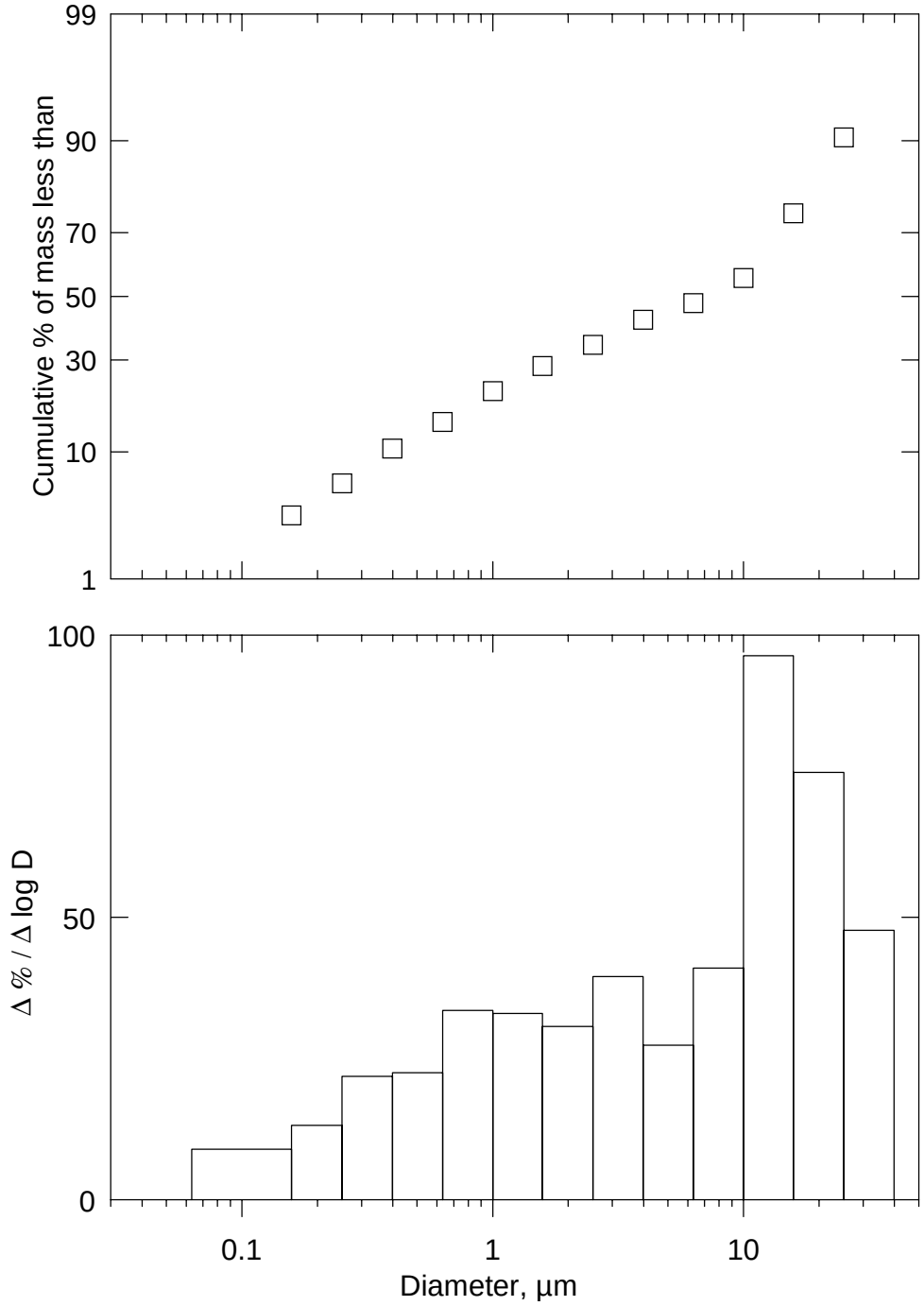

Figure 4-100. Cumulative and differential size distribution data measured for Herman Research Pty Ltd. Mulgrave test rig (Yallourn coal) gasification particulate (ID # 4197) measured with a Shimadzu SA-CP4 Centrifugal Particle Size Analyzer. The MMD of this distribution is 7.2 µm, and its geometric standard deviation is 5.5. (This size distribution data includes the assumption that the sample contains no particles smaller than 0.063 µm.)

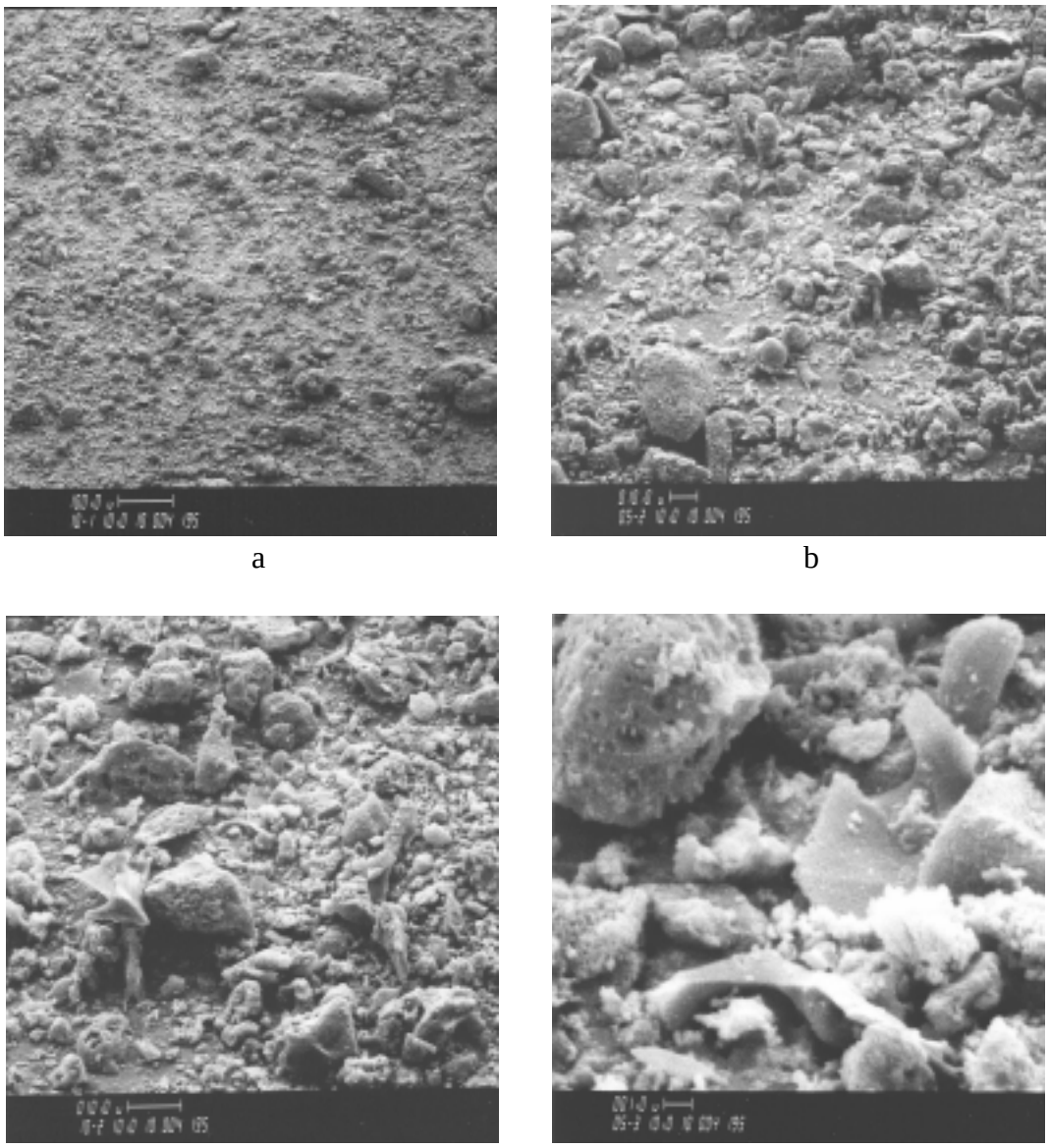

a b

c d

Figure 4-101. Representative scanning electron micrographs of Herman Research Pty Ltd. Mulgrave test rig (Morwell coal) gasification particulate (ID # 4195) taken at a) 100X, b) 500X, c) 1000X and d) 5000X.

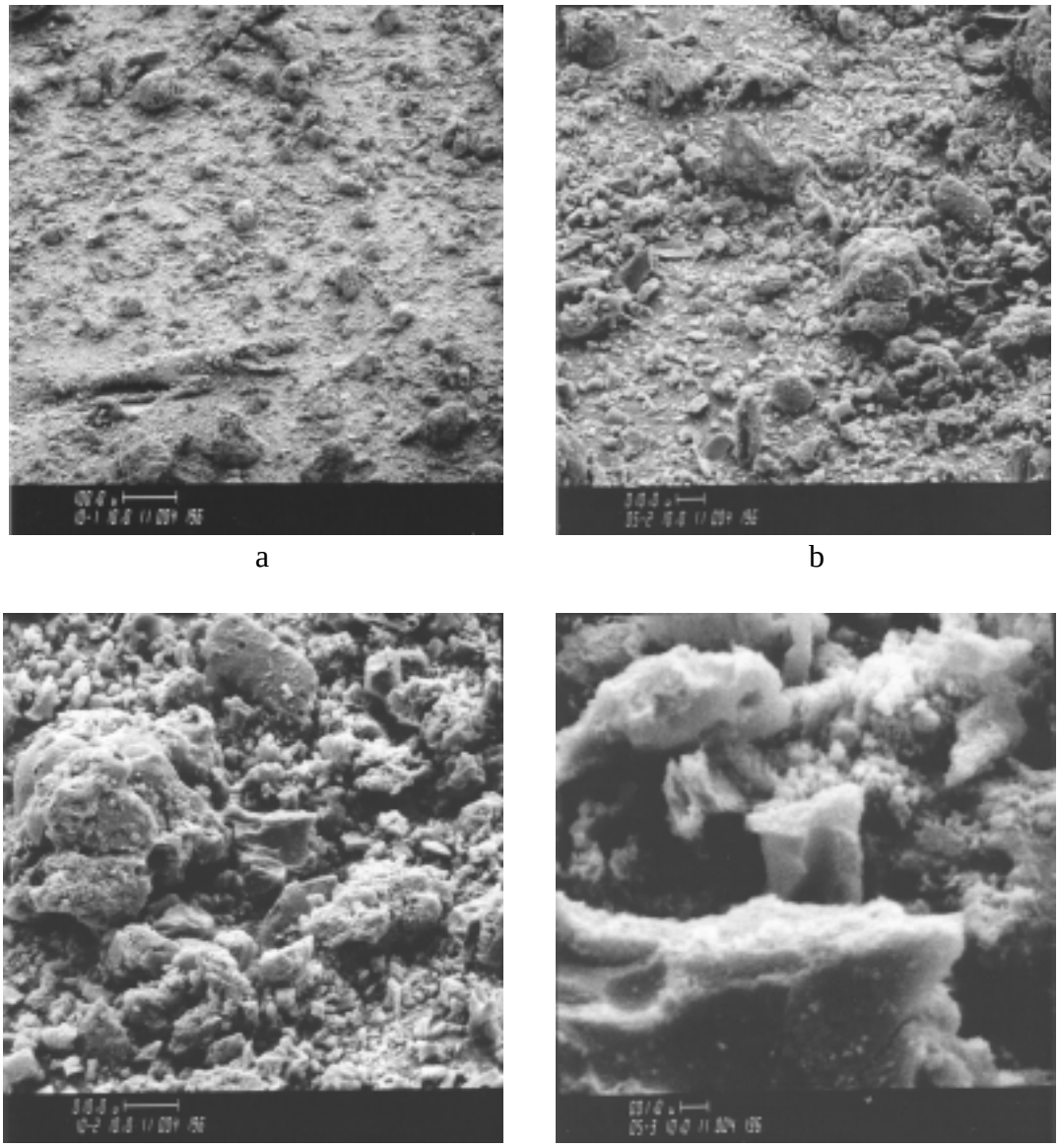

Figure 4-102. Representative scanning electron micrographs of Herman Research Pty Ltd. Mulgrave test rig (Loy Yang coal) gasification particulate (ID # 4196) taken at a) 100X, b) 500X, c) 1000X and d) 5000X.

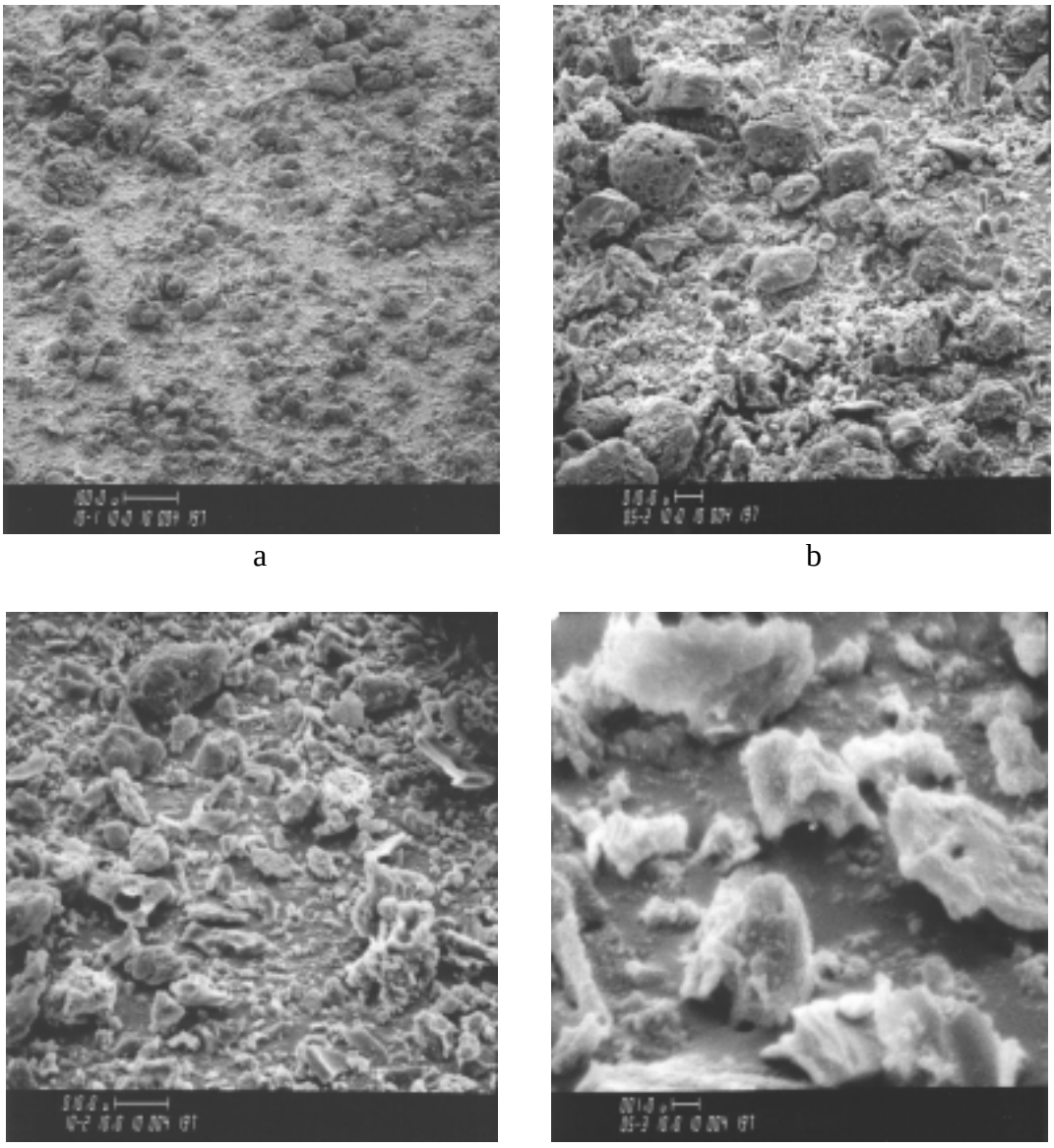

a b

c d

Figure 4-103. Representative scanning electron micrographs of Herman Research Pty Ltd. Mulgrave test rig (Yallourn coal) gasification particulate (ID # 4197) taken at a) 100X, b) 500X, c) 1000X and d) 5000X.

The three HRL particulate samples have similar physical characteristics. They all exhibit extremely high specific surface areas, and moderate drag-equivalent diameters and uncompacted bulk porosities (for gasification char particles). The specific gas flow resistances of these samples are not exceptionally large; however, these values could increase significantly if the actual filter cake porosities are much lower than the uncompacted bulk porosity values used to calculate these resistances. The size distributions of these samples indicate tests of the Loy Yang coal produced a finer distribution than the other two coals. However, the size distributions of the Loy Yang and Yallourn coal-derived char samples indicate that these two samples are very poorly approximated by log-normal distributions. There are various differences in the chemical characteristics of the three HRL samples. Because the relationships between chemical constituents and particulate behavior have not been established for gasification particulate, it is not possible to state whether the chemical differences in these three samples relate to their filtration behavior.

4.9 ADDITIONAL ANALYSES

4.9.1 Characterization of Additional Gasifier Char Samples

The discussion in this section includes analyses that were performed on gasifier char samples (described in Table 4-35) generated during tests carried out by Kellogg Brown & Root, Texaco, and KRW between 1988 and 1991. These analyses were intended to strengthen and clarify correlations that have been observed between particle size, specific surface area, uncompacted bulk porosity, specific gas flow resistance, and drag-equivalent diameter. The data measured for these additional char samples are presented in Tables 4-36 through 4-38. (Because of inadequate sample material, no analyses were performed on sample # 2563 other than examination with a scanning electron microscope.) Scanning electron micrographs of these char samples are presented in Figures 4-104 through 4-119.

Table 4-35
Additional Gasifier Char Samples from the HGCU Data Bank

ID #	Source	Brief description
2800	Kellogg Brown & Root	Transport Reactor Test Unit (TRTU) run G4 filter fines
2803	Kellogg Brown & Root	TRTU run G101 filter fines
2832	Kellogg Brown & Root	TRTU run H-1962-G3A filter fines
2834	Kellogg Brown & Root	TRTU run H-1962-G5C filter fines
2838	Kellogg Brown & Root	TRTU run H-1962-G7A filter fines
2840	Kellogg Brown & Root	TRTU run H-1962-G8A filter fines
2678	Texaco M.R.L.	run L8902-04 filter vessel ash pot solids
2550	KRW	fluidized bed gasification char (82 % carbon)
2556	KRW	TP-037-9: C-110 outlet particulate residue composite
2557	KRW	TP-037-9: C-115 outlet particulate residue composite
2558	KRW	TP-037-9: C-120 outlet composite
2559	KRW	TP-037-9: SC 41 hopper particulate residue composite
2560	KRW	TP-037-9: C-108 hopper particulate residue (4/25/88)
2561	KRW	TP-037-9: C-108 hopper particulate residue (5/1/88)
2562	KRW	TP-037-9: C-108 hopper particulate residue (4/28/88)
2563	KRW	TP-037-9: C-121 filter sample (4/28/88)

Table 4-36
Physical Characteristics of Texaco and Kellogg Brown & Root Gasification Chars

quantity ID #	2678	2800	2803	2832	2834	2838	2840
specific surface area, m^2/g	88	58	32	300	241	353	69
mass median diameter, µm	7.6	16	16	18	16	14	15
uncompacted bulk porosity, %	92	89	86	84	87	88	84
drag-equivalent diameter, µm	1.16	1.58	1.65	1.34	1.51	1.30	2.14
specific gas-flow resistance, in H_2O·min·ft/lb*	1.1	1.7	3.4	8.9	3.4	3.6	3.2
tensile strength, N/m^2	0.6	2.7	2.0	1.3	0.8	0.4	0.5
true particle density, g/cm^3	2.62	2.44	2.40	2.14	2.29	2.27	2.31

* specific gas-flow resistances were calculated for filter cake porosities equal to the uncompacted bulk porosity of the sample

Table 4-37
Physical Characteristics of KRW Gasification Chars

quantity ID #	2550	2556	2557	2558	2559	2560	2561	2562
specific surface area, m^2/g	278	112	108	184	135	218	381	293
mass median diameter, µm	0.22	16	17	1.4	16	3.1	0.38	0.36
uncompacted bulk porosity, %	94	93	93	95	92	95	95	96
drag-equivalent diameter, µm	0.14	0.99	0.93	0.28	0.95	0.26	0.26	0.25
specific gas-flow resistance, in H_2O·min·ft/lb*	45	1.3	1.5	6.4	2.0	7.4	7.8	4.5
tensile strength, N/m^2	3.5	0.3	0.3	2.5	0.3	3.0	1.8	1.1
true particle density, g/cm^3	2.17	2.11	2.08	2.14	2.18	2.12	2.12	2.17

* specific gas-flow resistances were calculated for filter cake porosities equal to the uncompacted bulk porosity of the sample

Table 4-38
Chemical Analyses of Kellogg Brown & Root Gasification Chars, % wt.

constituent ID #	2800	2803
Li_2O	0.02	0.02
Na_2O	0.59	0.51
K_2O	1.4	1.4
MgO	0.53	1.3
CaO	1.4	18.2
Fe_2O_3	5.8	4.6
Al_2O_3	58.9	42.3
SiO_2	29.6	22.5
TiO_2	0.67	0.5
P_2O_5	0.13	0.09
SO_3	0.94	8.6
LOI	47.2	40.7
soluble $SO_4^=$	0.36	3.5
Equilibrium pH*	8.2	11.1

* dimensionless

The size distribution data presented in Table 4-37 indicate that several of the KRW char samples (# 2550, # 2558, # 2561 and # 2562) are extremely fine (much like the MGCR char samples discussed in section 4.4). The specific surface areas of most of these char samples are extremely high, and all the samples have specific surface areas in excess of 32 m^2/g. The irregular morphologies of these char samples (and fine size distributions of several of them) are apparent in the micrographs.

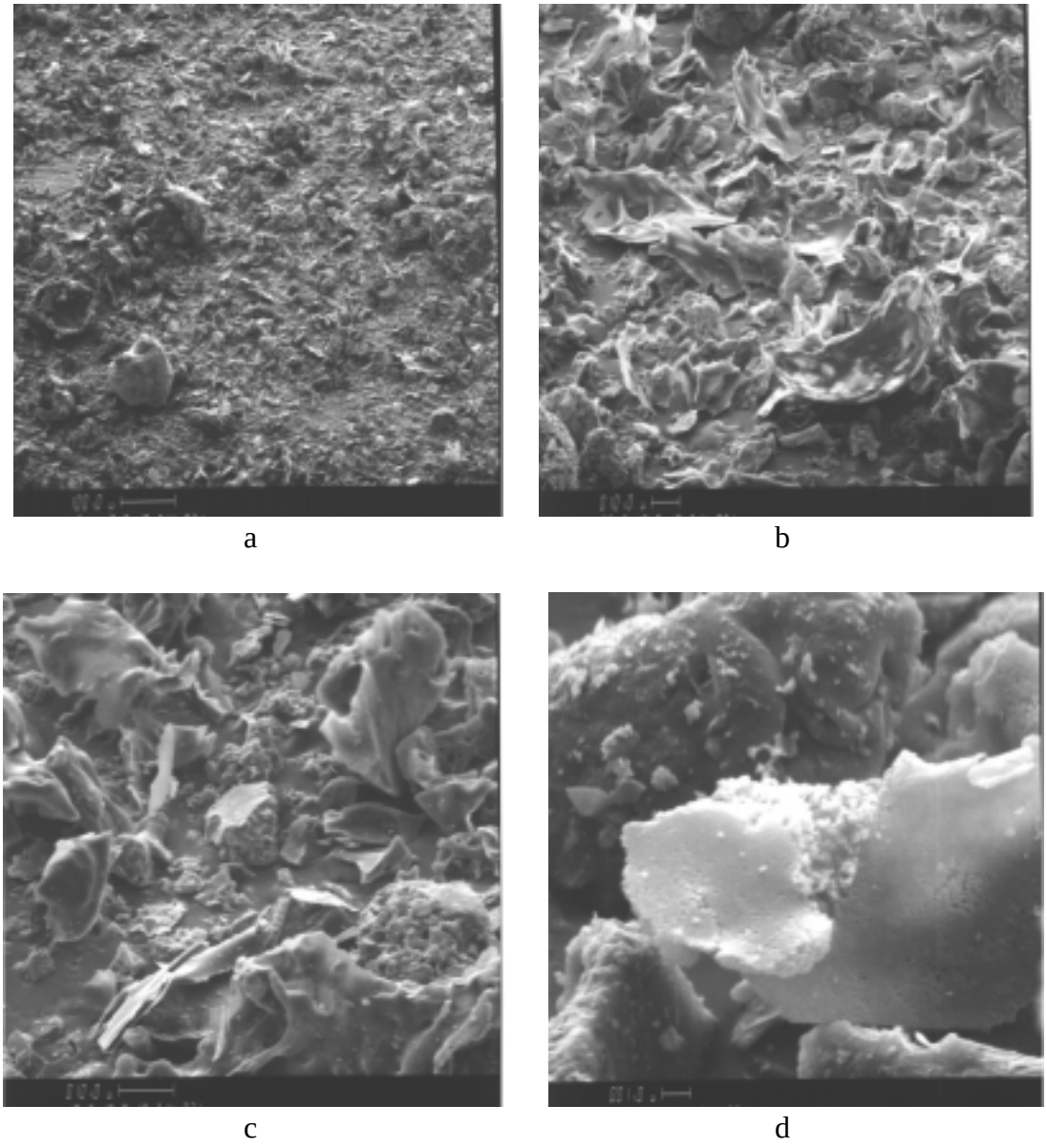

Figure 4-104. Representative scanning electron micrographs of Kellogg Brown & Root Transport Reactor Test Unit (TRTU) run G4 filter fines (ID # 2800) taken at a) 100X, b) 500X, c) 1000X, and d) 5000X.

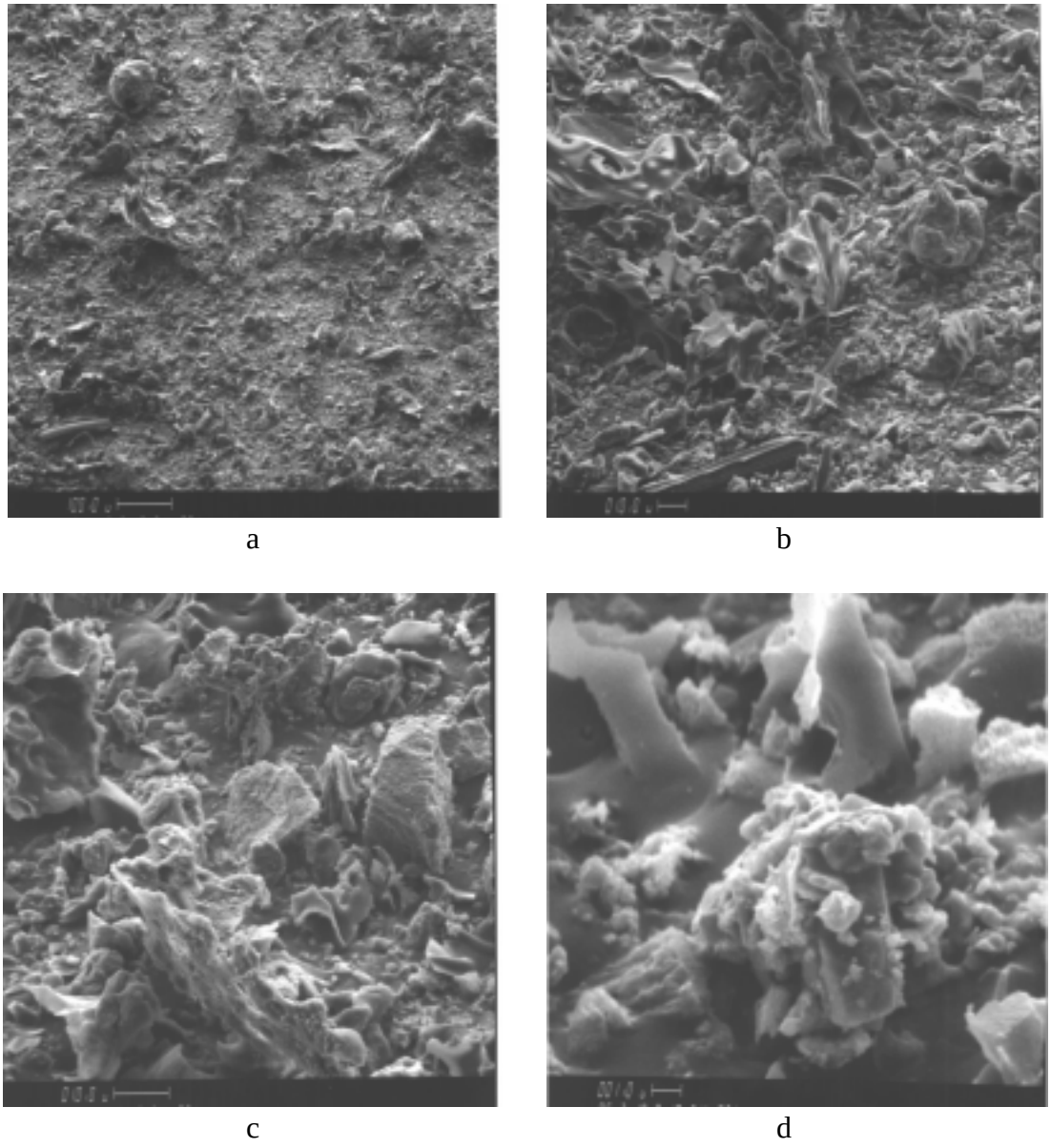

Figure 4-105. Representative scanning electron micrographs of Kellogg Brown & Root TRTU run G101 filter fines (ID # 2803) taken at a) 100X, b) 500X, c) 1000X, and d) 5000X.

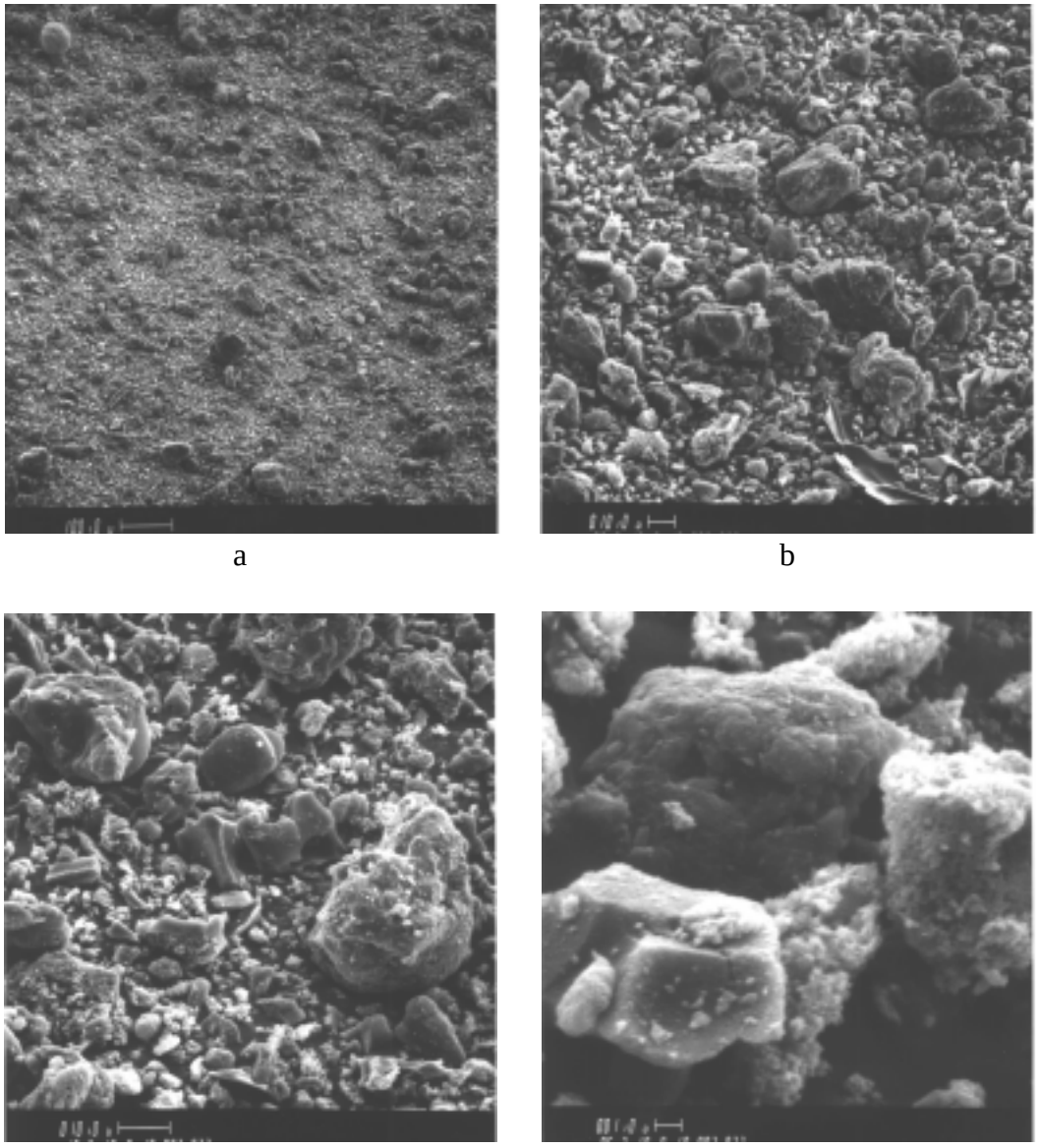

a b

c d

Figure 4-106. Representative scanning electron micrographs of Kellogg Brown & Root TRTU run H-1962-G3A filter fines (ID # 2832) taken at a) 100X, b) 500X, c) 1000X, and d) 5000X.

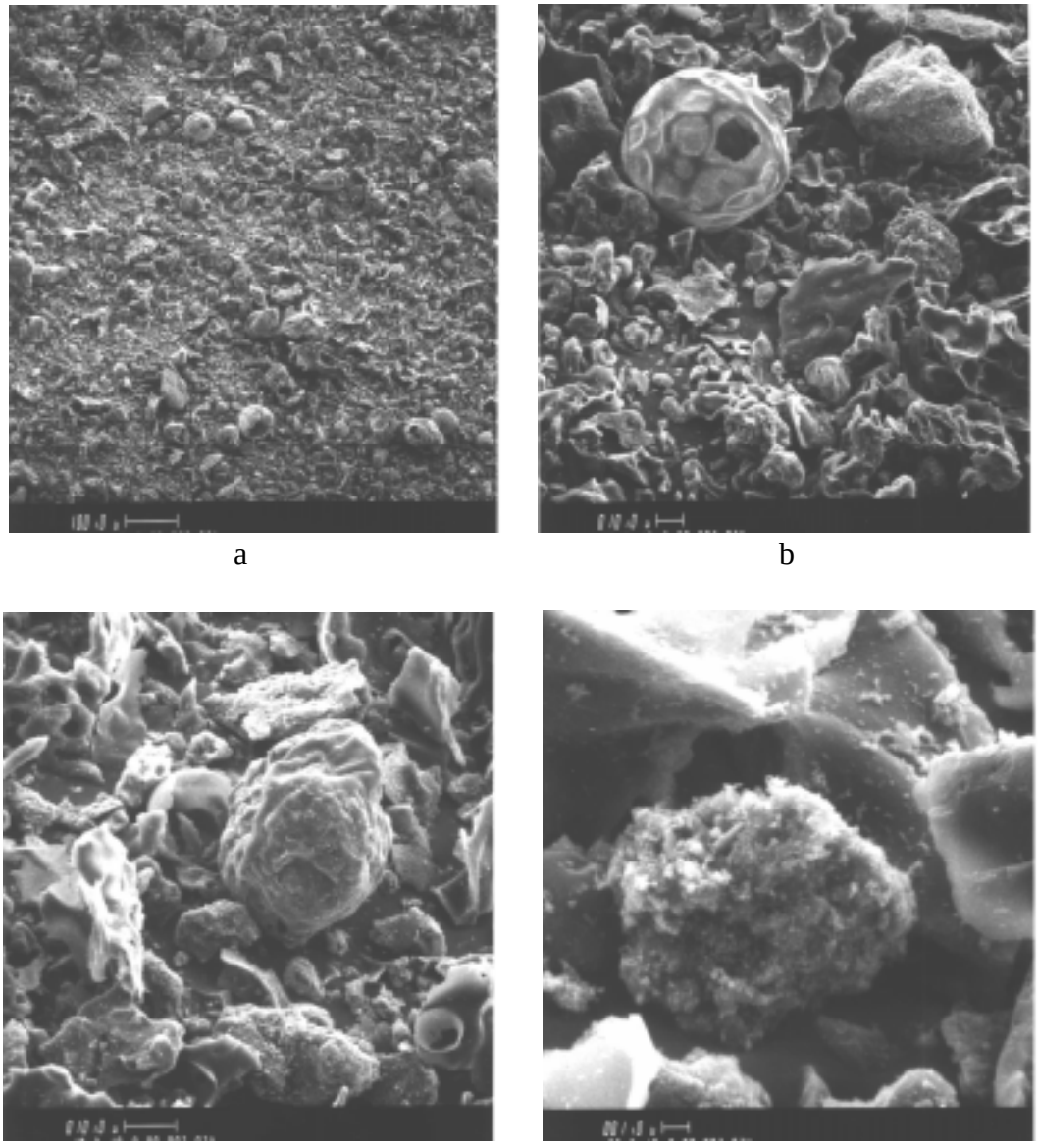

Figure 4-107. Representative scanning electron micrographs of Kellogg Brown & Root TRTU run H-1962-G5C filter fines (ID # 2834) taken at a) 100X, b) 500X, c) 1000X, and d) 5000X.

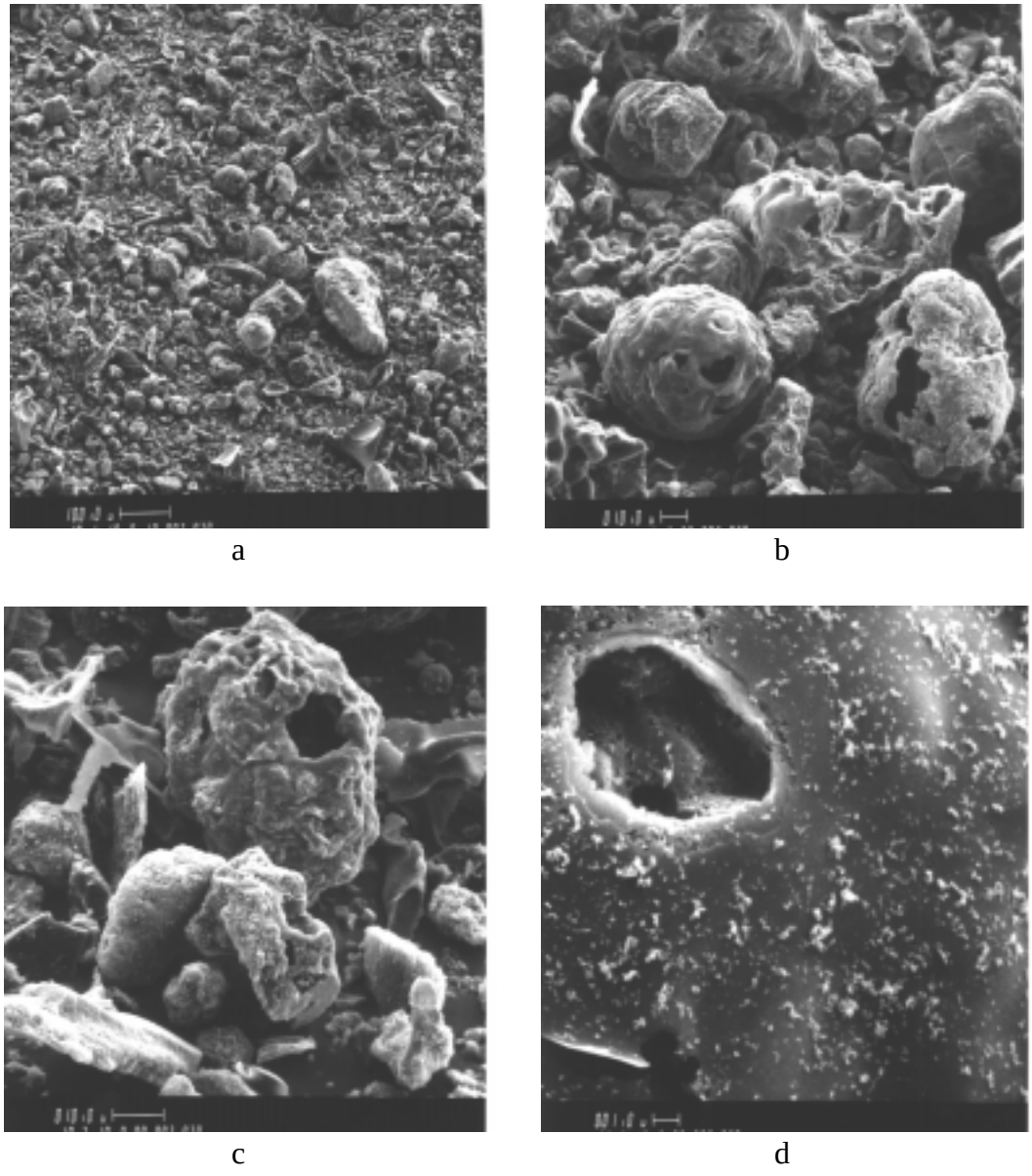

Figure 4-108. Representative scanning electron micrographs of Kellogg Brown & Root TRTU run H-1962-G7A filter fines (ID # 2838) taken at a) 100X, b) 500X, c) 1000X, and d) 5000X.

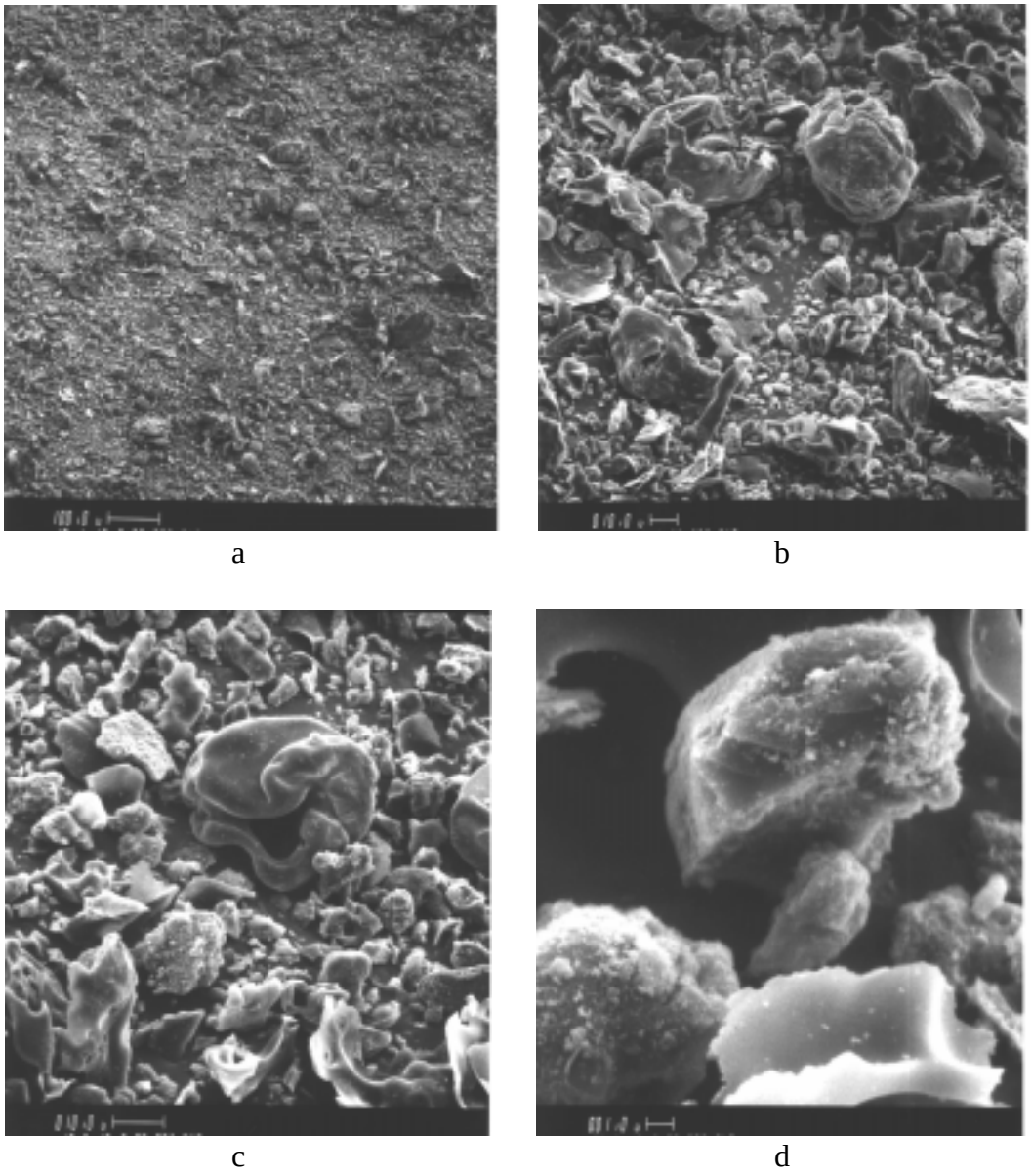

Figure 4-109. Representative scanning electron micrographs of Kellogg Brown & Root TRTU run H-1962-G8A filter fines (ID # 2840) taken at a) 100X, b) 500X, c) 1000X, and d) 5000X.

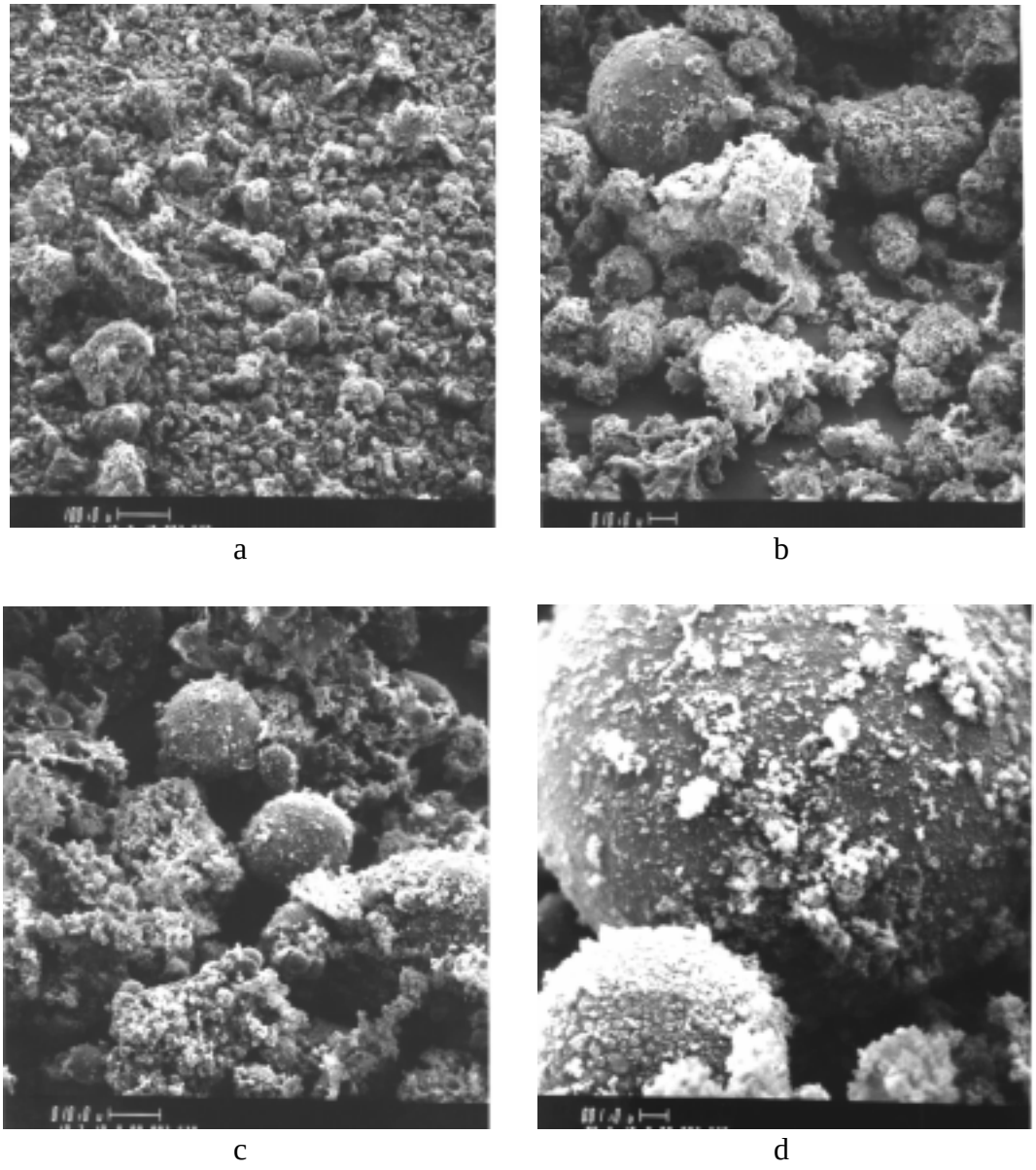

Figure 4-110. Representative scanning electron micrographs of Texaco Montebello Research Laboratory run L8902-04 filter vessel ash pot solids (ID # 2678) taken at a) 100X, b) 500X, c) 1000X, and d) 5000X.

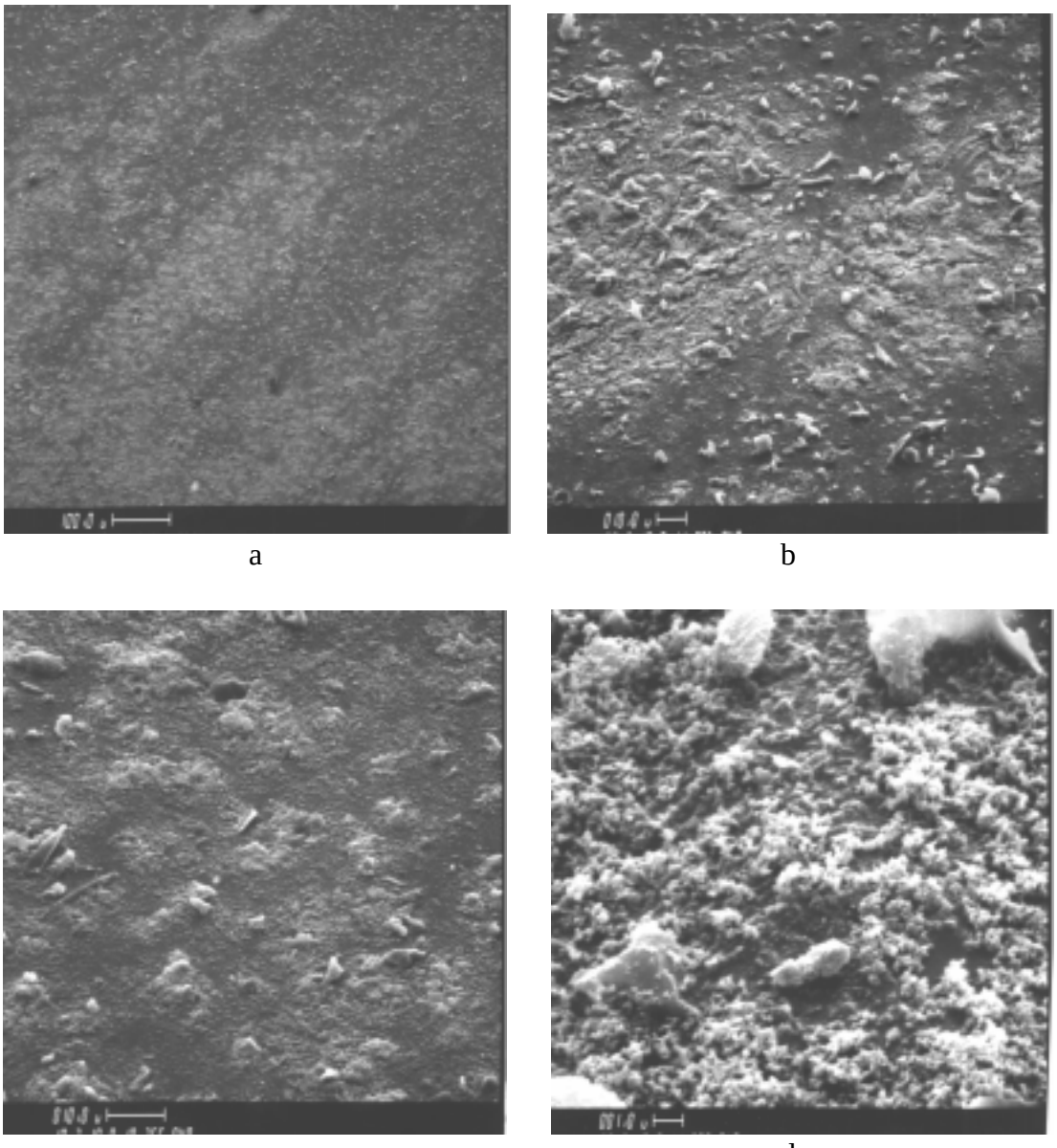

Figure 4-111. Representative scanning electron micrographs of KRW fluidized bed gasification char (ID # 2550) taken at a) 100X, b) 500X, c) 1000X, and d) 5000X.

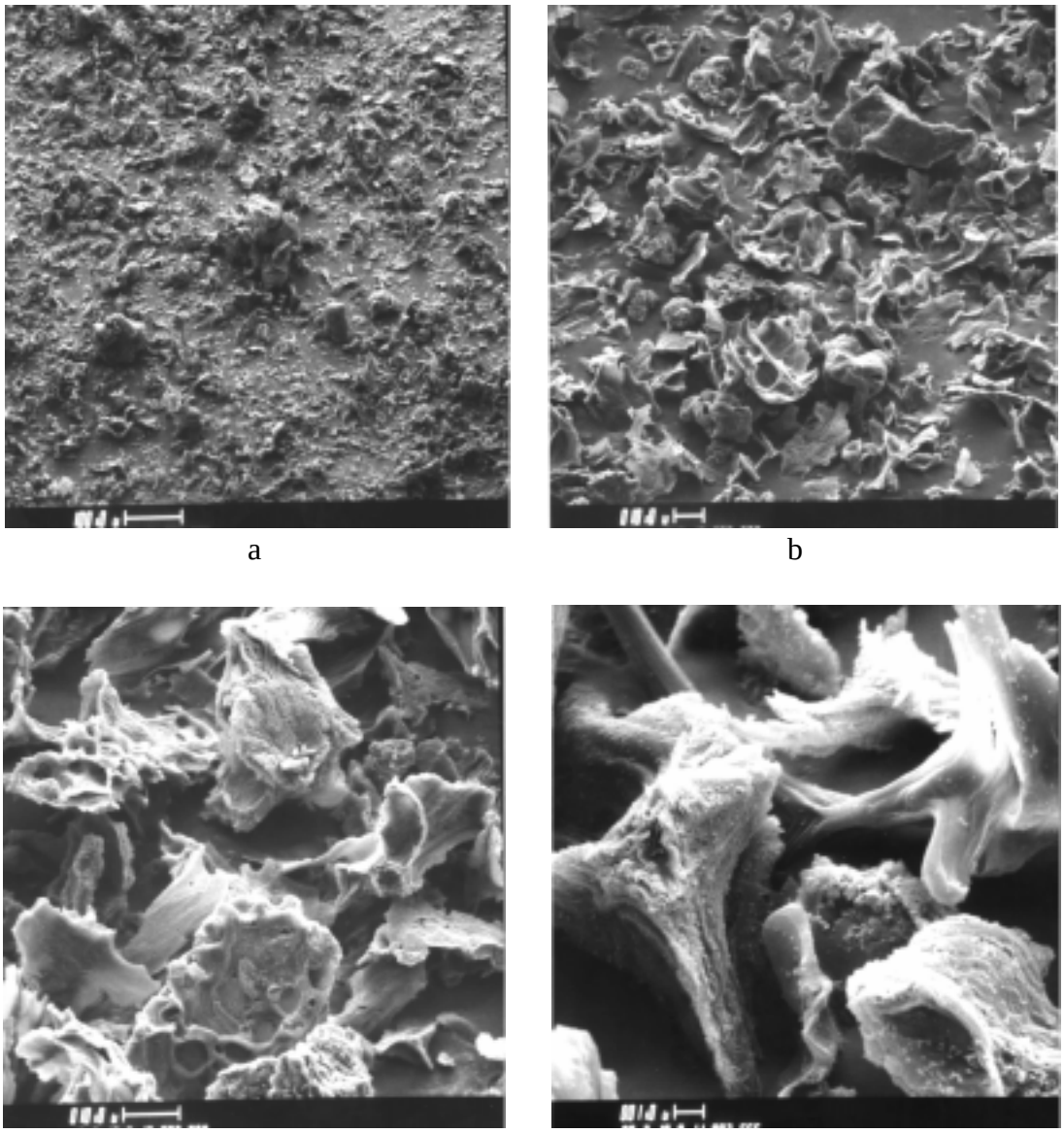

Figure 4-112. Representative scanning electron micrographs of KRW C-110 outlet composite gasification char (ID # 2556) taken at a) 100X, b) 500X, c) 1000X, and d) 5000X.

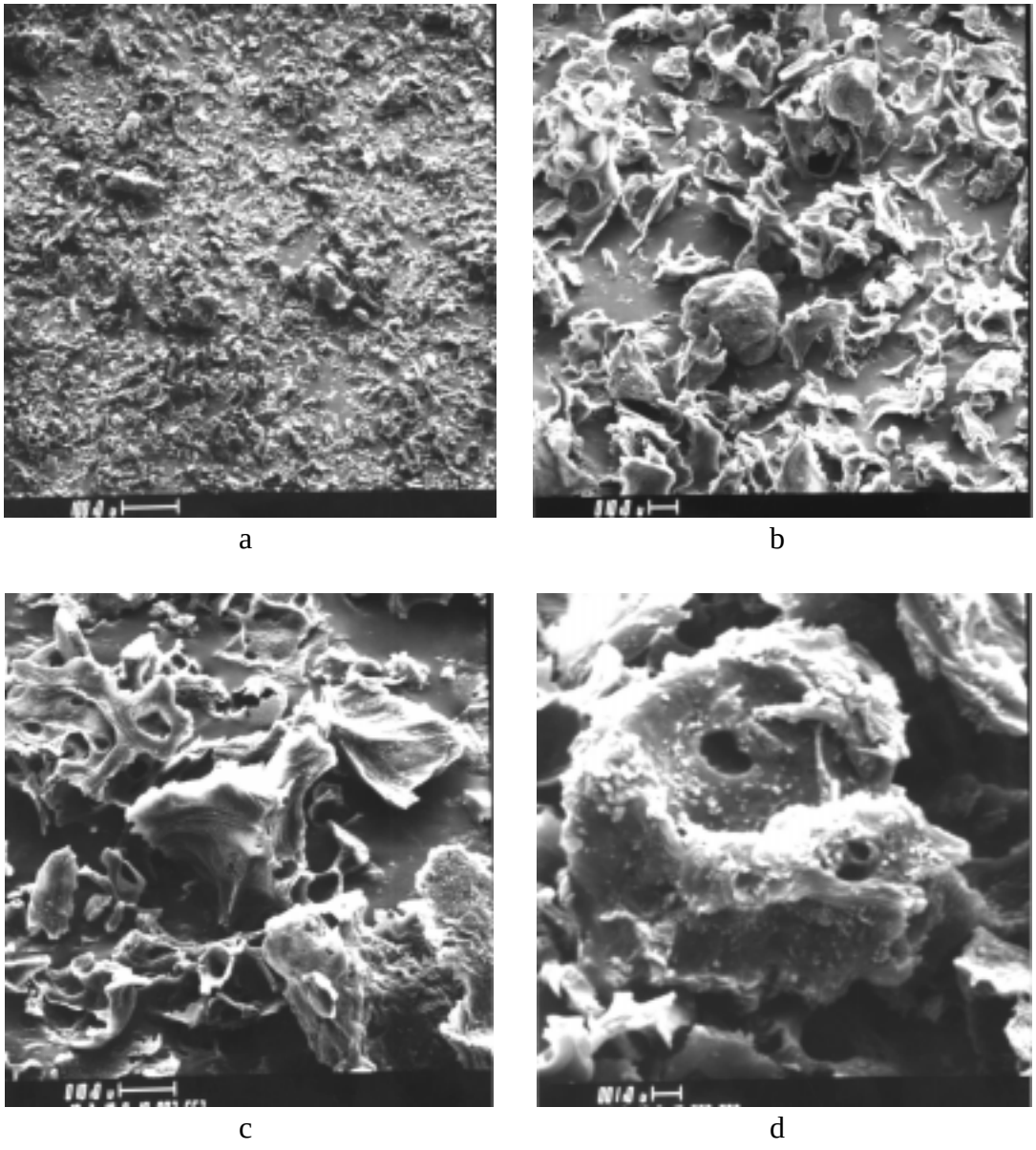

Figure 4-113. Representative scanning electron micrographs of KRW C-115 outlet composite gasification char (ID # 2557) taken at a) 100X, b) 500X, c) 1000X, and d) 5000X.

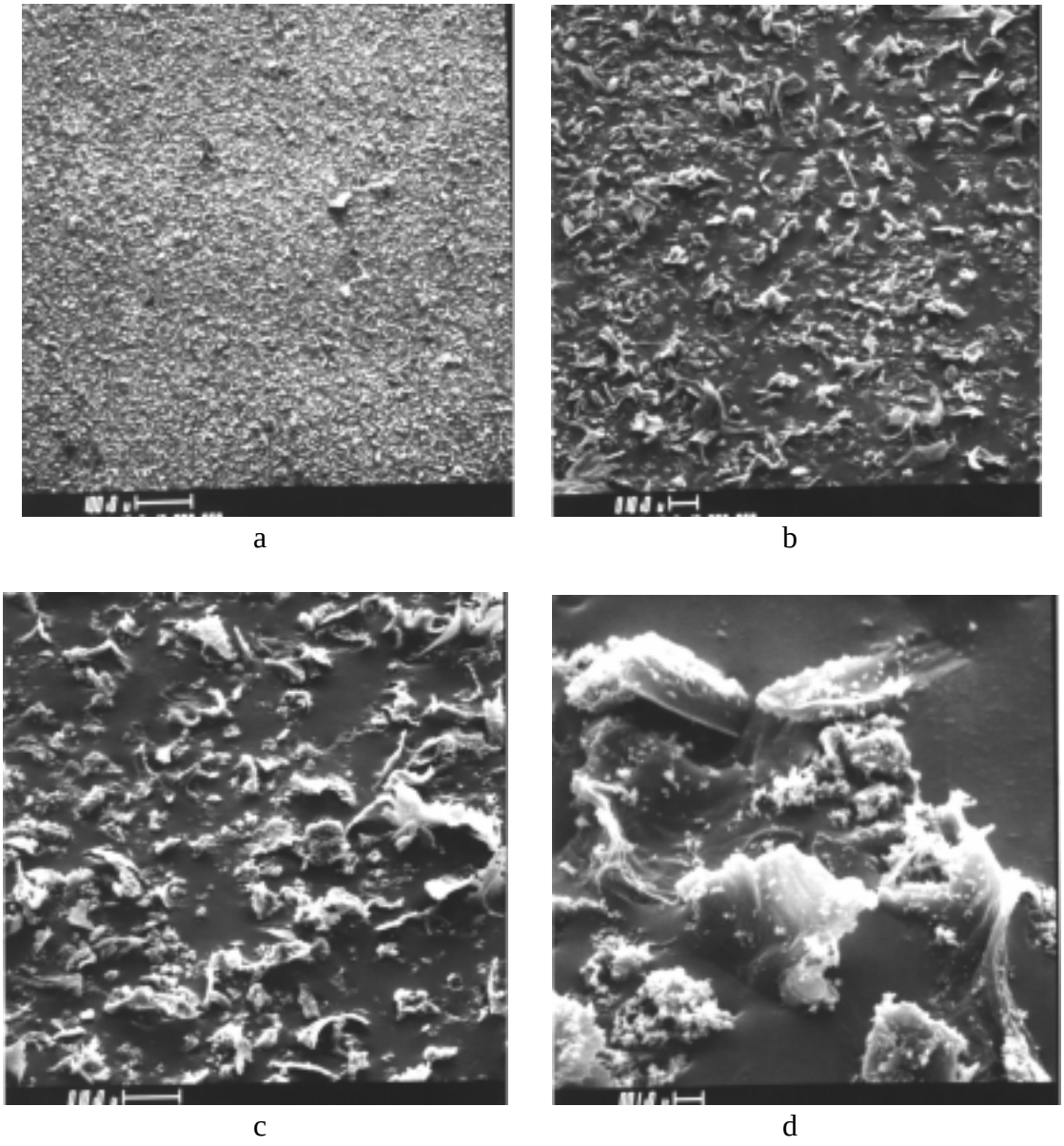

Figure 4-114. Representative scanning electron micrographs of KRW C-120 outlet composite gasification char (ID # 2558) taken at a) 100X, b) 500X, c) 1000X, and d) 5000X.

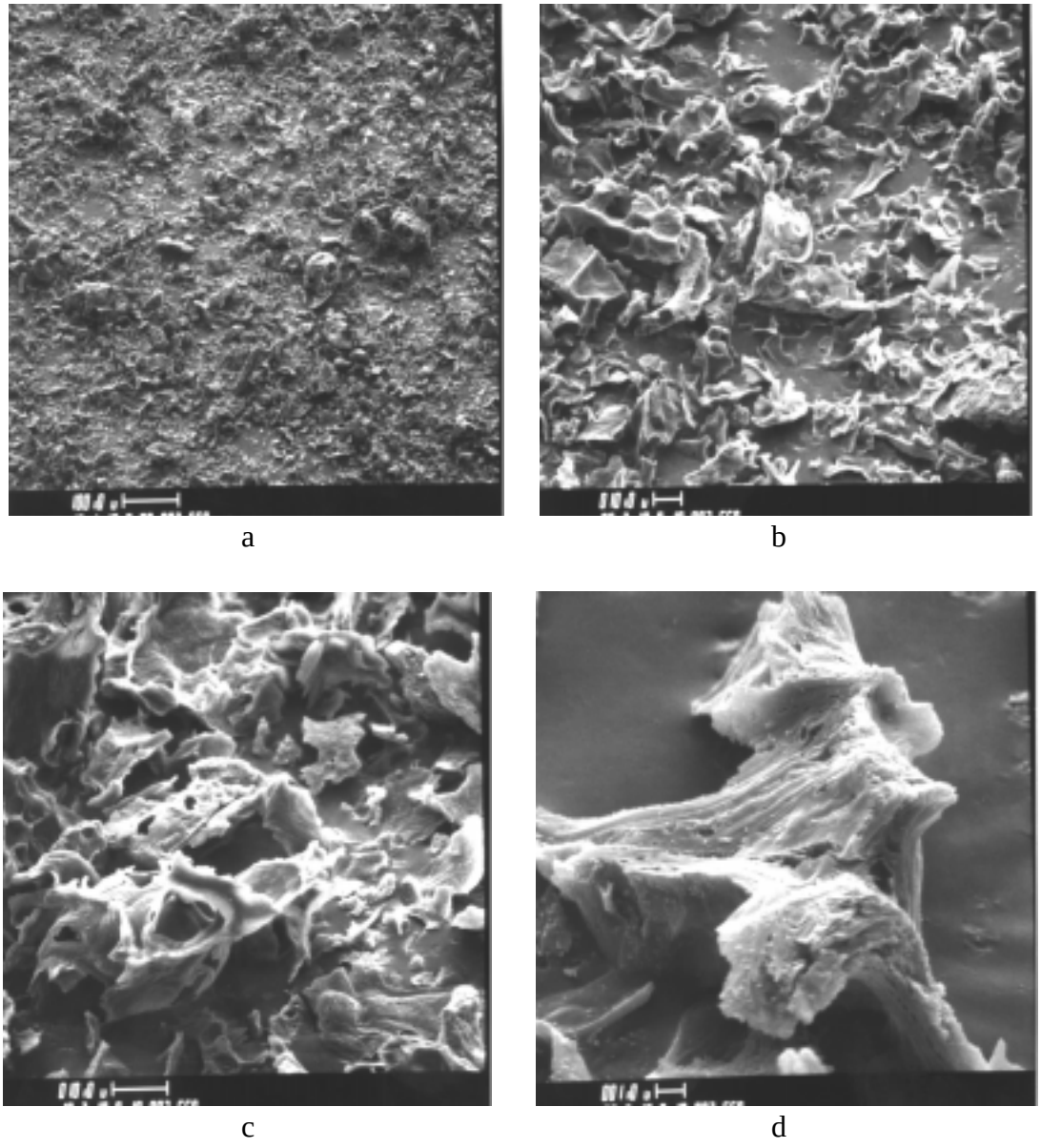

Figure 4-115. Representative scanning electron micrographs of KRW SC 41 hopper composite gasification char (ID # 2559) taken at a) 100X, b) 500X, c) 1000X, and d) 5000X.

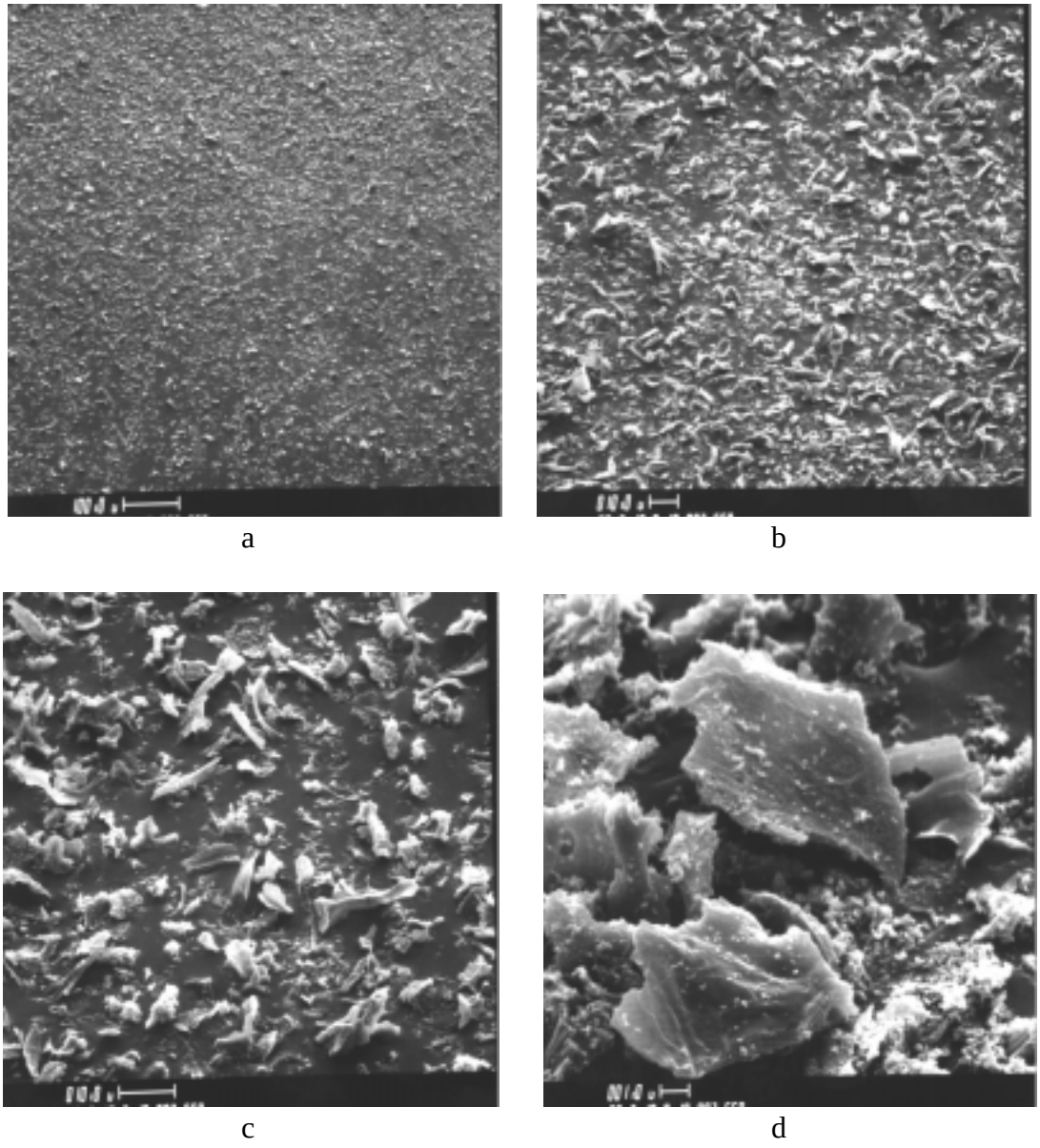

Figure 4-116. Representative scanning electron micrographs of KRW C-121 hopper (4/25/88) gasification char (ID # 2560) taken at a) 100X, b) 500X, c) 1000X, and d) 5000X.

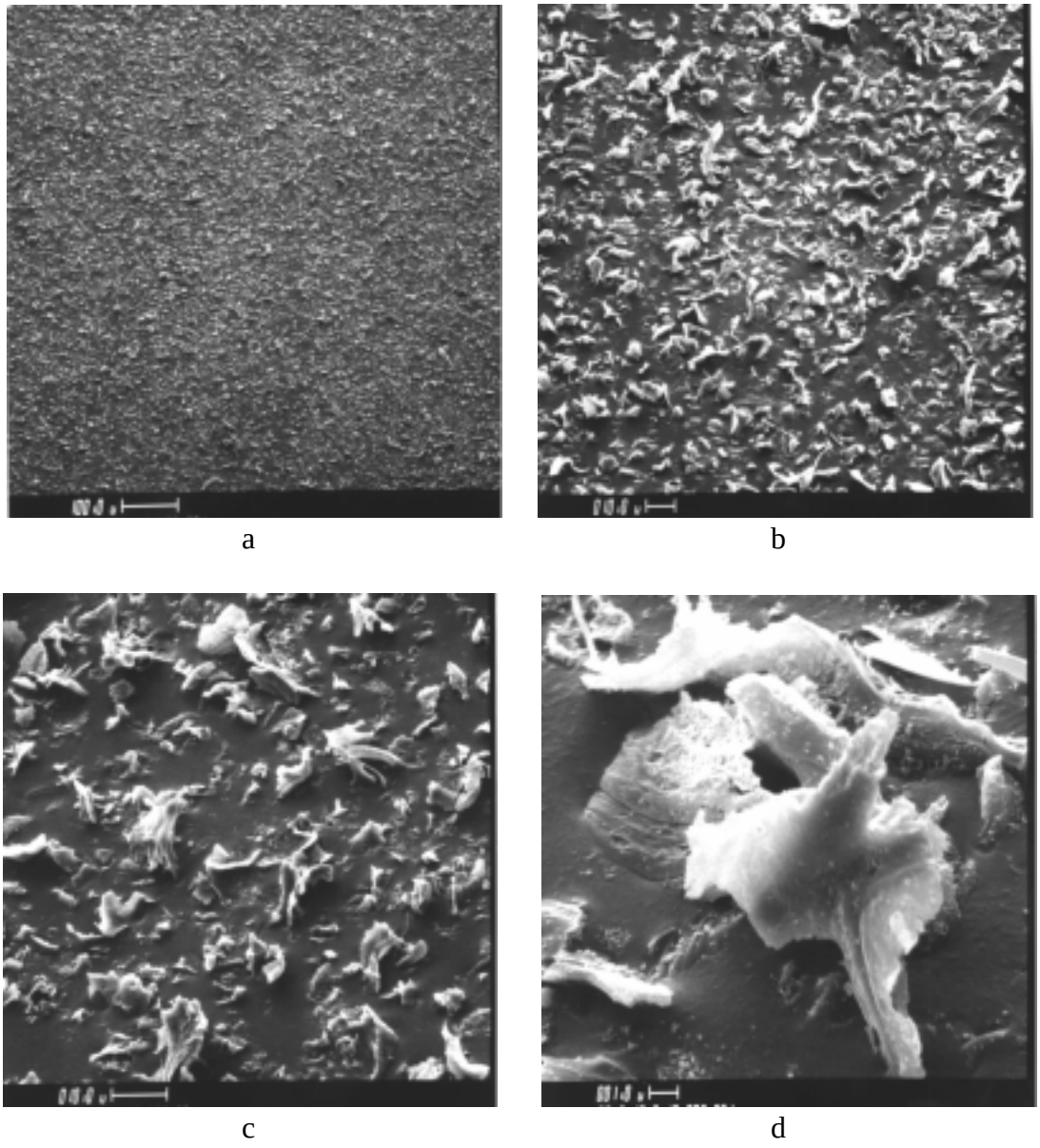

Figure 4-117. Representative scanning electron micrographs of KRW C-121 hopper (5/1/88) gasification char (ID # 2561) taken at a) 100X, b) 500X, c) 1000X, and d) 5000X.

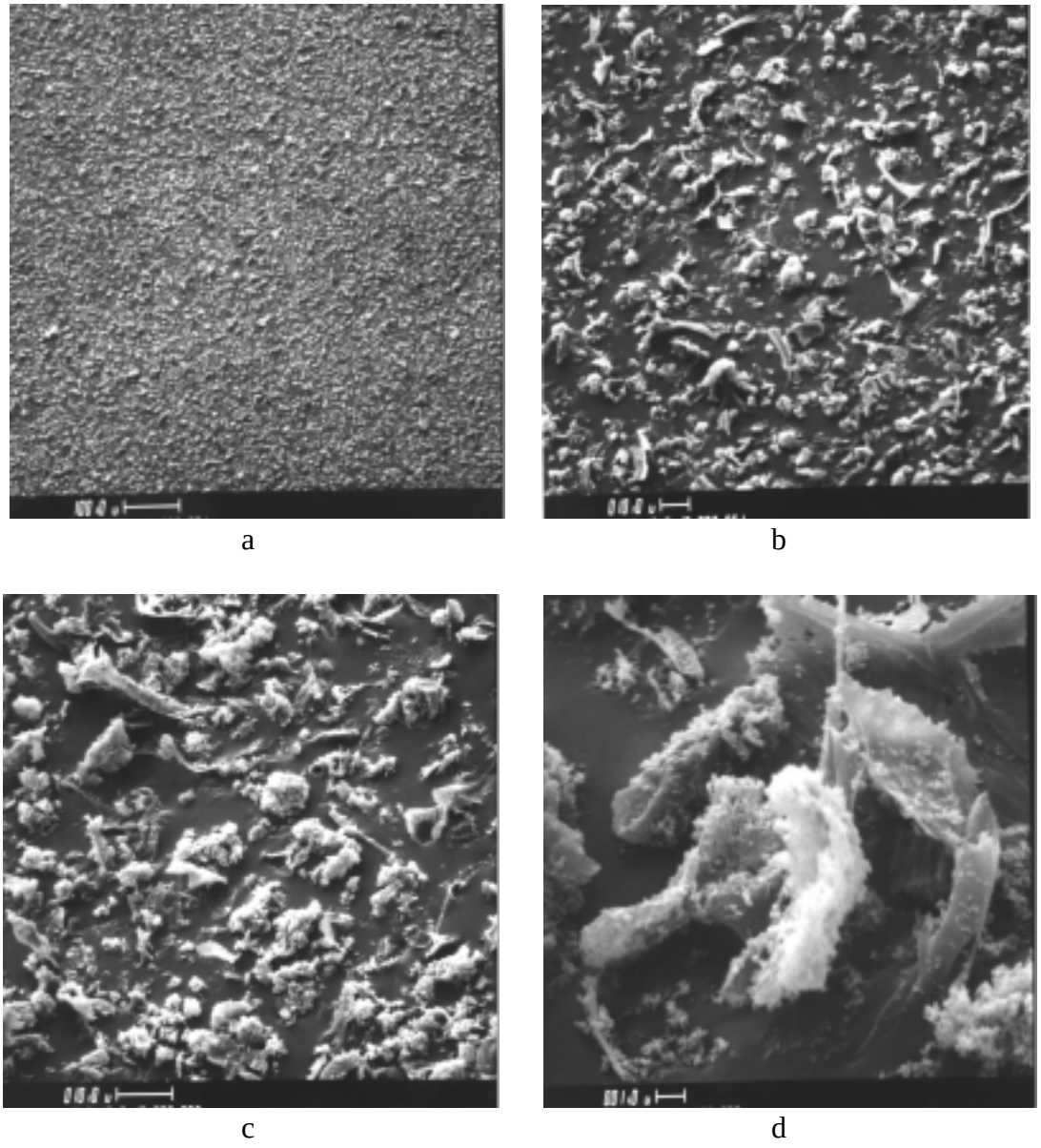

Figure 4-118. Representative scanning electron micrographs of KRW C-121 hopper (4/28/88) gasification char (ID # 2562) taken at a) 100X, b) 500X, c) 1000X, and d) 5000X.

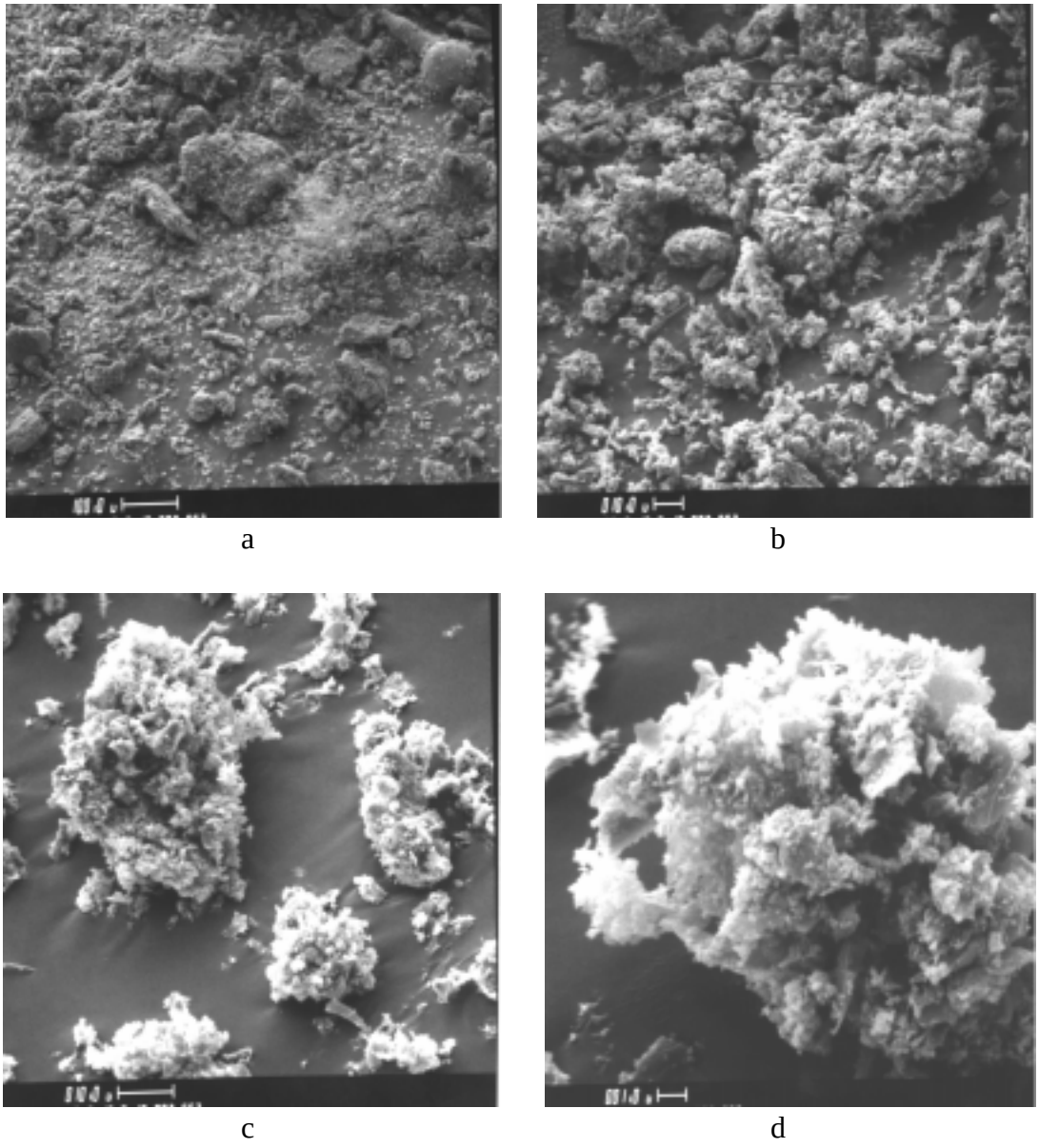

Figure 4-119. Representative scanning electron micrographs of KRW fluidized bed gasification char (ID # 2563) taken at a) 100X, b) 500X, c) 1000X, and d) 5000X. (This sample was collected via extractive sampling, and contained some fibers from the filter substrate.)

In general, the gasification chars analyzed have very high specific surface areas (> 100 m^2/g). Because filtering drag is accumulated as the gas being filtered passes over the surfaces of the particles in the filter cake, high specific surface areas generally correlate with small values of drag-equivalent diameter. (As discussed elsewhere in this report, drag-equivalent diameter incorporates the effects of particle morphology on filtering drag. The effect of the structure of the filter cake on drag is determined by the filter cake porosity. Therefore, filtering drag is a function of the shapes of the particles in the filter cake and the porosity of the cake.)

The relationships between the specific surface area data and drag-equivalent diameters measured for the gasification char samples listed in Table 4-35 are presented in Figure 4-120. (This figure also contains data measured, and presented earlier in this report, for char samples from Piñon Pine, HRL, the DOE/FETC MGCR, and the TRDU.) Process differences apparently cause each group of samples shown in Figure 4-120 to exhibit its own relationship between these two variables. Differences in the way the char particles were generated may have caused the distribution of pore sizes on the surfaces of the particles to differ. Similarly, the proportion of the total surface area that is contained within the char particles would be expected to differ according to the fuels and/or gasification process used. These two differences in the nature of the total surface area of the various char samples affect the correlation between specific surface area and drag-equivalent diameter. The KRW and TRTU samples (from April/May 1991, and also from August 1991) generally show decreasing values of drag-equivalent diameter with increasing values of specific surface area. This trend is not evident in the other groups of samples. The absence of this trend for these other groups of samples may be related to process parameters varied at a given facility, and/or the sampling method and location. In addition to these factors, the BET method for measuring surface area includes any surface area found in the interior of the particles. The vast majority of gas being passed through the simulated filter cake during the determination of drag-equivalent diameter (and flue gas passing through actual filter cakes) flows over the surfaces of the particles and not through them. Therefore the internal surface area measured by the BET method has little, if any, effect on filtering drag. In a similar manner, the BET method includes the surface area contained in very fine pores on the surfaces of the particles. However, gas flowing over the surfaces of the particles does not enter pores whose sizes are on the order of the mean free path of the gas molecules. This effect also causes the BET measurement to be more sensitive to surface area than the permeability measurement used to calculate the drag-equivalent diameter.

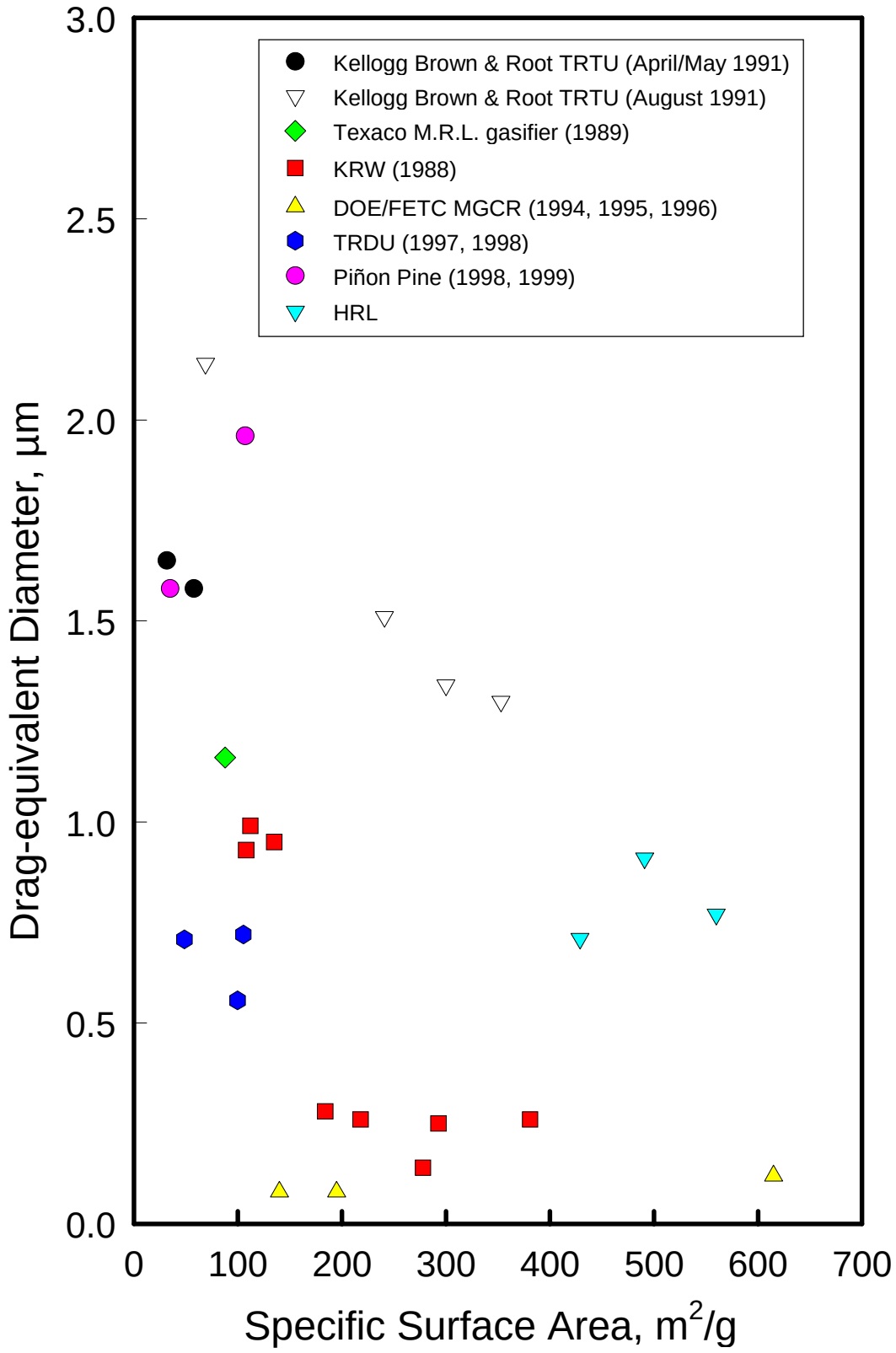

Figure 4-120. Drag-equivalent diameter as a function of specific surface area for char samples from a variety of HGCU installations.

The correlation between the drag-equivalent diameter and the mass median diameter of the same population of char samples plotted in Figure 4-120 is shown in Figure 4-121. Although there is a relatively strong overall correlation between drag-equivalent diameter and mass median diameter, the degree of correlation within each group of samples is much less distinct.

Although specific gas-flow resistance is highly dependent on the assumed filter cake porosity, the values of drag-equivalent diameter of several of these samples indicate that even if filter cake porosities remain high (near the uncompacted porosity value), their specific gas-flow resistances may be detrimentally high. (Of the samples listed in Table 4-35, ID # 2550 demonstrates this effect most strongly.) This circumstance of high specific gas-flow resistance for uncompacted filter cakes may lead to filter cake compaction, with even more serious pressure drop penalties.

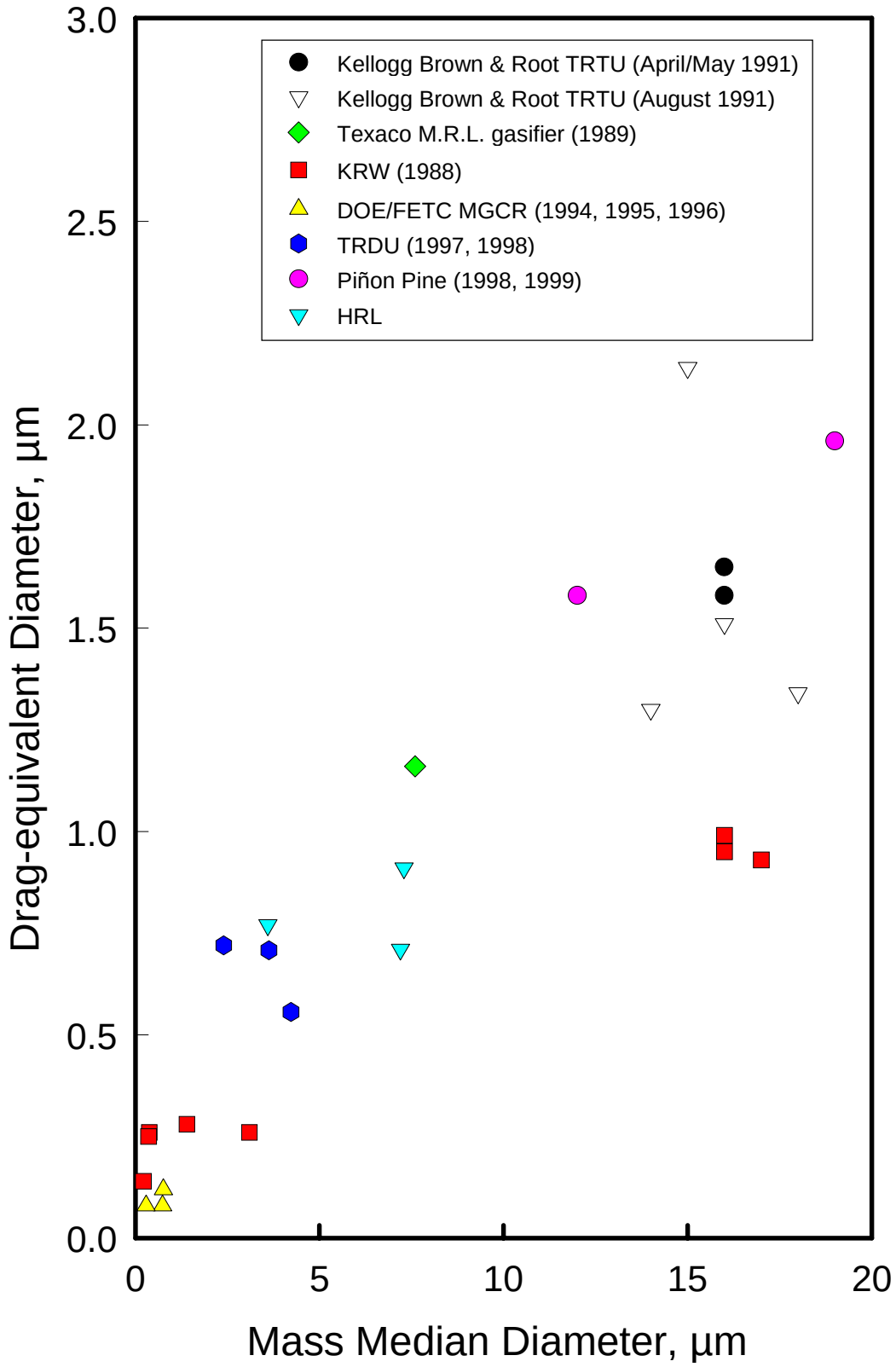

Figure 4-121. Drag-equivalent diameter as a function of mass median diameter for char samples from a variety of HGCU installations.

Like other gasifier residues studied under this task, the most distinctive of the chemical characteristics (shown in Table 4-38) of the two char samples from early gasification tests carried out at Kellogg Brown & Root's Transport Reactor Test Unit were their high values of loss-on-ignition (LOI) resulting from their high carbon content. Like samples from other processes where sorbents are used for sulfur control, the addition of sorbents during the gasification process is reflected in relatively high concentrations of calcium and/or magnesium in the chars. Of the two Kellogg Brown & Root samples described in Table 4-35, ID # 2800 was generated without added limestone, and limestone was added to the process during the generation of ID # 2803. This limestone addition is the source of the elevated Ca content of sample # 2803.

Overall, the observations of particulate samples from these gasification facilities indicate that gasification chars can exhibit extremely low permeabilities which can usually be traced to the presence of a high proportion of ultrafine particles and high specific surface areas. When these char characteristics combine with the potential for filter cake collapse, HGCU filtering pressure drops may become excessively high. Consequently, particle characteristics may make it difficult to maintain a reasonable pressure drop in the filtration of gasification char.

4.9.2 Laboratory Baking of Ash Nodules

A large nodule from sample ID # 4097 (Tidd: October 1994 - BP, AS) was broken into three pieces. The porosity of the first piece was measured with the ethanol-impregnation method. The second piece was baked at 1550 °F for three hours. The third piece was baked at 1550 °F for three days. The porosities of the two baked nodules were also measured with the ethanol-impregnation method. These data are summarized in Table 4-39.

Table 4-39
Effects of Baking Duration at 1550 °F on the Porosity of a Tidd Nodule (ID # 4097; BP, TS)

Duration, hr	Porosity, %
0	81.4
3	83.6
72	86.3

It is not certain what caused this apparent increase in porosity while the samples were being baked. Possibly the absorption and/or loss of water may account for these differences. Loose, sifted ash placed in the oven with these nodules consolidated slightly after 72 hours at 1550 °F during this trial.

Ash bridging in high temperature filters collecting PFBC ashes has been linked to the formation in the filter vessels of ash nodules with high inherent strength. Nodules with this characteristic have been collected from several PFBC filters, including Tidd (where ash bridging has been well documented), and Karhula. To determine whether nodule formation could be simulated in the laboratory, two experiments were performed to see if baking uncompacted beds of Tidd and Karhula ashes at 1600 °F could induce the beds to consolidate

and strengthen. For each of the four samples evaluated in the first test, two uncompacted beds of sifted ash were placed in a laboratory muffle furnace. The first of these two sample beds was prepared by simply sifting (through a 60-mesh screen) the ash into an open ceramic cup and scraping off the excess ash so that any change in the volume of the ash in the cup could be easily determined. The second sample bed was prepared in the same manner, except that the ash was thoroughly ground with a mortar and pestle before being sifted into the open cup. This grinding was intended to break apart as many of the particle-to-particle bonds as possible before exposing the sample to the 1600 °F environment in the muffle furnace. The samples used for this first experiment were ID #'s 4088, 4143, 4067, and 4182.

After each of the samples was sifted and loaded into an open cup, the cups were baked at 1600 °F for 72 hours. The Tidd ashes consolidated slightly (about 3 % loss in volume for a filter cake ash and about 10 % loss in volume for ash from the tubesheet deposit). The Karhula ashes did not measurably decrease in volume. The ashes were then baked for an additional 168 hours, but no additional losses in volume were observed for any of the samples. In each case, the samples ground with the mortar and pestle behaved just like the unground ash samples.

A second set of baking experiments was performed to more carefully control and monitor the water content of the samples throughout the baking process. Two Tidd ash samples (ID # 4049 and ID # 4088) were sifted into open cups. After their porosities were determined, they were dried for about 5 hours at 500 °F. After baking, some shrinkage was noted for sample # 4088; however, the loss in overall sample volume roughly corresponded to the loss in weight the samples experienced during baking at 500 °F. In other words, sample # 4088 decreased in volume, but its porosity remained essentially unchanged. The baking process was then continued by exposing the samples to 1600 °F for one week. Both samples lost weight and volume (about a 27 % decrease for the tubesheet deposit ash, and a 17 % decrease for the hopper ash). As was observed after baking at 500 °F, the loss in volume for these samples roughly corresponded to their loss in weight.

4.9.3 Additive Conditioning Tests

Tests were performed to determine if small amounts of powders with very fine size distributions could be used to condition PFBC ashes or gasifier chars. For some powders, it has been demonstrated that the addition of less than 5 % by weight of very fine particles to the powder can cause the relatively large powder particles to become coated with a layer of the fine conditioning particles.[17] Fine conditioning particles present on the surfaces of the particles cause these larger particles to be farther apart from each other, decreasing the van der Waals attraction between them. If a layer of fine particles could be effectively deposited on the surface of highly cohesive PFBC ashes or gasifier chars, these samples might become more free-flowing. This would tend to make them easier to remove from the filter vessel.

Tidd APF hopper ash (ID # 4049) and DOE/FETC MGCR hopper char (ID # 4170) were mixed with two additives (activated carbon and fumed silica). The activated carbon powder tested is a lignite-based commercial product known by the trade name Darco FGD, and was manufactured by Norit Americas, Inc. The amorphous fumed silica used in these tests was manufactured by the Cabot Corporation, and goes by the trade name Cab-O-Sil grade EH-5.

The basic properties of these additives are summarized in Table 4-40. To prepare the mixtures for testing, small amounts of additive were added to a container of each of these two samples, and the container was shaken thoroughly for two minutes. Mixtures were produced with 2.0 and 5.0 % by weight of additive. The results of the uncompacted bulk porosity (UBP) and tensile strength tests performed on these mixtures are presented in Table 4-41. (Measurements of uncompacted bulk porosity and tensile strength indicate relative cohesivity, but they do not provide a direct measurement of ash cohesivity.)

Table 4-40
Characteristics of Additives Used to Condition HGCU Hopper Ashes

quantity	fumed silica	activated carbon
specific surface area, m^2/g	380*	395
uncompacted bulk porosity, %	--	86.8
Stokes' MMD, μm	0.007**	19
drag-equivalent diameter, μm	--	0.588
specific gas flow resistance, in $H_2O \cdot min \cdot ft/lb$	--	15
tensile strength, N/m^2	--	4.5
true particle density, g/cm^3	2.2	2.06

* value reported by Cabot Corporation

** value reported by Cabot Corporation (calculated from specific surface area data assuming monodisperse, smooth, spherical particles)

Table 4-41
Uncompacted Bulk Porosities of Mixtures of Hopper Samples and Conditioning Additives

Source hopper sample	additive	% wt. additive	UBP, %	tensile strength, N/m^2
DOE/FETC (ID # 4170)	none	0.0	97.0	0.2
DOE/FETC (ID # 4170)	fumed silica	2.0	97.3	0.1
DOE/FETC (ID # 4170)	fumed silica	5.0	97.4	0.3
DOE/FETC (ID # 4170)	activated carbon	2.0	97.6	0.3
DOE/FETC (ID # 4170)	activated carbon	5.0	96.9	0.4
Tidd APF (ID # 4049)	none	0.0	89.6	5.1
Tidd APF (ID # 4049)	fumed silica	2.0	88.4	4.9
Tidd APF (ID # 4049)	fumed silica	5.0	90.1	3.4
Tidd APF (ID # 4049)	activated carbon	2.0	89.0	8.0
Tidd APF (ID # 4049)	activated carbon	5.0	87.3	9.0

The results shown in Table 4-41 indicate that the only significant effect of these conditioning agents was a small change in the case of the Tidd hopper ash (ID # 4049) mixed with activated carbon. In fact, the modifications in uncompacted bulk porosity and in tensile strength indicate opposite trends. As the amount of activated carbon added to the sample is increased, the uncompacted bulk porosity decreases slightly, which indicates a decrease in

cohesivity. The measured tensile strength data contradicts this trend. In general, the uncompacted bulk porosity is a more reliable indicator of trends in cohesivity than the measured tensile strength because of effects related to sample preparation. Similarly, the addition of fumed silica to the Tidd hopper ash (ID # 4049) and the DOE/FETC gasification char (ID # 4170) resulted in somewhat different values of tensile strength; however, these differences can probably be attributed to uncertainties in the measurement procedure.

The small change in the cohesivity of the Tidd APF hopper ash (ID # 4049) with the addition of activated carbon is attributed to a lubricating effect by which the additive interferes with the cohesive forces among the particles. It is believed that the fumed silica had virtually no effect because its size is so small in comparison with irregularities in the surfaces of the ash and char particles.

The effectiveness of this type of conditioning may be limited by the proportion of submicron particles already present in the ash to be conditioned. Conditioning may also be limited by the basic morphology of the particles in the ash to be conditioned. Either the presence of a large proportion of submicron particles or rough, irregular particle surfaces may serve to separate the primary ash particles prior to the addition of any conditioning agent. The results obtained in these experiments indicate that, depending on the specific characteristics of the ash and the additive, it may be possible to use small amounts of a conditioning powder to reduce the apparent cohesivity of the ash. However, the results reported above do not indicate that the use of such additives are likely to be highly effective or economical in HGCU processes.

4.9.4 Ash Compaction Tests

As was done for DOE/MGCR sample # 4170 (Figure 4-48), measurements were made of the response of KRW hopper char (ID # 2562) and Tidd APF hopper ash (ID # 4049) to compacting forces. The compaction data, which were measured at room temperature for these two samples, are presented in Figures 4-122 and 4-123. These data were obtained with a compaction device marketed by Jenike and Johansen Inc. The test procedure involves filling an open-topped cylinder with uncompacted sample and then gradually applying load to the top surface of the sample by adding weights to a circular plate placed on top of the sample. The circular plate acts as a loose fitting piston to transfer the applied load directly to the sample. A depth gauge is used to measure the height of the sample as it decreases with increasing applied load. The data in Figure 4-122 show that a filtering pressure drop of 3.4 psi (94 in. H_2O) may be sufficient to reduce the porosity of a filter cake formed from the KRW hopper char (ID # 2562) from around 93 % to a porosity of about 86 %. (This change is equivalent to compacting the filter cake into half its original thickness.) This data demonstrate the detrimental decrease in porosity that might be expected if gasification char filter cakes are subjected to significant pressure drops. Any reduction in filter cake porosity would cause a significant increase in specific gas flow resistance.

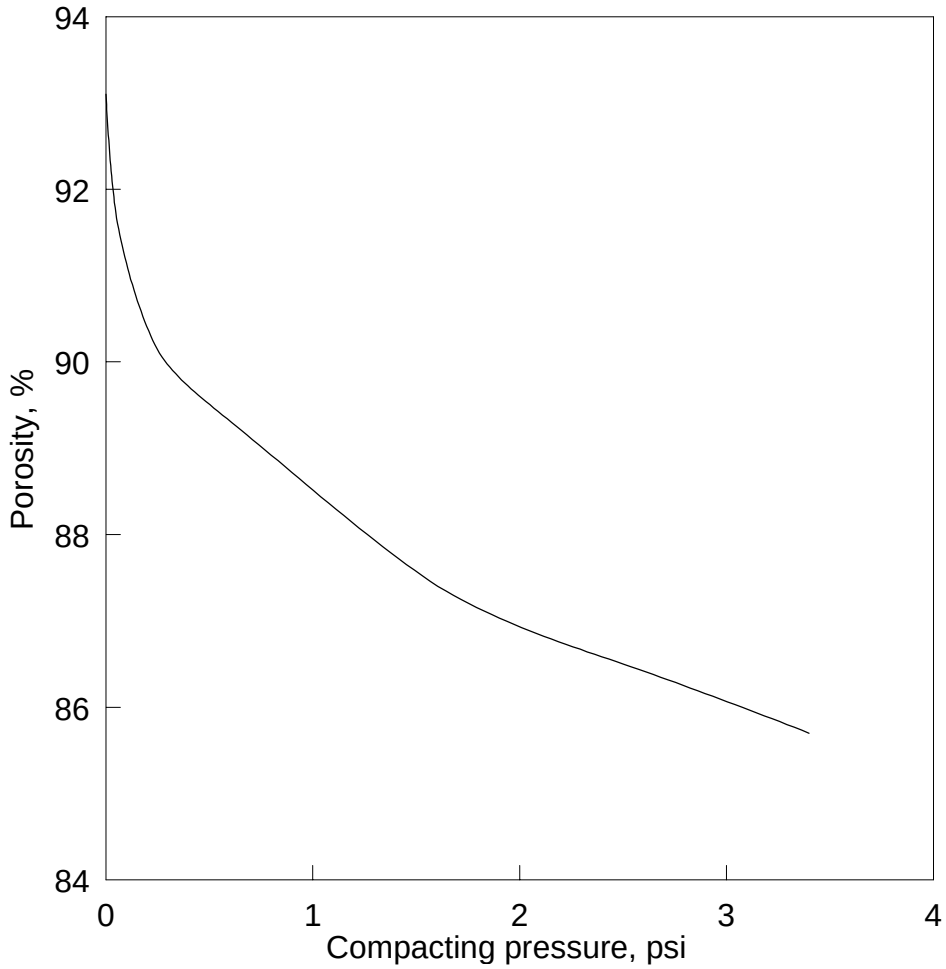

Figure 4-122. Data measured for KRW gasification hopper char (ID # 2562) showing the dependence of porosity on mechanical pressure applied across the sample.

Figure 4-123 presents the effects of compacting pressure on samples of Tidd APF hopper ash (ID # 4049) prepared in two different ways. In the first trial, unsifted ash was loaded into the sample cup used in these tests as gently as could be accomplished with a small spoon. This procedure resulted in a porosity of about 85 % for the ash in the cup. In the second trial, the ash was sifted into the cup as is done in measurements of uncompacted bulk porosity. This technique resulted in the ash filling the sample cup with a porosity of around 89 %. Although these two loading methods generated different initial conditions for the compaction tests, the porosities of the two samples converged as the compacting forces increased. These data support the contention that filter cakes and passively deposited ash that are originally deposited in HGCU filters are fragile and susceptible to compacting forces. Regardless of the procedure used to load the ash into the sample cup, the data in Figure 4-123 indicate that filtering pressure drop can be expected to exert a strong compacting force on PFBC filter cakes.

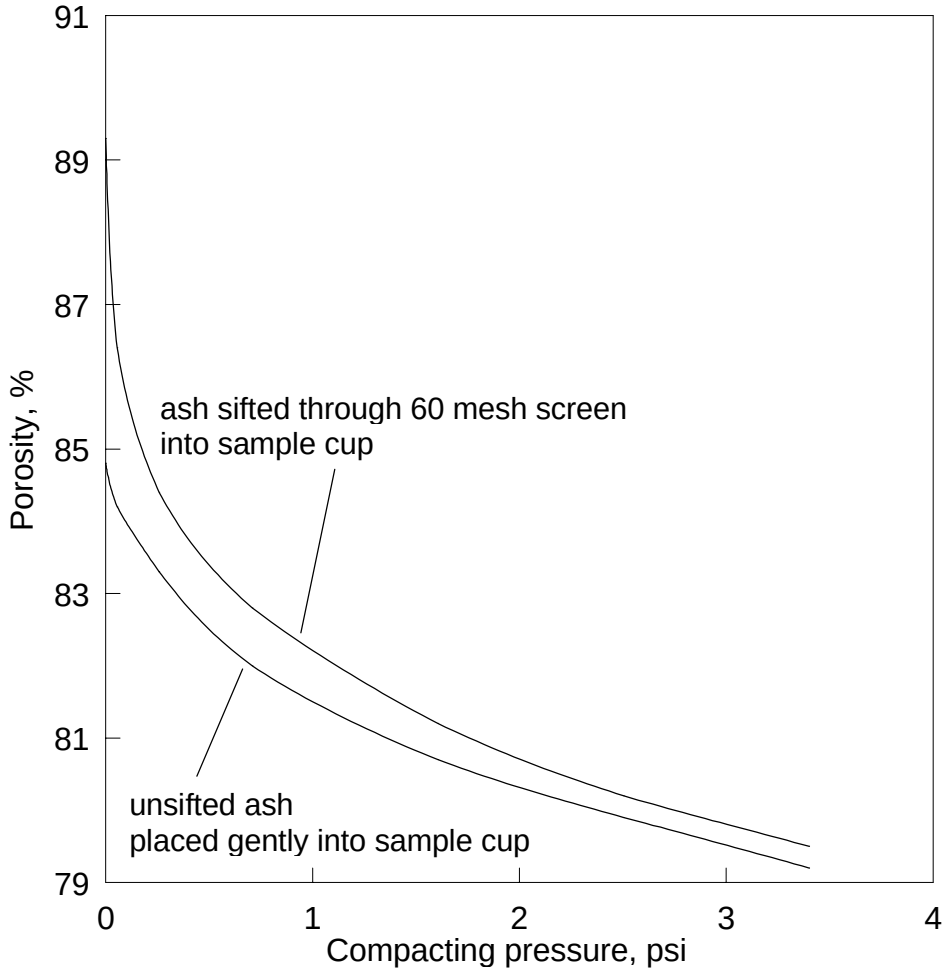

Figure 4-123. Data measured for the Tidd APF hopper ash (ID # 4049) showing the dependence of cake porosity on mechanical pressure applied across the cake. The procedures used to load the sample container caused initial differences in the porosity of the sample prior to compaction. As compacting pressure increased, the differences in porosity due to the different loading procedures diminish.

5.0 MODELING PARTICULATE BEHAVIOR

Laboratory analyses and mathematical models provide a variety of useful information to assess particulate characteristics and HGCU filter performance. The following discussions cover a range of topics studied under this task. The first four of these topics are related to the measurement of permeability in the laboratory. Specific issues related to permeability that have been addressed include the effect of irregular particle morphology on the empirical model used in the laboratory, the effect of non-uniform porosity of the sample in the permeability cell, relating values measured in the laboratory to environmental conditions in HGCU vessels, and the applicability of permeability data measured at ambient pressure to filter cake behavior in the filter (at pressures of 10 to 15 bar). The next two topics concern the reproducibility and techniques used for some of the laboratory analyses. A discussion is also presented which describes a method for estimating the non-filtering collection (inertial impaction and gravitational settling) in a HGCU filter vessel. Another discussion describes some of the mechanisms thought to lead to consolidation and bridging of PFBC ash deposits. The last discussion presents some extrapolations based on the measured characteristics of char collected in the DOE/FETC MGCR.

5.1 EMPIRICAL PERMEABILITY MODEL

The mathematical permeability model Southern Research Institute developed in 1986 was based almost exclusively on empirical data measured for pulverized-coal ashes.[7] One ash produced by atmospheric fluidized-bed combustion was also included in this modeling. This model, which relates the characteristic gas flow resistance of a porous bed of ash particles with the porosity of the bed, was based on the work of Kozeny[3], Carman[4], Langmuir[5], and Davies[6].

This model was used in the analyses of bulk samples of HGCU ashes and chars to estimate the characteristic gas flow resistance of filter cakes formed from the sample being analyzed. Two key parameters determine this characteristic flow resistance: porosity and particle diameter. However, during the development of the model, it was found that simple measurements of physical diameter obtained with various laboratory devices (Coulter Counter, Bahco Classifier, or Shimadzu centrifugally-augmented sedigraph) do not correlate well enough with measured permeability data to accurately predict gas-flow resistance. Therefore, empirical permeability data were used to define the drag-equivalent diameter, a value calculated for each sample tested, which accurately ranks the gas flow resistance of different samples at equal filter cake porosities.[18]

As the data bank of HGCU samples expanded, it was found that the permeability data measured for these samples comprising small, irregular particles was not satisfactorily fit by the model developed in 1986 primarily for larger, spherical particles. In almost every case, the 1986 model would tend to overestimate the gas-flow resistance values of uncompacted filter cakes. To correct these estimates, permeability data measured for 34 samples composed of small, irregular particles were used to develop an adjusted permeability model. Most of these 34 samples were generated at HGCU facilities. The adjusted model, which is presented in equations (5) and (6) below, was also presented as equations (1) and (2) in the section *Laboratory Methods Used to Characterize Samples*.

$$R = \Delta p/(UW) \quad (5)$$

$$R = 10^8 \cdot (\mu/D^2) \cdot (1/\rho) \cdot [111-211\varepsilon+100\varepsilon^2]^2 \quad (6)$$

where: R = specific gas-flow resistance of the porous bed, μbar·sec·cm/g
Δp = pressure drop across the porous bed, μbar
U = face velocity of the gas through the sample in the test cell, cm/s
W = areal mass loading of the sample in the test cell, g/cm^2
μ = gas viscosity, poise
D = drag-equivalent diameter of the sample, μm
ρ = average true density of the sample particles, g/cm^3
ε = porosity of the sample in the test cell, dimensionless ($0 < \varepsilon < 1$).

When this equation is converted to the English units commonly used in filtration, R is expressed in units of in H_2O·min·ft/lb.

This adjusted form of the permeability model was then used to recalculate the drag-equivalent diameters and relative gas flow resistances of all of the HGCU samples for which permeability had been measured. These recalculated values are the ones included in this report and entered in the HGCU data bank.

5.2 EFFECT OF NON-UNIFORM DUST CAKE POROSITY ON GAS FLOW

In measuring the permeability of a sample of dust it is sometimes tacitly assumed that the sample is reasonably homogeneous. To evaluate the effects of an inhomogeneous spatial distribution of porosity in a test apparatus, some simple, but relatively extreme cases can be examined by calculation. In the following discussion gas flow resistance is compared in three cases (see Figure 5-1). Common among the three cases are the total mass of the sample, and its total volume. Also, the total cross-sectional area A and the total thickness H are held the same for all three cases. In the first example the sample is a single homogeneous disc, as might be used in a permeability cell. In each of the other two examples the dust is divided into three domains of different porosity. In one, the domains are arranged such that the gas flows through the three separately (in parallel), and in the other, the gas passes sequentially through three layers (in series).

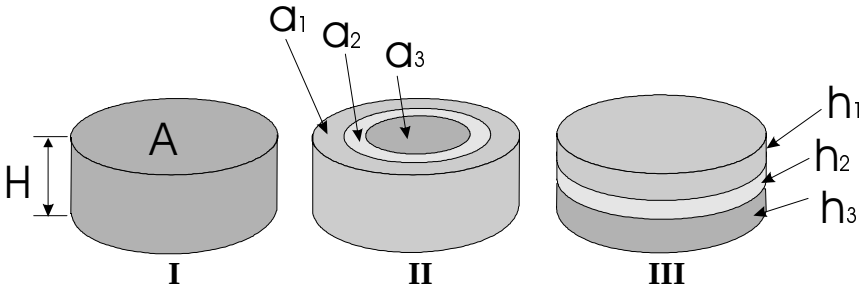

Figure 5-1. Configurations for dust samples.

The first sample is a straightforward application of gas flow through a uniform, homogeneous dust layer of thickness H. The cross-sectional area A is bounded at the cylindrical surface, so

that the gas flow is all along a direction normal to the surface A. This condition is similar to that of a sample in a cylindrical permeability cell. The normalized gas-flow resistance R is the ratio of the pressure drop p to the gas volume flow rate per unit area q/a for unit dust cake loading λ =m/A (mass per unit area of dust cake).

$$R = \left[\frac{p}{q/A}\right]\frac{1}{\lambda} \tag{7}$$

Given porosity ε and particle density ρ, the mass is simply $m = \rho AH(1-\varepsilon)$, and $\lambda = \rho H(1-\varepsilon)$, and

$$R = \frac{Ap}{q\rho H(1-\varepsilon)} \tag{8}$$

Defining r_h, the resistance of a specific homogeneous sample, as the ratio of pressure drop to total gas volume flow rate gives

$$r_h = \frac{p}{q} \tag{9}$$

$$= \frac{RH}{A}\rho(1-\varepsilon) \tag{10}$$

In the second sample, there are three parallel regions. The flow rate through each region is q_i (i =1,2,3) the gas flow resistance for each is r_i, and the cross-sectional area of each is a_i. Since the pressure drop P across the cell must be the same for all parts of the cell, then $P = q_i r_i$. The total gas flow Q must be the sum of the q_i, so

$$Q = \sum_i \frac{p_i}{r_i} \tag{11}$$

$$= \frac{P}{H\rho}\sum_i \frac{a_i}{R_i(1-\varepsilon_i)} \tag{12}$$

The gas flow resistance r_p for the sample is the ratio of P to Q, which results in

$$r_p = \left[\frac{1}{H\rho}\sum_i \frac{a_i}{R_i(1-\varepsilon_i)}\right]^{-1} \tag{13}$$

In the third sample, the flow rate through all three layers must be the same ($Q = q_i$), but the pressure drop p_i across each is defined by $p_i = Q r_i$. The total pressure drop is the sum of the p_i, so

$$P = Q\sum_i r_i \tag{14}$$

and r_s is simply

$$r_s = \frac{1}{A}\sum_i h_i r_i \rho(1-\varepsilon_i) \tag{15}$$

Example:

In the following simple illustration, only three different regions are used for cases two and three. For consistency, the overall porosity and the overall dimensions are required to be the same for all three cases. A porosity $\varepsilon = 85\%$ yields $R = 4.43$ for the homogeneous case, as noted above. The following values agree with this condition.

Table 5-1
Assumed Distributions of Volume, Mass, and Porosity
for Series and Parallel Examples (Configurations II and III in Figure 5-1)

i	v_i	ε_i, %	m_i	R_i	a_i	h_i
1	0.25V	82	0.30M	7.94	0.25A	0.25H
2	0.50V	85	0.50M	4.43	0.50A	0.50H
3	0.25V	88	0.20M	2.22	0.25A	0.25H

In this table, v_i is the volume of the i^{th} region in terms of the total volume V, and m_i is the mass of the i^{th} region in terms of the total mass M.

Based on these distributions of volume and mass (and consequently, porosity), the relative values of normalized flow resistance in these three cases can be calculated and expressed as:

$$r_h = 0.665\frac{H\rho}{A}, \tag{16}$$

$$r_s = 0.756\frac{H\rho}{A} \tag{17}$$

and

$$r_p = 0.536\frac{H\rho}{A}. \tag{18}$$

The relative values of normalized flow resistance in these three cases can also be expressed as:

$$r_s = 1.14 r_h \tag{19}$$

and

$$r_p = 0.81 r_h. \tag{20}$$

Therefore, these calculations demonstrate that even in the two extremely non-uniform cases described above, the overall effect of non-uniformity of porosity in the permeability cell is not too severe. The series-type non-uniformities would tend to overestimate the flow resistance of a uniform sample by a factor of 1.14, while the parallel path-type uniformities would tend to underestimate the flow resistance of a uniform sample by a factor of 0.81. In fact, because the types of non-uniformities that would most likely be encountered in a prepared sample in the cell would combine parallel and series path effects, these effects would tend to mitigate each other, and the overall value measured would probably quite closely approximate the flow resistance of a uniform sample. Additionally, because every effort is made to load the permeability cell uniformly in preparation for the laboratory measurement, the poor distribution of porosity assumed for the series and parallel-path cases probably represent worst-case boundaries for the technique.

5.3 TRANSLATING LABORATORY PERMEABILITY DATA TO HGCU CONDITIONS

Measuring the permeability of simulated filter cakes formed from HGCU samples was a key component of the characterizations conducted under this task. These permeability measurements were used to estimate or rank the on-line filtering pressure drop associated with actual filter cakes formed from these samples. To generate reliable estimates from the laboratory measurements, it is crucial that the key characteristics of the filter cake and flue gas as they exist during high temperature filtration are accurately known.

The permeability of filter cakes depends in part on the morphology of the filter cake (expressed by the drag-equivalent diameter and the porosity of the cake). The amount (areal loading) of filter cake and the true density of the filter cake particles also influence the overall pressure drop associated with a given cake. The other factors that determine the pressure drop (face velocity and gas viscosity) are dependent on the characteristics of the flue gas. Laboratory measurements of bulk permeability and the porosity of filter cakes removed from HGCU filters in combination with SEM observations of actual HGCU filter cakes have allowed the morphology of these cakes to be accurately characterized. Assessments of areal loading must be performed on site. True particle density has been accurately determined in the laboratory for many ash samples obtained from HGCU filters and is essentially unchanged at HGCU flue gas conditions. Face velocity and flue gas viscosity are significantly different in HGCU filters than in the laboratory. However, the overall effect of increased temperature and pressure can be accurately estimated based on filtration theory and basic theories of fluid dynamics.

Because the morphology of the filter cakes in operating HGCU filters has been accurately characterized, translating laboratory permeability data (acquired at ambient temperature and pressure) to HGCU operating conditions is relatively simple. The increased temperature and increased pressure in the HGCU filter vessel cause changes in gas volume and gas viscosity. In turn, these two factors affect the filtering pressure drop. Based on the conditions included in Table 5-2, equation 19 demonstrates the translation from laboratory to HGCU conditions for a typical HGCU facility operating at 10 atmospheres and 1600 °F (1144 °K).

Table 5-2
Comparison of Laboratory Conditions with Typical HGCU Filter Conditions

condition	Laboratory	Typical HGCU	effect on pressure drop
temperature, °K	295	1144	increase by a factor of 3.88
gas viscosity, poise	184	456 *	increase by a factor of 2.48
pressure , Atm	1.0	10	decrease by a factor of 0.1

* These calculations use the values associated with air to approximate flue gas.

$$\Delta p(\text{HGCU conditions}) = \Delta p(\text{laboratory conditions}) \text{ X } 3.88 \text{ X } 2.48 \text{ X } 0.1 \qquad (21)$$

Coincidentally, these multiplicative factors combine to an overall factor of approximately 1.0. Therefore, when the permeability of a simulated filter cake is measured at laboratory

conditions, the values obtained applies directly to filter cakes in operating HGCU filters at the baseline conditions specified above (10 atmospheres and 1600 °F).

5.4 PERMEABILITY AS A FUNCTION OF GAS PRESSURE

The ultimate value of a laboratory determination of the specific gas-flow resistance of a sample is in estimation of, or comparison to, operating data from high-temperature, high-pressure HGCU filters. The gas laws governing the actual volume of a gas as a function of temperature and/or pressure are well established. However, most of the filtration theories describing the pressure losses generated as a known actual volume of gas passes through a porous bed are at least partly derived from empirical data, which is usually obtained from ambient pressure and ambient temperature measurements. Because the conditions in HGCU filters differ significantly from ambient conditions, an experiment was designed to verify the effect of absolute gas pressure on the permeability of a particulate sample. (A similar experiment was conceived to verify the effects of temperature on permeability measurements, but was not carried out under this task.)

To determine whether all changes in the specific gas-flow resistance of a particulate sample measured at two widely different absolute pressures could be entirely explained by differences in actual gas volume, the device shown in Figure 5-2 was constructed. To perform the measurements of specific gas-flow resistance, the permeability cell located in the pressure vessel was loaded with PSDF filter cake ash (ID # 4294). The ash in the cell was thoroughly compacted to prevent cracks from developing in the ash sample. (Cracks can develop in the sample in the permeability cell if the sample is highly porous, and/or if the pressure drop across the sample is too great. If cracks form in the sample, the test must be aborted and the sample reloaded.) To induce flow through the sample, the pressure in the vessel was increased to 24.7 psia. At this vessel pressure, the pressure drops across the ash sample and across the orifice were measured. The vessel pressure was then increased to 164.7 psia. (This was the highest pressure that could be obtained with the gas regulator.) The flow through the sample was adjusted to provide the same pressure loss across the orifice that was observed at an absolute vessel pressure of 24.7 psia. The temperature monitors in the device verified that no corrections for gas volume resulting from temperature differences were necessary. Therefore it was possible to directly compare the ratio of the two absolute vessel pressures with the ratio of the two pressure losses across the ash sample at the two absolute vessel pressures. These two ratios agreed within 6 %. Other runs made with the device yielded similar results. Therefore no significant correction to permeability measurements made at ambient pressures (other than correction for actual gas volume) need to be performed to apply these permeability data to filter cakes in high-pressure environments.

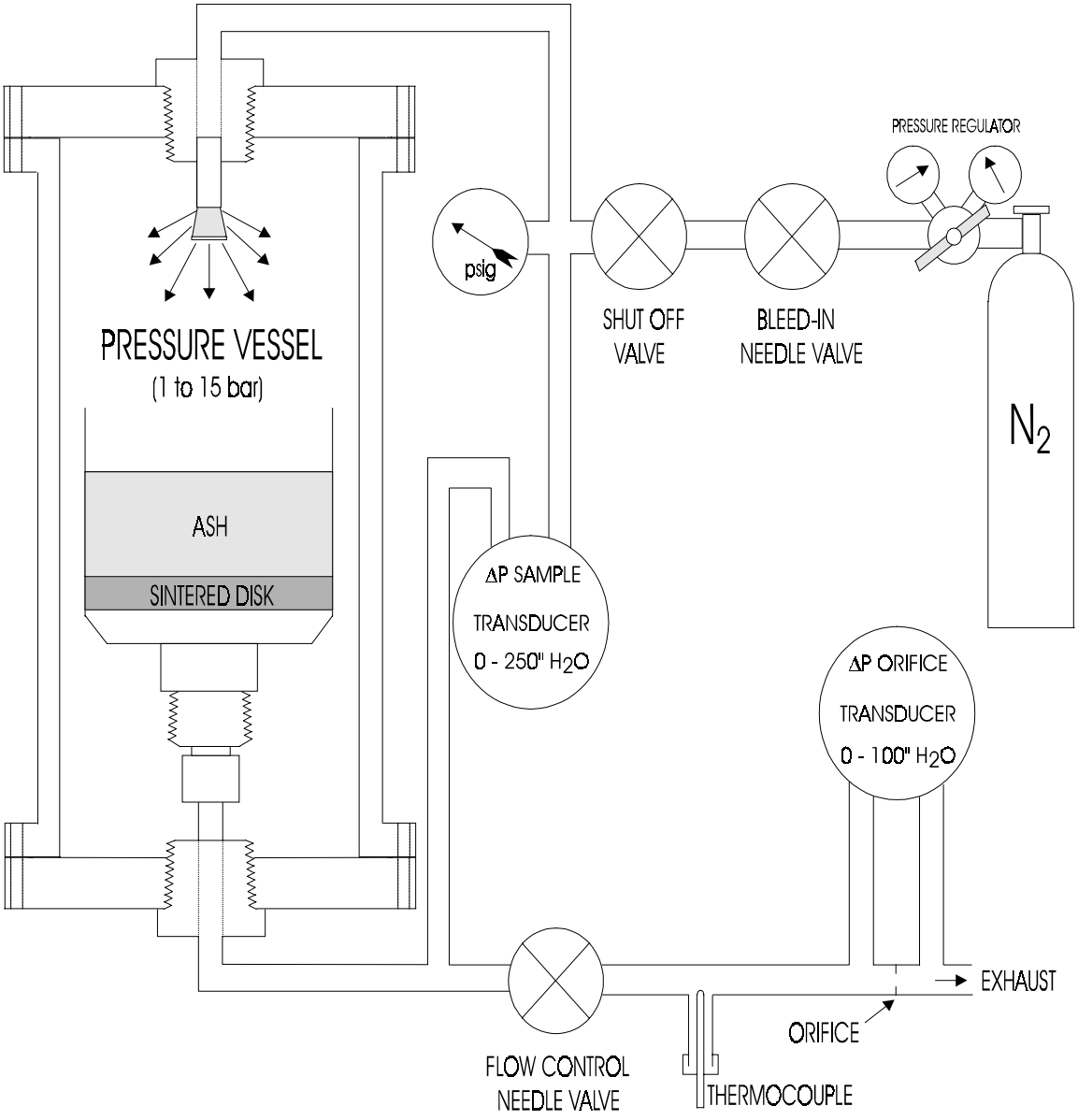

Figure 5-2. Schematic diagram of a setup for evaluating the effect of absolute gas pressure on the specific gas-flow resistance of a particulate sample.

5.5 REPRODUCIBILITY OF MEASUREMENTS

5.5.1 Specific Gas-Flow Resistance

The method used to obtain the permeability of an ash sample in the laboratory is described in section *4.0 Laboratory Methods Used to Characterize Samples*. Using this method, replicate measurements were performed on one of the PSDF filter cake ashes (ID # 4294) obtained on January 20, 1998 (see the discussion of analyses of PSDF ash samples for more descriptions of this sample). The results of four repetitions of the measurement of specific gas-flow resistance are summarized in Table 5-3. The quantity $1/D^2$ is calculated and shown for each test because this is the value that enters directly into equation 2 for the calculation of specific gas-flow resistance.

Table 5-3
Specific Gas-Flow Resistance Measurements of PSDF Filter Cake Ash (ID # 4294)

test point #	porosity, %	D, µm	$1/D^2$
1	77.4	2.155	--
1	70.9	2.348	--
1	67.6	2.376	--
point #1 average	--	2.293	0.1902
2	77.8	2.271	--
2	72.2	2.363	--
2	67.6	2.409	--
point #2 average	--	2.348	0.1814
3	76.4	2.237	--
3	69.9	2.353	--
3	67.9	2.338	--
point #3 average	--	2.309	0.1876
4	76.4	2.182	--
4	72.2	2.340	--
4	67.8	2.374	--
point #4 average	--	2.299	0.1892
overall average	--	2.312	0.1871

The data shown in this table indicate that the laboratory technique used for the measurement of specific gas-flow resistance provides consistent values of drag-equivalent diameter.

5.5.2 Uncompacted Bulk Porosity

Four replicate measurements of uncompacted bulk porosity were also performed on sample ID # 4294. These measurements are summarized in Table 5-4.

Table 5-4
Uncompacted Bulk Porosity Measurements of PSDF Filter Cake Ash (ID # 4294)

trial #	UBP, % (60-mesh screen)
1	83.6
2	83.6
3	83.9
4	85.0
average	84.1

These data indicate, that as with the measurements of specific gas-flow resistance, the technique for determination of uncompacted bulk porosity yields reproducible values. (The influence of mesh size on uncompacted bulk porosity is discussed below.)

5.6 EFFECT OF SCREEN MESH SIZE ON UNCOMPACTED BULK POROSITY

The uncompacted bulk porosity of a sample is one of the estimates that has been used in this task to estimate filter cake porosity when no direct measurements on existing filter cakes can be made. Although there is some evidence to suggest that uncompacted bulk porosity may overestimate filter cake porosity, it is useful for ranking sample cohesivity, and may be a component of any eventual model for estimating filter cake porosity from the range of bulk sample characteristics that can be measured in the laboratory. The technique that is currently used for measuring uncompacted bulk porosity has been described earlier in this report, and uses a 60-mesh screen (250 µm opening) to break up large agglomerates and establish uniformity of the sample. However, it is reasonably certain that many relatively large agglomerates still exist in the sample after it has passed through the 60-mesh screen. Therefore two measurements of uncompacted bulk porosity of sample # 4294 were made using a 325-mesh screen with openings of 45 µm. These measurements are summarized in Table 5-5. Although these smaller openings still allow agglomerates of particles to pass through, the overall porosity of the sample deposited in the wide, short, open-topped cylinder was expected to depend on the size of the screen openings.

Table 5-5
Uncompacted Bulk Porosity Measurements of PSDF Filter Cake Ash (ID # 4294)

trial #	UBP, % (325-mesh screen)
1	87.5
2	87.8
average	87.6

The data in Table 5-5 demonstrate that using the 325 mesh screen generated consistent results; however, the average value of uncompacted bulk porosity measured (87.6%) was significantly greater than the average value determined using the 60 mesh screen (84.1%).

5.7 ESTIMATING FILTER VESSEL INERTIAL COLLECTION FROM SIZE DISTRIBUTION DATA

In most filter applications, particles entering the filter vessel are apparently segregated based on their physical characteristics. If the coarser entrained particles are large enough, they will impact on nearby surfaces as the flue gas changes direction in the filter vessel. This may result in deposits on the outer wall or shroud surrounding the tubesheet and filter elements. As the gas entering the vessel slows in the vicinity of the filter elements to the filtering face velocity, previously entrained particles with higher settling velocities will tend to divert from the flow paths of the flue gas. Instead of continuing to be entrained in the flue gas, their trajectories can become governed by the force of gravity, causing them to settle into the hopper without ever reaching the filter cake. Finer particles with low enough settling velocities will continue to be entrained in the gas until they impact and are retained on the surface of the filter cake. The same mechanism of selective continued entrainment would also apply to particles ejected from the filter cake during cleaning pulses. Individual particles, or agglomerates of particles with small enough settling velocities will reentrain in the flue gas and be recollected on the filter cake. Particles and agglomerates of particles with sufficiently high settling velocities ejected from the surface of the filter element will permanently leave the filter cake and settle into the hopper.

The degree to which particulate matter collected in a HGCU hopper contains large particles not found in the corresponding filter cakes can be inferred from finely-resolved size distribution data measured for corresponding hopper and filter cake samples collected in the vessel. The basis of this approach is the assumption that the finest portion of the size distribution of the filter cake sample should match (in terms of the shape of the differential size distribution) the corresponding portion of the measured size distribution of the sample collected from the HGCU hopper. For the purposes of this estimation, the hopper sample is assumed to be well-mixed and representative of particles collected in the hopper over several filtration cycles. In a single filtration cycle, particles are collected in the hopper by passive dropout while the flue gas is being filtered, and by the capture of particles or agglomerates ejected from the filter cakes immediately following cleaning pulses. (These distinct mechanisms may cause samples taken from the particulate disposal system to have different characteristics depending only on the time within the filter cycle that the samples were deposited in the hopper.)

The size distribution data used in this analysis were obtained with a Leeds and Northrup Microtrac X-100 particle sizing device. During the preparation of particulate samples for the measurement of size distribution with this device, a small portion of the sample is suspended in a clear fluid (usually isopropyl alcohol), and submitted to ultrasonic agitation for several minutes. This procedure is intended to break up any agglomerates of particles that may have formed either during the collection process (on surfaces in the filter vessel), or during the storage of the samples prior to their analysis. Provided this agitation successfully breaks up all these agglomerates in the samples, the measured size distributions of the filter cake samples should represent the size distribution of the entrained particles when they reached the surface of the filter cake, and the measured size distribution of the hopper sample should be representative of the size distribution of the entrained particles entering the filter vessel.

In this discussion, char samples from run P051 at the TRDU are used to demonstrate how size distribution data can be used to estimate non-filtering collection in HGCU filter vessels. The measured size distributions of the char sample obtained from the filter cake (ID # 4325) and the hopper (ID # 4324) are both shown in Figure 5-3. The differential size distribution data measured for the filter cake char have been scaled down by a factor of 0.673 to match the magnitude of the corresponding differential size distribution data measured for the hopper char. (This scaling is adjusted to match, to as large an extent as possible, the shapes of these differential size distributions for the smallest particles represented in these distributions.) After this scaling has been applied, the two distributions coincide well up to a particle size just over 1 µm (Figure 5-3). Particles found in the TRDU hopper but not found in the filter cake char can be observed in the size distribution data shown in Figure 5-4. The calculated size distribution of the particles assumed to have settled prior to reaching the filter surface shown in this figure is obtained by subtracting the scaled-down differential size distribution data measured for the filter cake material from the differential size distribution data measured for the material collected in the hopper. (No scales are presented for the ordinate axes in the differential size distribution plots shown in Figures 5-3 and 5-4 because of the scaling applied to the filter cake char data.) The factor of 0.673 applied to the filter cake char size distribution implies that during run P051 about 33 % of the mass of the entrained particles entering the filter vessel settled out prior to reaching the filter cake surface.

Although the type of comparison described above can estimate particle settling in the filter vessel, several factors can diminish its accuracy. Process parameters that affect the characteristics of the particles entering the filter vessel can change between the time the material collects in the hopper and the formation of the filter cake. In this case, comparisons of these two materials may be compromised. As mentioned above, the material collected from the hopper must be well-mixed. Because periodic cleaning cycles in HGCU filters could cause layers of settled and cleaned particles to develop in the hopper, care must be taken to obtain hopper ash that is representative of a complete filtration cycle. Another complicating factor is continuing chemical reactions in the filter cake prior to its collection for analysis. As is noted elsewhere in this report, PFBC ash usually contains some incompletely-utilized sorbent material that is available to react with SO_2 in the flue gas. Also, if the eutectic reactions described in section 5.8 have time to occur, the ash particles in the filter cake may agglomerate. It is possible that these chemical reactions could alter the size distribution of the filter cake material prior to its collection and analysis.

It should also be noted that gravitational settling of coarser entrained particles prior to collection on the filter cake is not the only possible explanation for physical differences in hopper and filter cake ashes. Preferential cleaning and/or reentrainment of different-sized particles may also contribute to these differences. Other parameters that would affect the proportion of material settling out prior to filtration include inlet particle size distribution, face velocity, flow patterns in the filter vessel, and candle geometry. Despite these limitations, it is highly desirable to quantify the amount of material that reaches the surface of the filter cake. Because the performance of HGCU filters is strongly dependent on the rate at which particle mass is collected on the cake, filter operators should use all available methods and samples to assess this parameter.

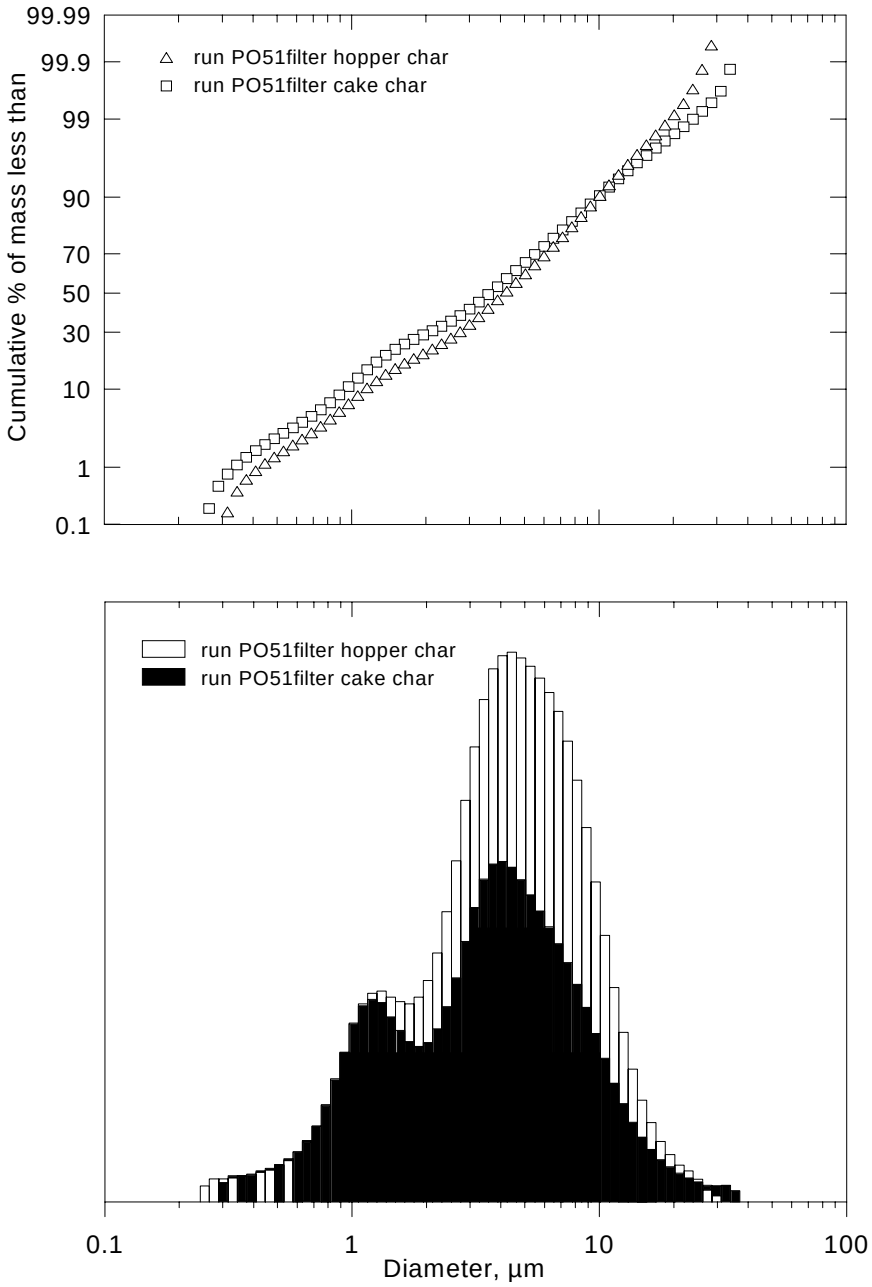

Figure 5-3. Cumulative and differential size distribution data for P051 filter cake char (ID # 4325) and filter hopper char (ID # 4324) measured with a Leeds and Northrup Microtrac Particle Size Analyzer. The differential data for the filter cake char in the lower graph have been scaled down by a factor of 0.673 to align the finest portion of its size distribution with that of the filter hopper char.

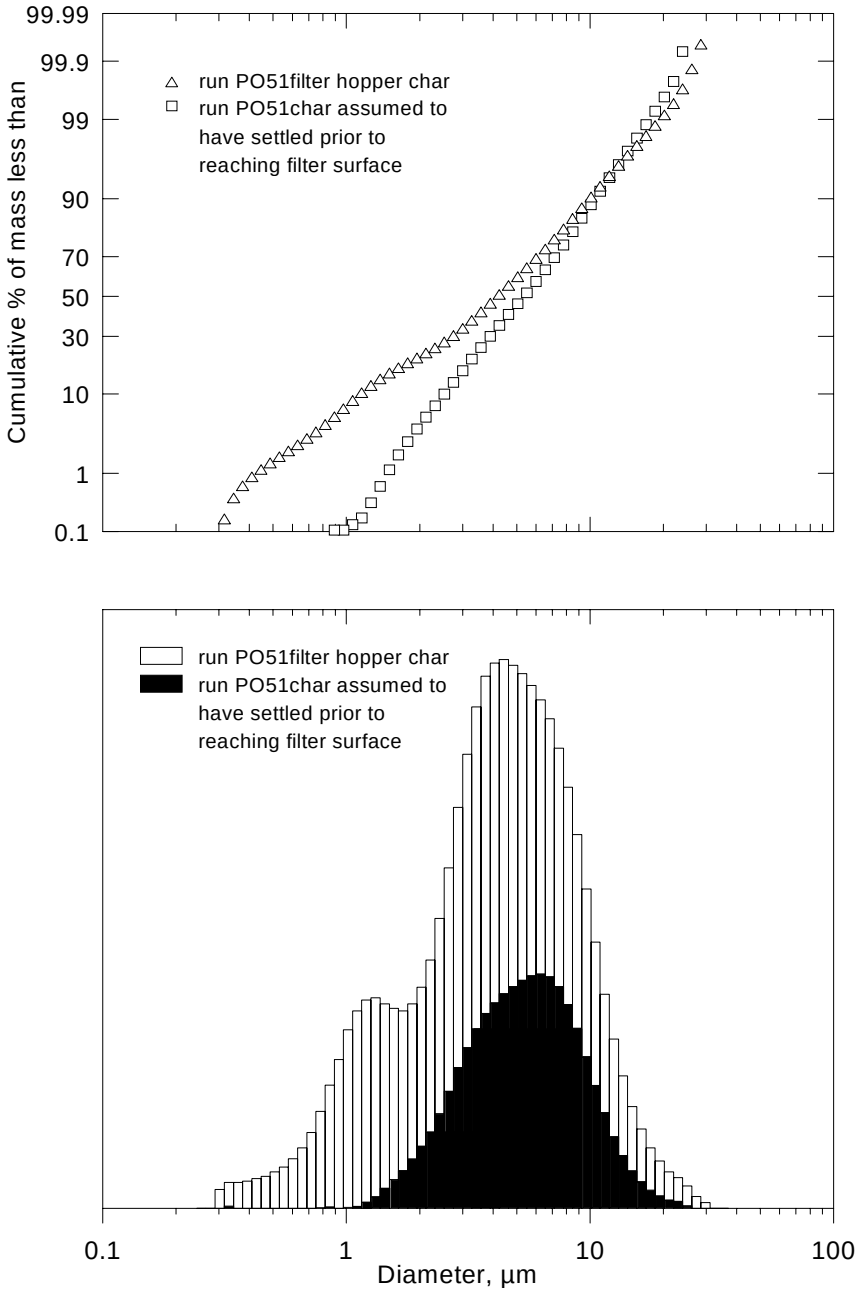

Figure 5-4. Cumulative and differential size distribution data for P051 filter hopper char (ID # 4324) and the portion of the char entering the filter vessel that is assumed to have settled out prior to reaching the surface of the candle filters. The calculation for assumed settling was derived from the comparison and scaling shown in Figure 5-3.

5.8 CONSOLIDATION AND BRIDGING OF PFBC ASH DEPOSITS IN HGCU FILTERS

Operating experiences at Grimethorpe, Karhula, and Tidd illustrated the propensity for PFBC ash to form strong ash structures that could lead to catastrophic filter element failures. The clearest evidence for this behavior was obtained from site observations made at the Tidd APF. (The four site visits Southern Research Institute personnel made to this facility have been summarized under the section *Site Visits*.) These observations demonstrated that given sufficient residence time, PFBC ash at Tidd would form extensive, strong deposits on the candle surfaces and on many of the passive, non-filtering surfaces in the APF. Furthermore, the location and nature of the ash bridged between and around filter elements, and the condition of the filter elements strongly suggested that large ash agglomerates that dislodged from various places in the APF were becoming trapped in the APF before they could fall into the hopper for removal. After becoming trapped, these agglomerates served as platforms on which more ash could collect. When this ash was trapped against the surface of filter elements, the weight of the ash was transferred laterally to the elements, leading ultimately to element breakage.

Laboratory analyses of ash samples and deposits from Tidd, Grimethorpe, and Karhula were performed to identify the mechanism(s) governing the formation of these high-strength ash deposits. In particular, scanning electron micrographs of the internal structure of the deposits, and measurements of their porosity were combined with chemical analyses and literature reviews to evaluate the various mechanisms that might be responsible for the formation of these deposits. The following discussion details the analyses performed on samples collected from the Tidd APF after instances of extensive deposit formation. These data are then used to evaluate several mechanisms cited as potential causes for deposit formation.

In general, analyses of the ash samples from the Tidd APF showed that the ash that collects at various places throughout the filter vessel initially forms loose, weak, uncompacted deposits that are 85 to 90 % porous. (After the cyclone was completely bypassed, the ash formed deposits that were initially around 80 % porous.) A consistent difference was observed between the porosity of these newly-deposited regions of ash aggregates and the porosity of portions of the aggregates that were exposed to the temperatures in the APF for extended periods (as low as 72 % for the portions of filter cakes adjacent to candle surfaces, and 74 % for deposits formed on non-filtering surfaces). In other words, the newly-deposited regions of the agglomerates formed before the cyclone was bypassed are no more than 15 % solid, whereas the solid content of more aged deposits could be as high as 28 %. These data are illustrated in Figure 5-5, which shows the porosity gradient through one of the thick filter cake specimens collected on September 30, 1993 from the Tidd APF. In almost all cases, the exposure of these deposits to the temperatures in the APF (1200 - 1550 °F) apparently caused them to gradually consolidate and transform into much stronger structures with much reduced porosities.

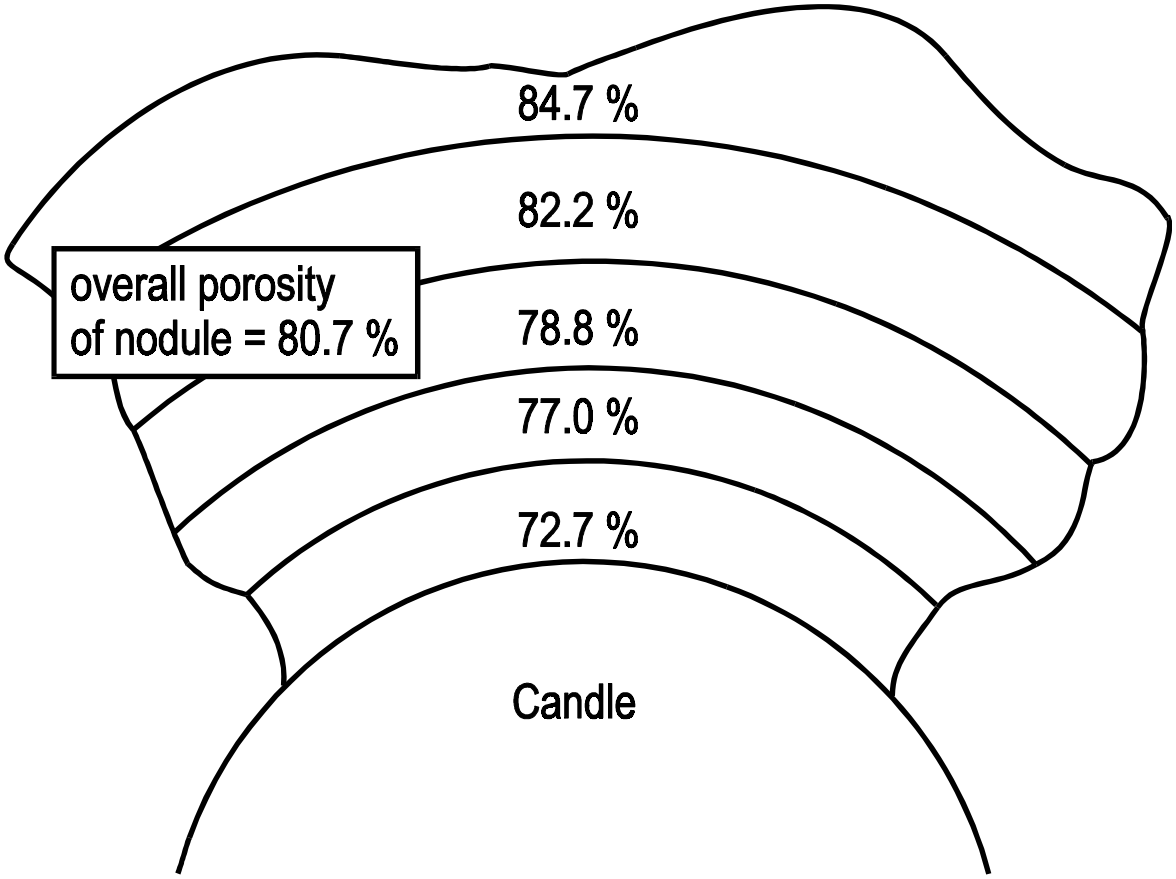

Figure 5-5. Porosity gradient through one of the thick filter cake specimens collected on September 30, 1993 from the Tidd APF.

SEM examinations of fresh fracture surfaces of a filter cake nodule obtained from Tidd on September 30, 1993 (Figure 5-6), and an ash deposit taken from one of the ash sheds at Tidd on October 27, 1994 (Figure 4-35) provide valuable circumstantial evidence as to the nature of the mechanisms involved in ash deposit formation. The micrographs in Figure 5-6 strongly suggest that the ash particles initially deposited on the filter cake have undergone significant structural changes. This fracture surface apparently shows particles that have been enveloped in interparticle bonds, possibly as a result of melting. The microscopic structure of this sample suggests that this ash deposit would have significant physical strength, which was confirmed by mechanical tensile strength measurements which returned a value in excess of 12.5 psi. The micrographs in Figure 4-35 also suggest that adjacent particles have softened and welded together, although the degree of apparent melting is somewhat less pronounced than in Figure 5-6.

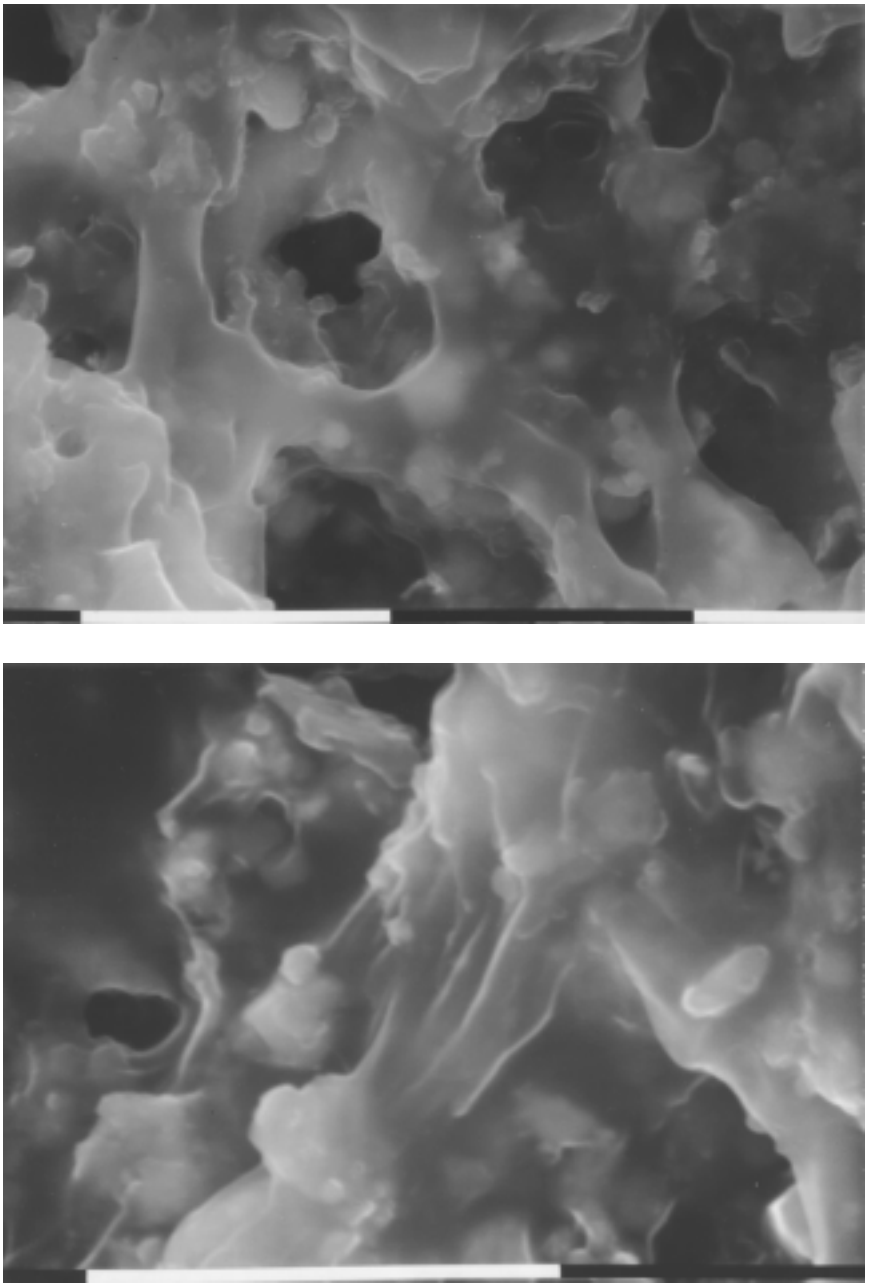

Figure 5-6. Scanning electron micrographs of internal fracture surfaces of a filter cake ash nodule from Tidd (ID # 4012). The white bars at the bottom of the micrographs represent lengths of 10 µm.

As can be seen in Figure 5-6, the primary ash particles are nearly completely imbedded in a pervasive amorphous mass. The keys to determining the mechanism(s) responsible for the development of this type of amorphous mass include physical observations of the porosity of fresh and aged deposits, and comparisons of the chemical composition of aged ash deposits with APF hopper ashes.

The first mechanism postulated to support the porosity gradient illustrated in Figure 5-5 is the compaction of filter cake as a result of the pressure drop applied across it by the passage of flue gas through the cake. However, this mechanism does not account for the apparent differences in the porosities of fresh and aged portions of passively formed ash deposits. As mentioned earlier, the outer, more recently deposited portions of these passive deposits were fluffy (83 to 85 % porosity) and had low mechanical strength, while the deeper, older regions of the deposit were much stronger and had measured porosities around 74 %.

Two other mechanisms are available which may account for the consolidation and strengthening of ash deposits. The first of these involves the adsorption of compound(s) out of the flue gas onto the surfaces of the previously collected ash particles. If this adsorbed material occupies enough of the interparticle voids, its presence could account for the decreased porosity of the ash deposit. The compound in the flue gas most likely to be available for this type of mechanism is SO_2. Because the PFBC process at Tidd captured only about 90 % of the sulfur in the coal, a significant concentration of SO_2 was present in the flue gas entering the APF. The ash that collected in the APF contained significant amounts of unspent calcium and magnesium with which the SO_2 could react. Calcium sulfate and magnesium sulfate are the compounds most likely to be formed as a result of the chemical adsorption of SO_2 by ash particles. Because these alkali-sulfate salt molecules are physically larger than the original alkali molecules, the formation of these salts after the ash particles have been collected may result in lowered porosity, increased aggregate strength, and possibly the formation of the type of consolidated deposit mentioned above. Another basic mechanism that may account for the consolidation of ash deposits is that eutectic mixtures are formed directly from the ash and sorbent particles in the deposit. In this mechanism, the ash particles soften significantly and gradually rearrange themselves into a more compact structure. Evidence supporting or refuting these two mechanisms is discussed in the following paragraphs.

For adsorbed material to account for the apparent consolidation of ash deposits, a sufficient amount of material must be added to the deposit to yield the reductions in porosity (or increases in % solid volume) that have been observed. Since this material would have a different composition than the originally deposited PFBC ash particles, and would be gradually added to ash deposits in the APF, aged deposits such as thick filter cakes or thick passive deposits should contain more of the adsorbed or condensed material than APF hopper ashes. In addition, the intimate contact of flue gas with the ash particles in the filter cake would most likely enhance this adsorption for filter cake ash over passively deposited ash. The type of ash available from Tidd for analysis that would experience the least chance of this type of reaction would be ash collected in the APF hopper. By comparing the chemical compositions of hopper and filter cake ash from Tidd, and from Karhula (see the results for Tidd in Tables 4-3 and 4-4, and the discussion of sulfate ion contents of the Karhula ash

under section 4.3), the likelihood of the adsorption of SO_2 from the flue gas causing the consolidation of ash deposits can be evaluated. Because the sulfur contents of hopper and filter cake ashes from both these facilities are not significantly different, it is unlikely that enough SO_2 becomes captured by the unreacted sorbent in the ash after an ash deposit is initially formed to account for the substantially increased amount of solid material in consolidated ash deposits.

Another way to compare the chemistries of hopper and filter cake ashes is to examine their relative concentrations of non-volatile components. If the flue gas contributed large amounts of mass to the aggregate through condensation or adsorption, the chemical constituents of this added mass would be limited to compounds that could exist as a vapor at the normal operating conditions of the APF. Although many compounds could satisfy these requirements, some of the major constituents found in the fly ash do not. Three major constituents that will not be found in a gaseous state in the APF are iron, aluminum and silicon. When we compare the mineral analyses of Tidd APF hopper ashes with mineral analyses of aged Tidd filter cake ashes (see Tables 4-3 and 4-4), the iron, aluminum, and silicon contents of the two types of samples are very similar. Because the concentrations of these three non-volatile elements are not significantly lower in filter cake ash than in hopper ash, it is apparent that essentially all of the mass of the filter cake is derived from the original ash particles, and not from any significant additional deposition of gas-phase constituents from the flue gas. These results do not preclude formation of calcium and/or magnesium sulfate in the Tidd APF; however, the chemical analyses do not support the production of these compounds as the primary mechanism by which ash deposits consolidate.

This leaves one plausible mechanism that might be responsible for the extreme consolidation of these agglomerates of ash. This mechanism, which is consistent with the observations and analyses presented above, is a physical rearrangement of the previously collected ash particles (or the material composing the particles). This description is based on site observations made at the Tidd PFBC, field and laboratory analyses of ashes and nodules collected from Grimethorpe, Tidd and Karhula, and a review of literature describing eutectic formation, sintering, and consolidation of boiler tube deposits. The formation of eutectic mixtures at the contact points between particles could provide the driving force for this type of consolidation. The distributions of chemical constituents among collected PFBC ash particles provide local, highly concentrated chemical species that promote reactions between adjacent particles that can ultimately cause strong, nodular deposits to form in the filter vessel. These deposits can lead directly to bridging and filter element failure.

The amorphous masses shown in Figure 5-6 apparently formed in the filter vessel after the particles were initially collected. The formation of strong, consolidated ash deposits begins with direct contacts between collected particles comprising highly concentrated, dissimilar chemical compounds. Chemical species exist in high local concentrations in particles collected in HGCU filters applied to PFBC processes because of the nature of the process. In conventional pulverized coal combustion, the fly ash particles are generated through carbon burnout, melting, or vaporization/condensation processes. These latter two mechanisms produce individual ash particles containing a broad array of chemical compounds. In the PFBC process, the coal and sorbent particles introduced into the combustor are never exposed to high enough temperatures to undergo either significant rapid melting, or

vaporization and condensation. The chemical compositions of the entrained particles that leave the combustor result from either carbon burnout around mineral inclusions in the coal, or carryover of alkaline sorbent particles that have been mostly sulfated in the combustor. Therefore the individual particles entering the HGCU filter are much more likely to be predominantly composed of a single compound. Distinct chemical compositions of various individual particles found in ash deposits obtained from the Tidd APF have been observed with SEM microprobe analyses (discussed earlier in this report). Consequently the ash deposits in a PFBC HGCU filter contain a high proportion of intimate interparticle contacts between highly concentrated, distinct chemical compounds. Although HGCU temperatures are not high enough to melt these concentrated compounds, solid-to-solid diffusion gradually occurs between dissimilar compounds in direct contact. The formation of interparticle melts that could result from these direct contacts is shown generically in Figure 5-7.

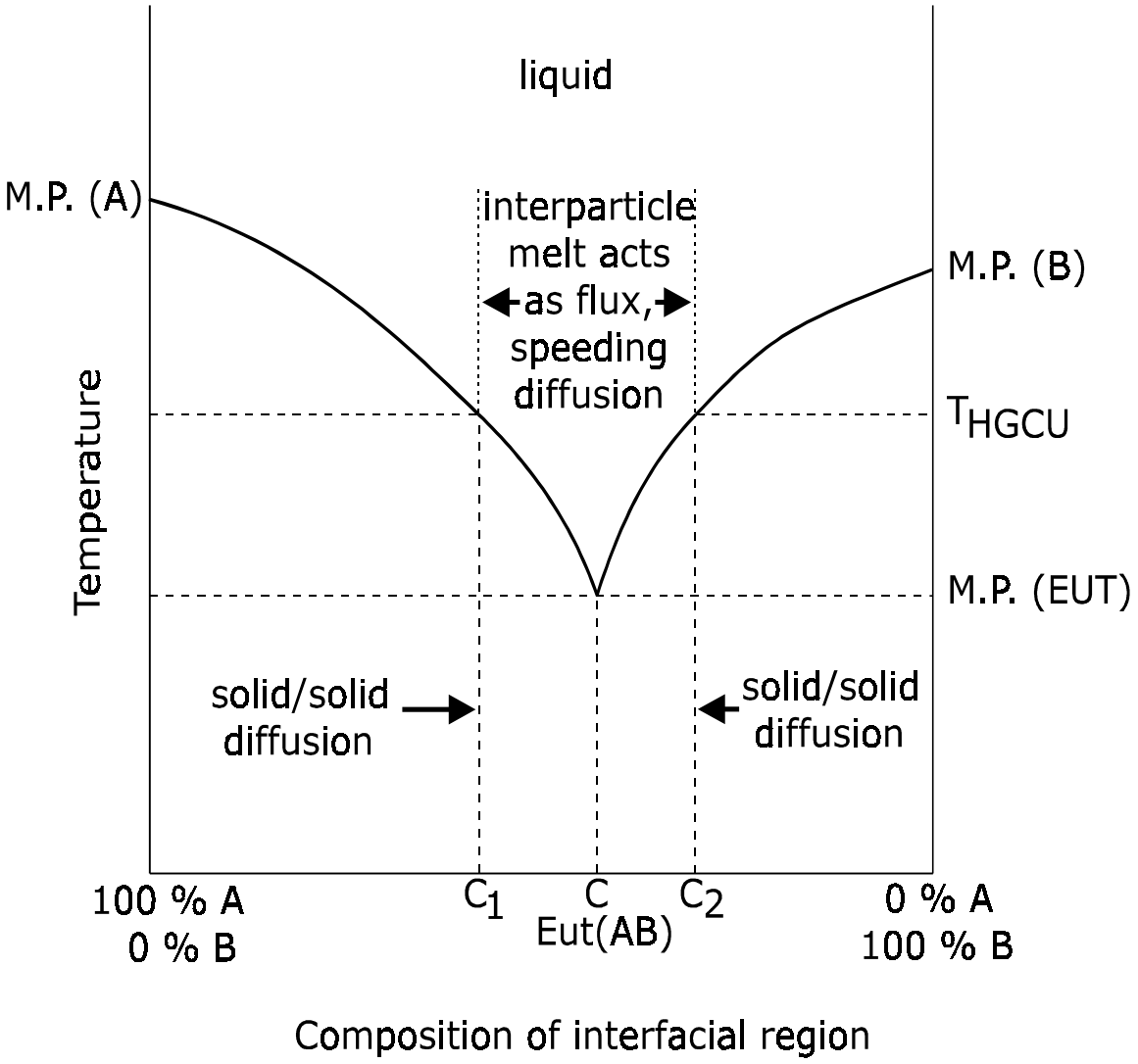

Figure 5-7. Binary phase diagram showing the formation of a eutectic (AB) resulting from surface diffusion between solid compounds A and B in contact. Eutectic AB has a melting point less than the temperature of the HGCU filter. Compositions C_1 and C_2 have melting points equal to the temperature of the HGCU filter.

As the compounds diffuse together in the region of particle contact, compositions are eventually obtained that begin to melt at the HGCU operating temperature. (The points corresponding to these compositions are labeled C_1 and C_2.) The interparticle melts that form act as fluxing agents, speeding the diffusion of chemical species into the region of interparticle contact. Eventually, the composition of the interparticle melt reaches the eutectic composition, which is established by minimizing the overall system energy for the combination of compounds involved in the process. The eutectic composition is the specific combination of the compounds that yields the minimum melting point. The melting point of the eutectic is lower, often by a significant amount, than the melting points of any of the chemical compounds contained in the eutectic composition.[19]

Therefore, any adjacent particles that place two distinct compounds in direct contact will tend toward the formation of a eutectic at the interparticle contact point. The rate at which the eutectic composition is approached is determined by several factors. These include the purity of the component compounds, the geometry of the interparticle contact (particle size and contact area), the pressure of contact between the particles, the temperature of the particles, and the fluxing action of intermediate compositions of the component compounds.[12] In addition, other factors that exist in HGCU filters may also influence the rate of eutectic formation. These include the presence of gaseous compounds in the pressurized flue gas surrounding the particles, and additional compounds that are probably present in relatively low concentrations in the contacting particles. (In general, the melting point of a eutectic will be further decreased by the addition of more chemical species into the eventual eutectic composition.)

Based on the nature of the PFBC process and the measured bulk compositions of various ash samples obtained from APFs at PFBC facilities, there are several compounds that are likely to be available in PFBC ash deposits. Some of the compounds that may be found in high concentrations in individual PFBC ash particles include K_2SO_4, $CaSO_4$, $MgSO_4$, Na_2SO_4, K_2O, MgO, SiO_2, Al_2O_3, and Fe_2O_3. A review of multicomponent system phase diagrams involving combinations of these compounds was conducted.

The tertiary phase diagram for the system K_2SO_4 - $MgSO_4$ - $CaSO_4$ is presented in Figure 5-8. The formation of calcium sulfate or magnesium sulfate on the surfaces of incompletely reacted sorbent particles in the agglomerate after their initial collection may contribute to eutectic formation. Although the melting points of these compounds in their pure state exceed the operating temperature of the APF; these compounds may still become part of eutectic mixtures like the ones discussed above. In this way, adsorption of SO_2 from the flue gas and its subsequent chemical reactions with alkali components of the ash may play an important role in the consolidation of ash deposits.

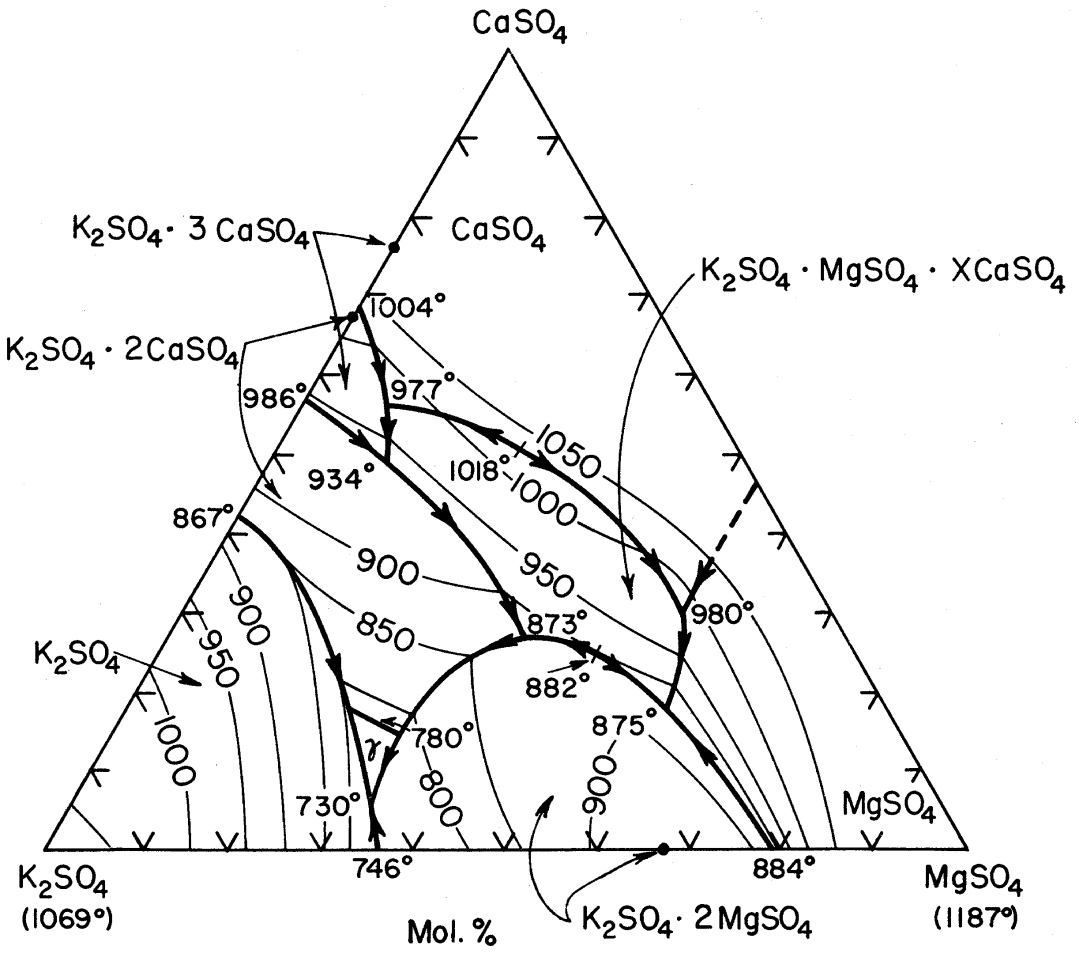

Figure 5-8. Phase diagram for the system K_2SO_4 - $MgSO_4$ - $CaSO_4$.

The silica ratio and $R_{b/a}$ values presented for the Tidd, Karhula and PSDF ashes in Sections 4.2, 4.3, and 4.5 indicate that the Tidd and Karhula ashes, unlike those from the PSDF that are analyzed in this report, could be interpreted as having a high probability of slagging if present in a PC boiler.[12] The slagging propensity for the PSDF ashes analyzed in this report, as indicated by these two quantities, is less than that of the Tidd or Karhula ashes. These quantities also indicate that the slagging propensity of the Tidd ashes exceeds that of the Karhula ashes. These trends correlate with the fact that ash bridging and the formation of strong ash deposits were extensive at Tidd, intermittent at Karhula, but have not been a problem at the PSDF for the periods of operation covered in this report. It is interesting to note that these two quantities are calculated from the amounts of Si, Fe, Ca, Mg, K, Na, Al, and Ti, but do not depend on the amount of S measured in the ashes. (Alkali sulfate compounds are often found in low-melting-temperature eutectic compositions.) The correlation of these two quantities with the experiences at these three facilities do not provide proof of any mechanism for the formation of high-strength ash deposits. Specifically, other factors, such as temperature and particle size, are ignored in this first-order correlation. However, this correlation does indicate that the roles that the various compounds containing the elements used to calculate the silica ratio and $R_{b/a}$ should be carefully examined as the

fundamental mechanisms(s) that control these processes continue to be investigated. Furthermore, the silica ratio and $R_{b/a}$ may ultimately prove useful as a means of predicting the development of high-strength PFBC ash deposits in HGCU filters.

Table 5-6 lists systems (combinations of compounds) identified in this review with eutectic compositions that melt below 1600 °F and their eutectic melting points.[19]

Table 5-6
Selected Systems Containing Compounds that can Combine and Melt Below 1600 °F

System	Relative Amounts, % wt.	Melting Point, °F
K_2SO_4 - $MgSO_4$ - $CaSO_4$	70-25-5	1346
K_2SO_4 - $MgSO_4$	72-28	1382
Na_2SO_4 - K_2SO_4	79-21	1513
SiO_2 - K_2O - Na_2O	69-23-8	1004
Na_2SO_4 - $MgSO_4$ - K_2SO_4	55-30-15	1193
Na_2SO_4 - $MgSO_4$ - $CaSO_4$	59-36-5	1202
SiO_2 - Na_2O - MgO	63-29-8	1315
SiO_2 - K_2O	67-33	1382

It is evident from the melting points in the preceding table that APFs collecting PFBC ash and operating at or near 1600 °F probably provide the conditions necessary for the development of melts at many of the interparticle contact points in the various ash deposits formed in the filter. Given enough time, these interparticle melts will develop. As the volume of an interparticle melt grows, the surface capillary force exerted by the surface tension of the liquid melt gradually rearranges the collected particles into a more compact structure. This effect is shown schematically in Figure 5-9. A diagram is also shown in Figure 5-10 which highlights the mechanisms governing this type of consolidation. In addition to the detrimental effects this consolidation (reduction in the porosity of the deposit) has on filtering pressure losses, the interparticle bonding forces increase, causing the overall deposit to have significantly greater strength.

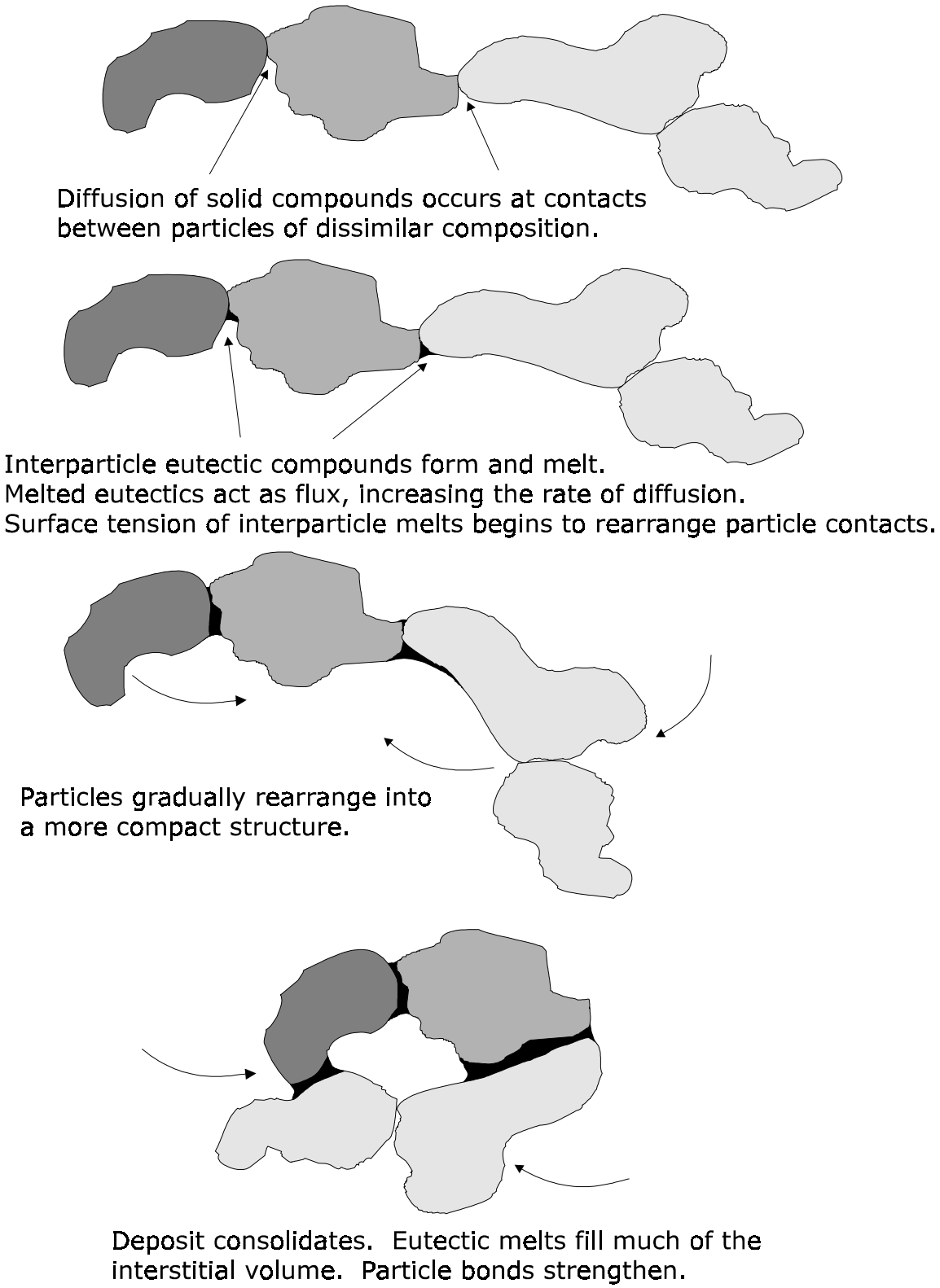

Figure 5-9. Schematic representation of the consolidation of ash deposits.

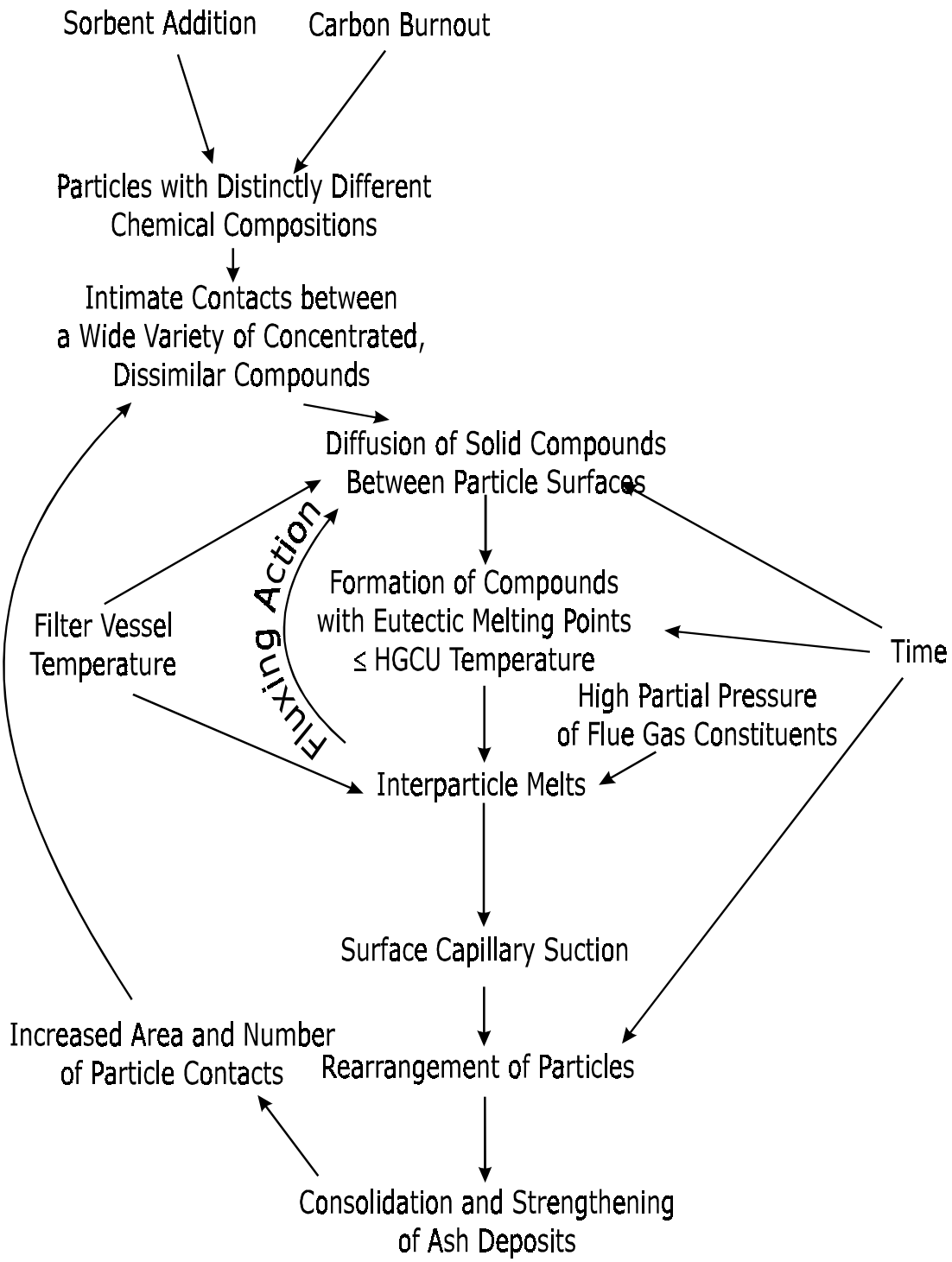

Figure 5-10. Mechanisms governing consolidation resulting from the formation of eutectic melts between PFBC ash particles.

Because the environment in which a PFBC ash deposit is present in a HGCU filter includes all of the ingredients necessary to form these detrimental, consolidated deposits, it is important to consider all of the factors that influence the rate at which these deposits will consolidate. The consolidating force, which results from the development of interparticle melts between adjacent particles, is dependent on the particle size, the viscosity and surface tension of the interparticle melt, as well as the time of exposure of the particles to the forces exerted by the surface tension of the melt.[12, 20] The size distribution of the particles in the ash deposit is controlled by the parameters of the PFBC process, the characteristics of the coal and sorbent, any inertial collectors included in the process stream, and the design of the particle filter (which may promote inertial collection within the filter vessel). The viscosity and surface tension of the melt are functions of the chemical composition of the melt, and the HGCU temperature.[12] Figure 5-11 shows the dependence of the dimension of the interparticle melt on particle size.[12]

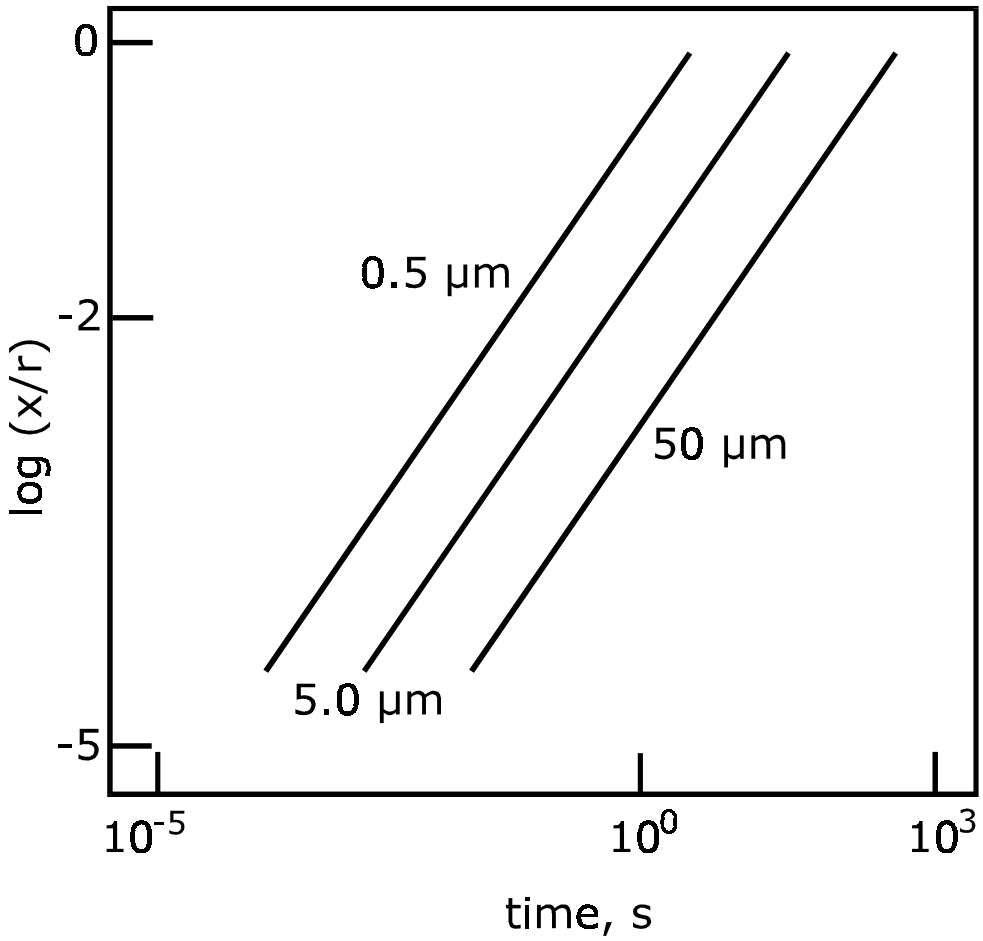

Figure 5-11. Sintering as a function of time for a range of particle sizes. Sintering is expressed as x/r, where x = the radius of the interparticle interface, and r = the particle radius.

Figure 5-12 demonstrates that if given sufficient time, even an interparticle melt that is highly viscous at HGCU conditions will eventually cause the formation of particle bonds with significant size[4].

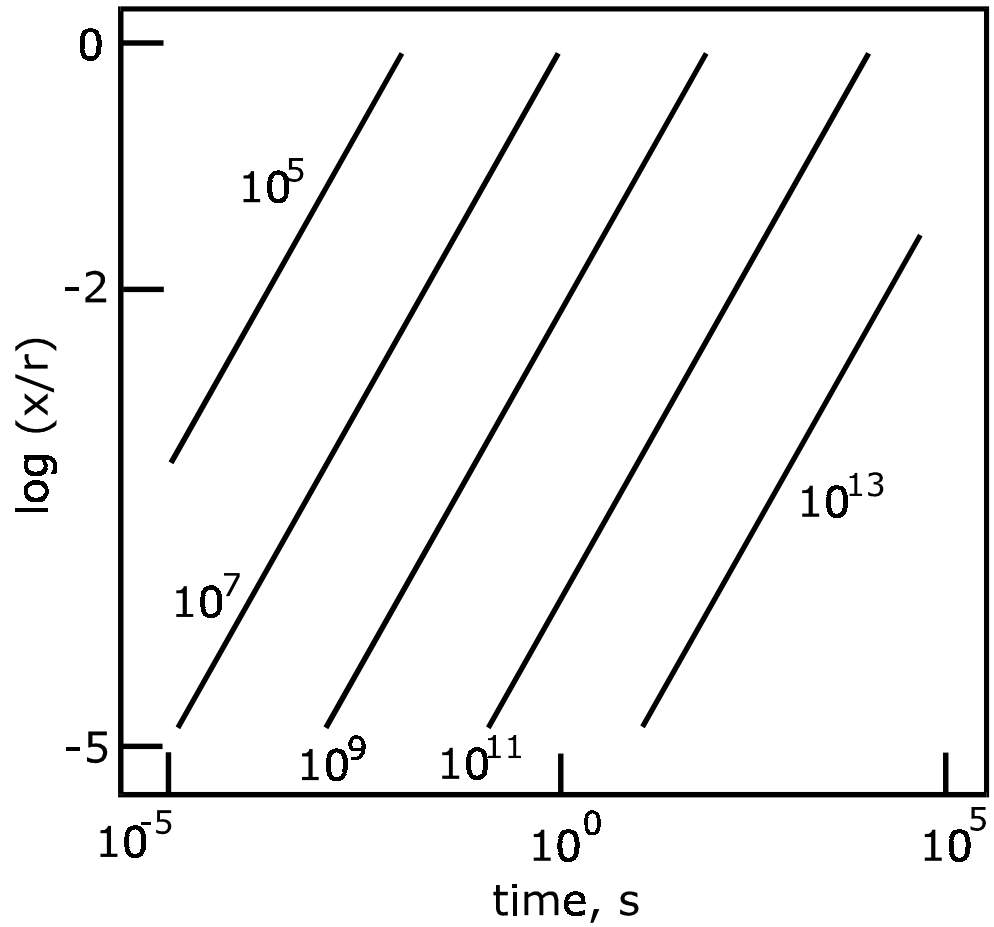

Figure 5-12. Sintering as a function of time for a range of viscosities. Sintering is expressed as x/r, where x = the radius of the interparticle interface, and r = the particle radius. Values of viscosity are given in poise.

Process changes such as slightly lowering the temperature in the HGCU filter, sorbent switching, or addition of a conditioning agent may be able to affect the formation of these eutectics and the subsequent consolidation and strengthening of the ash aggregates. There is some evidence that maintaining the HGCU filter at reduced temperatures may slow or prevent the formation of consolidated ash aggregates. Because magnesium and calcium are both excellent fluxing agents, altering the type of sorbent used in the PFBC process may be unable to alter the tendency for eutectic formation. Finally, the addition of any conditioning agent to the eutectic system is only likely to lower its melting point even further. The optimum solution to the problems caused by the ash aggregates that have been consolidated and strengthened by pervasive eutectic formation is the removal of ash aggregates from the filter before these eutectics have had enough time to develop. A large measure of success was achieved at Tidd by bypassing the cyclone upstream of the HGCU filter. This increased the size distribution of the particles forming the various ash deposits (filter cakes and passive deposits), thereby decreasing their inherent cohesivity. These agglomerates of lower

cohesivity did not have sufficient strength to remain in the APF long enough to undergo consolidation. The effects of gravity and vibration caused them to fall off the surface on which they initially formed.

A diagram was constructed illustrating the various factors that can contribute to filter system failure at barrier filters collecting PFBC ashes. This diagram is presented in Figure 5-13. Most of the relationships shown in this diagram are based on the four on-site observations of the Tidd APF when it was opened for inspection and/or refitting. The diagram is not meant to imply that all of these factors are present in every PFBC/barrier filter application. It is meant to illustrate how filter design, PFBC ash characteristics, and the properties of filter materials can combine to create significant problems in a ceramic candle-based barrier filter vessel.

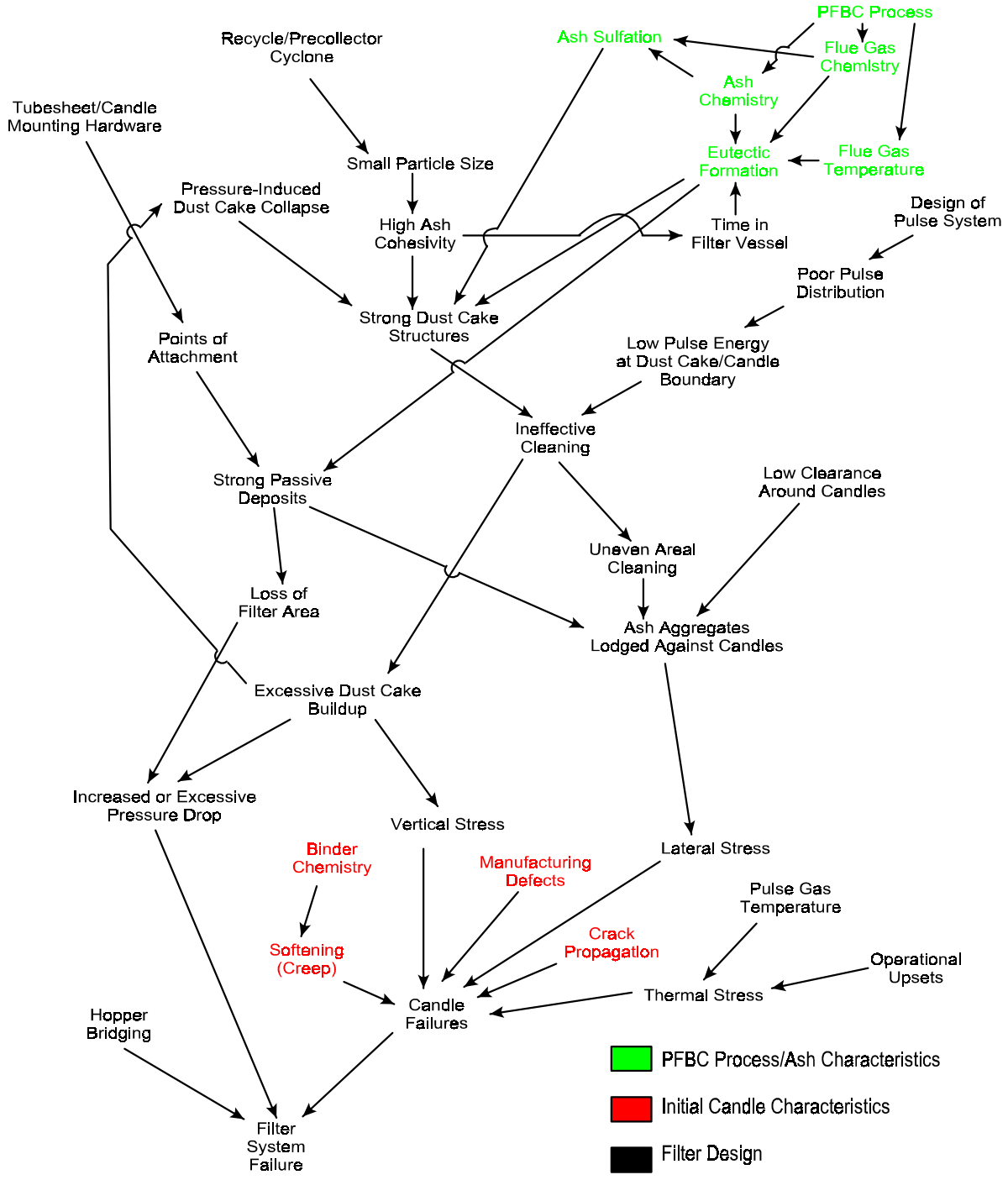

Figure 5-13. Diagram illustrating the various factors in a ceramic candle barrier filter collecting PFBC ash that can combine to cause filter failures.

5.9 PERFORMANCE ESTIMATES FOR DOE/FETC MGCR PARTICULATE RESIDUE

Based on the measurements performed on one of the DOE/FETC gasifier residue samples (ID # 4170), calculations have been made of some quantities relating to the type of filter performance that might be expected during filtration of this type of gasifier residue. The goals of the calculations performed were to estimate the rate of filter cake and pressure drop accumulation for a ceramic candle type barrier filter collecting a gasifier residue like that produced by the DOE/FETC Advanced Gasification and Hot Gas Cleanup Facility. Inlet particulate loading to the barrier filter is assumed to be 4000 ppmw and the temperature and pressure in the filter vessel are assumed to be 1150 °F and 20 atmospheres, respectively. The filter is also assumed to have an active filter area able to handle a flow of 10 acfm/ft^2 (or 10 ft/min), and the viscosity of the gas being filtered is assumed to equal the viscosity of air at equivalent conditions. The specific gas-flow resistance of this gasifier residue is 18 in. H_2O/[(acfm/ft^2)·(lb/ft^2)] for a filter cake having a porosity of 97 %. (The units for specific gas-flow resistance have been expanded to clarify the calculations presented below.) A filter cake porosity of 97 % has been assumed because this is the uncompacted bulk porosity of this material. (As discussed elsewhere in this report, the filter cake may compact as a result of the filtering pressure drop across the sample.) The true density of the residue particles is 2.87 g/cm^3.

An inlet loading of 4000 ppmw at 20 atmospheres and 1150 °F is approximately equal to 0.0019 lb/acf. Therefore at a face velocity of 10 acfm/ft^2 it will take about 53 minutes to deposit 1.0 lb of residue on each square foot of active filter area. For a filter cake with a porosity of 97 %, the volume of each pound of filter cake is about 320 in^3. Under these conditions, a standard candle with an outer diameter of 60 mm will accumulate a filter cake 1.4 inches thick in 53 minutes. (These calculations are adjusted for the cylindrical geometry of the candle, and also assume the filter cake does not compact, but maintains a porosity of 97 %.)

The pressure drop that would be accumulated over the 53 minutes it would take to build the cake described above can be calculated from the specific gas-flow resistance of the residue, the actual face velocity of the gas, the areal density of the filter cake, and the viscosity of the gas at 20 atm and 1150 °F. Therefore the specific gas-flow resistance of the residue (18 in. H_2O/[(acfm/ft^2)·(lb/ft^2)]) must be multiplied by 10 to account for the face velocity, 1.0 to adjust for the areal density (which was defined for this example to be equal to 1.0 lb/ft^2), and 2.11 to adjust for the increase in gas viscosity. (The viscosity of air increases from 184 poise at the laboratory conditions under which the specific gas-flow resistance was measured, to 389 poise at 1150 °F.) Therefore, in the absence of any cake removal, and under the assumed conditions described above, the pressure drop across the filter will increase by 380 in. H_2O during a 53 minute filtering cycle. It is important to note that this pressure drop could increase many fold if the filter cake compacts to a porosity of near or below 90 % as a result of filtering pressure drop.

6.0 INTERACTIVE DATA BANK

SRI has accumulated 387 HGCU particulate samples and has performed various analyses on over 160 of these samples. The results of all of these analyses are included in the interactive, computerized data bank constructed as a deliverable item under this task. This data bank comprises samples and information from a broad selection of advanced combustion processes and facilities developed and operated by a wide range of power systems developers, power producers, and researchers. The facilities represented range from bench-scale units to large pilot-scale demonstration plants. Because the processes being tested were under development and optimization (as well as demonstration) when samples and operating data were obtained, the data presented in the data bank may not always be representative of normal, or optimized, process operation. In fact, a significant proportion of the data and the samples obtained for analysis were included precisely because they were representative of unusual, or troublesome, system behavior. In addition, the characteristics of particulate samples are especially sensitive to the locations in the processes from which the samples were obtained, and also to a wide range of process operating parameters. Although the data bank provides for comprehensive querying and analysis of measured sample characteristics, users of the data bank are cautioned against relying too heavily on comparisons between different processes or sample analyses. The data bank is intended to provide the user with information describing the characteristics and behavior of specific samples and test facilities. When sufficient operating data, samples, and sample analyses were available to draw conclusions about system or process behavior, the data bank includes discussions of these conclusions. In addition, a number of references and key personnel are listed for the processes and facilities represented in the data bank. The user is directed to these sources for more detailed information.

The data bank accomplishes two principal functions. In addition to archiving the results of laboratory analyses of HGCU samples for interactive access (shown schematically in Figure 6-1), the data bank is structured to identify relationships between the HGCU particulate properties that have been measured and the performance of the HGCU filters. Upon activating the data bank, the user initially views a title page and then a page that provides some instructions for properly using and interpreting the information and constructing comparisons between data. (On-line help for the various options is available throughout the data bank.) The user is then directed to a screen that both serves as a main navigation screen, and as an invitation for the user to contribute samples and/or data to the data bank. The first of the principal functions of the data bank is accessed through this main navigation screen and allows the user to perform interactive queries on the data that were measured to physically and chemically characterize the HGCU samples. Parameters available to specify the sample population in this user-controlled querying include the HGCU facility where the sample was generated, the conversion process used, and the type of ash sample (the location in the process stream where the sample was obtained). During querying, the user assembles the specifying parameters in a stepwise process. As the specifications for each parameter are set, the data bank displays the number of samples satisfying these specifications. If the user desires, parameters can be restructured. In addition to allowing the user to build custom sets of parameters to constrain the data population, the data bank also offers the user several preexisting sets of parameters from which analytical data can be selected and plotted.

After defining all the parameters that will be used to specify the samples included in the data comparison, the user has three options: outputting the population with its associated data set to a Windows clipboard, examining all available data for any specific sample in the population (including scanning electron micrographs, and any specialized analyses performed on the sample), or proceeding to select analytical quantities for a plotted display of the data. The analytical quantities that have been measured and can be plotted are listed in Table 6-1. When the user selects the analytical quantities that will be plotted, a summary is provided of the number of samples in the sample population that contain numerical values for the quantities the user has selected. Depending on whether one or two quantities are selected for the data population, this plot will be displayed either as the distribution and range of values measured for a single quantity (vs. the tracking ID # of the sample), or as data pairs for two different quantities. Once data from the sample population is selected and graphed on the screen by the data bank, the user may modify the numerical limits of the axes and the axes titles to change the appearance of the plot. The user then has the option of obtaining a hard copy of the plot, or of returning to the data bank for further comparisons.

The second principal function of the data bank is utilized when sufficient operating data, samples, and sample analyses were available for SRI to draw conclusions about system or process behavior. This portion of the data bank is shown schematically in Figure 6-2. In this case, the data bank includes prepackaged discussions of these conclusions. The user can select from a list of in-depth discussions of ash behavior and/or analyses procedures. The first of these discussions presents one of the principal findings of Task 1 of Contract No. DE-AC21-94MC31160 - a coherent mechanism describing how and why consolidated ash deposits may form in PFBC filter vessels. This description is based on site observations made at the Tidd PFBC, field and laboratory analyses of ashes and nodules collected from Grimethorpe, Tidd and Karhula, and a review of literature describing eutectic formation, sintering, and consolidation of boiler tube deposits. The next three in-depth discussions review the factors in a PFBC that contribute to filter system failure, inertial particle collection in barrier filter vessels, and the potential for rapid increases in the thickness of transient IGCC filter cakes. The fifth and sixth discussions accessible for review from this screen detail the procedures and sampling protocol used during site visits, and the techniques used in the laboratory to characterize particulate samples. The seventh discussion describes laboratory equipment constructed to allow fragile filter cakes to be hardened with cynoacrylate vapor while still on the surface of the filter element.

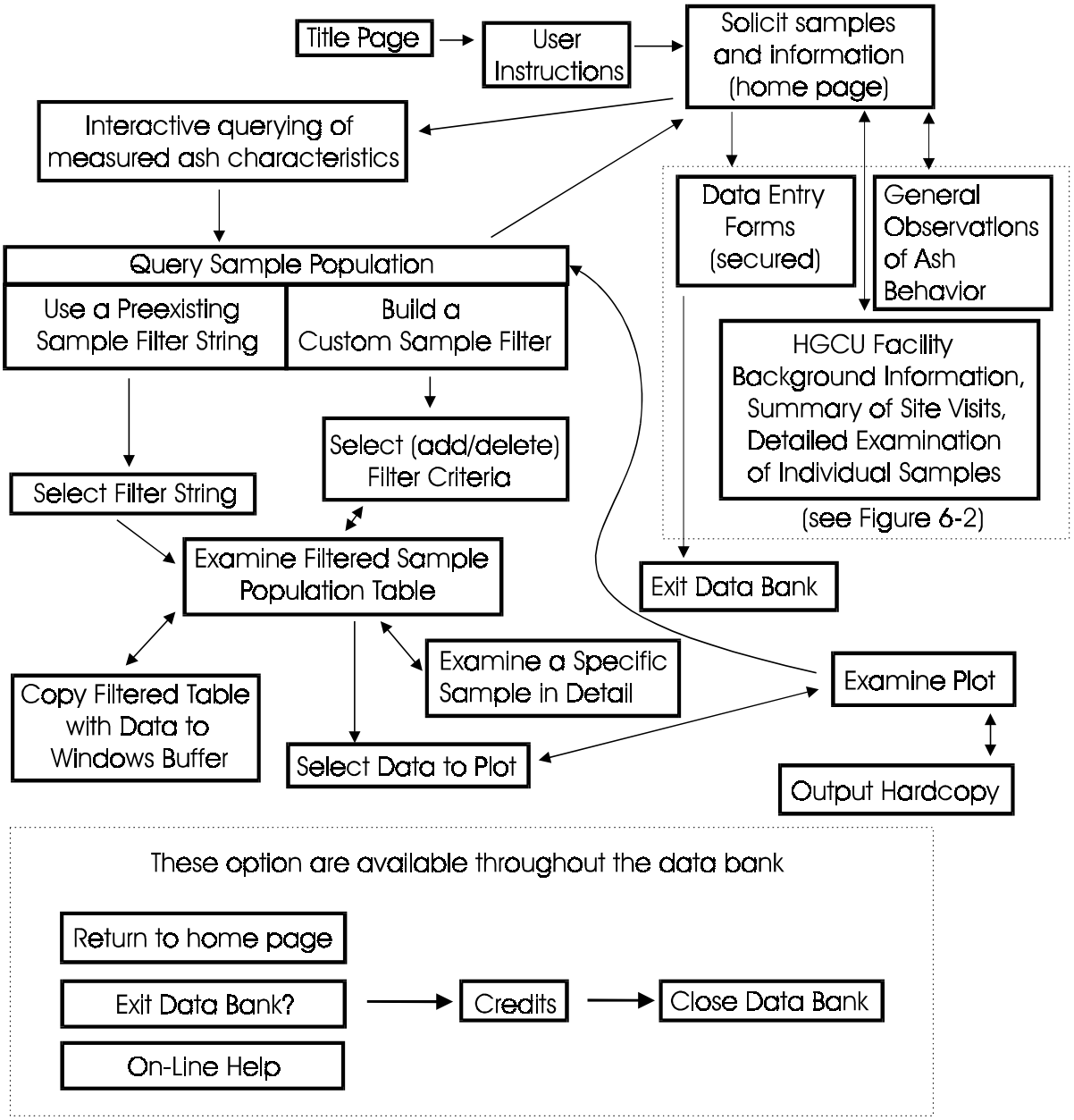

Figure 6-1. Schematic representation of the portion of the data bank controlling the interactive querying and plotting of sample analyses data.

Table 6-1
Analytical Quantities that can be Selected and Plotted as part of Interactive Querying

Analytical Quantity	units
Mass Median Diameter	µm
true particle density	g/cm^3
specific surface area	m^2/g
uncompacted bulk porosity	%
morphology factor	dimensionless
drag-equivalent diameter	µm
specific gas-flow resistance	in H_2O·min·ft/lb
tensile strength	N/m^2
Li_2O content in ashed sample	% wt.
Na_2O content in ashed sample	% wt.
K_2O content in ashed sample	% wt.
MgO content in ashed sample	% wt.
CaO content in ashed sample	% wt.
Fe_2O_3 content in ashed sample	% wt.
Al_2O_3 content in ashed sample	% wt.
SiO_2 content in ashed sample	% wt.
TiO_2 content in ashed sample	% wt.
P_2O_5 content in ashed sample	% wt.
SO_3 content in ashed sample	% wt.
loss-on-ignition during ashing of sample	% wt.
soluble sulfate content of as-received sample	% wt.
equilibrium pH of as-received sample	dimensionless
porosity of ash deposit	%

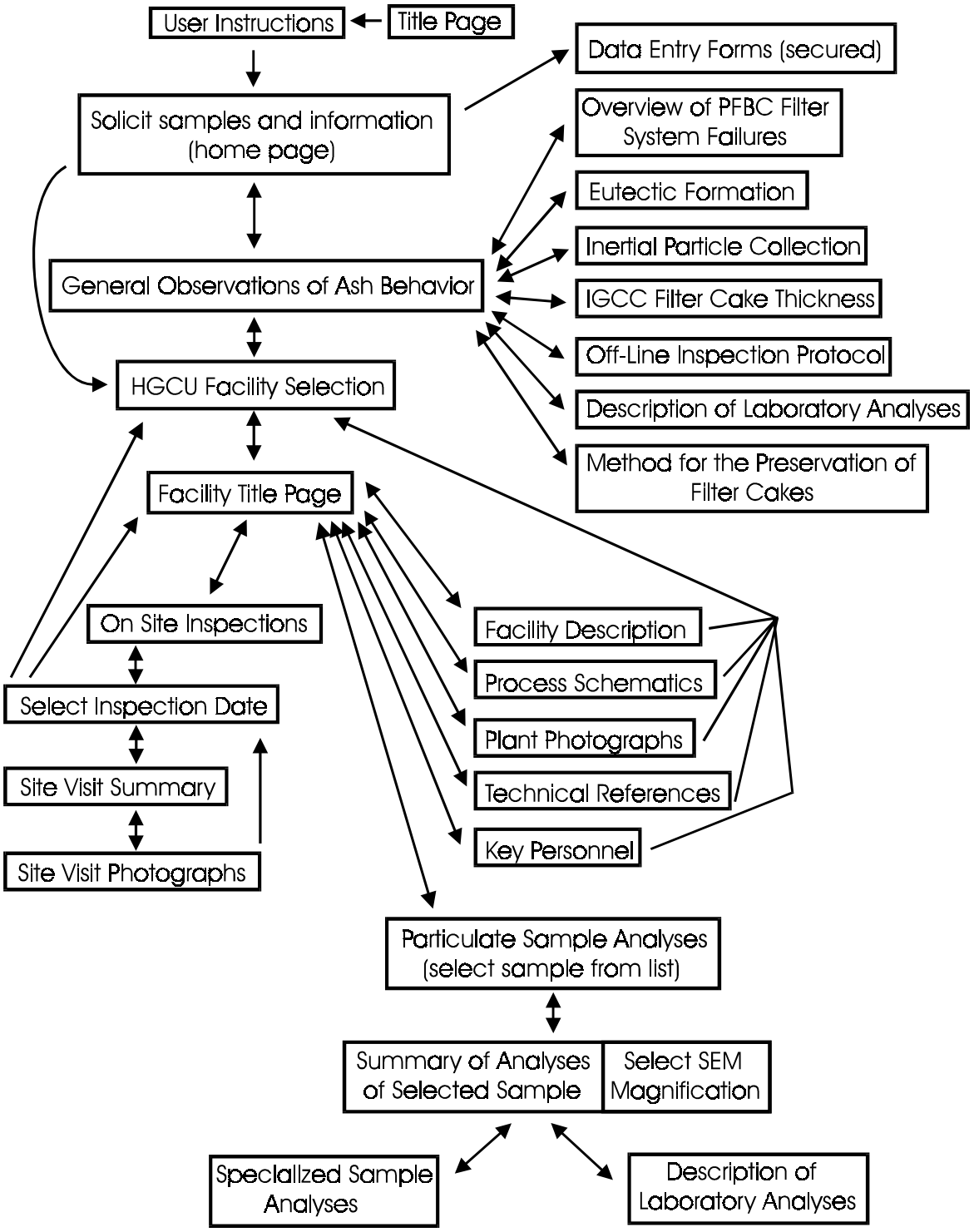

Figure 6-2. Schematic representation of the portion of the data bank controlling the review of project findings, site visits, background information on the HGCU facilities, and detailed analyses of individual samples.

From the main navigation screen, the user may also proceed to examine data and samples for specific facilities. If this option is selected, the user chooses one of the fifteen HGCU facilities to examine. These facilities are listed in Table 6-2. Once a facility has been selected, the data bank lists the primary participating organizations and principal contact personnel for the facility. The user can then select and review one of the six categories listed: brief description of the facility; process schematics; plant photographs; technical references; on-site inspections; or particulate sample analyses. Under the first category, brief descriptions (up to two pages of text) are provided for each of the facilities in the data bank from which the various particulate samples were obtained. Series of process schematics and plant photographs can be scrolled through by selecting the second or third category. The fourth category provides the user with references to more detailed information about the facility. The category for on-site inspections contains information gathered during filter inspection and sampling trips made by Southern Research Institute personnel. Information in this category covers four site visits to the Tidd PFBC, one visit to the MGCR at Morgantown, and six inspection and sampling trips to the PSDF. After selecting a particular site visit to review, the data bank provides a brief summary of the condition of the filter, the sampling procedures and the particulate samples obtained, and some of the key data obtained during the visit. A series of photographs of the filter cakes and ash deposits observed during the visit can also be reviewed.

Table 6-2
HGCU Facilities Represented in the Data Bank

FETC Fluid Bed Gasifier with the Modular Gas Cleanup Rig
Transport Reactor Development Unit located at the University of North Dakota's Energy and Environmental Research Center
Foster Wheeler Development Corporation Integrated Carbonizer/CPFBC Pilot Plant at Livingston, New Jersey
Kellogg Brown & Root Advanced Transport Reactor at the Department of Energy / Southern Company Services Power Systems Development Facility
Foster Wheeler's 10 MWt Pressurized Circulating Fluid Bed Facility in Karhula, Finland
Sierra Pacific Power Company's Piñon Pine Power Project
American Electric Power Service Company's 70 MWe Tidd Pressurized Fluidized-Bed Combustor
Grimethorpe PFBC
Siemens Westinghouse cross-flow filter at the Texaco Montebello Research Laboratory Gasifier
Kellogg Brown & Root Transport Reactor Test Unit located in Houston, Texas
New York University's Bubbling Bed PFBC
Iowa State University's Atmospheric, Circulating Fluidized-Bed Combustor
General Motors' Allison Coal-Fueled Turbine
KRW Process Development Unit
Herman Research Pty Ltd. Mulgrave Gasification Research Facility, Australia

When the user wishes to review the analyses of samples obtained from a particular facility, a scroll-down list of the samples from that facility is displayed. Included with this listing are

brief descriptions of the samples, and where and when they were obtained. After a sample is selected to examine in detail, a screen is displayed that summarizes the physical and chemical analyses that have been performed on that sample. Physical attributes that have been measured and are included in this display include median particle size, specific surface area, particle morphology, bulk ash cohesivity, permeability, and tensile strength. This screen also provides access to scanning electron micrographs of many of the samples in the data bank. In general, these micrographs were obtained and can be viewed at four different magnifications. Chemical analyses of the selected sample are also summarized on this screen. Some of the samples collected which have unusual histories or unique characteristics have been analyzed with specialized techniques. When specialized analyses have been performed on the selected sample, the results of these analyses can also be accessed from this screen. This screen also provides a direct link to descriptions and explanations of the various analyses used to characterize the samples.

Another option available through the main navigation screen is the entry of additional data obtained during the analysis of particulate samples. This option is password-protected so the integrity of data included in the data bank can be maintained. The entry of additional data into the data bank can be accomplished using forms customized to accept sample identification information and the results of the analyses listed in Table 6-2.

7.0 CONCLUSIONS

Ceramic barrier filters operating in HGCU environments face several potential challenges that may result from the characteristics of the ash or char being collected. The condition that has received the most attention since the first testing of these filters is the formation of tenacious ash deposits in the filter vessel. These deposits can form bridge-like structures that often result in lateral mechanical forces being exerted on the filter elements. In some cases, these lateral forces have apparently been sufficient to fracture some of the ceramic filter elements. Ash bridging can also become extensive enough to significantly reduce active filter area, and ash deposits can become large enough to cause damage to filter elements if the deposits dislodge and strike filter elements as the deposits fall to the hopper. The experiences with bridging observed in this study were confined to PFBC operation. Although experiences at Tidd and Karhula led to improved filter elements and filter system design to minimize the damaging effects of these ash deposits, operating experiences and supporting laboratory studies indicate that these improvements are not sufficient to completely remove the potential for ash bridges to form. Residence time in the filter vessel combined with filter temperature, and ash and flue gas chemistry, can provide conditions sufficient for strong PFBC ash deposits to form in HGCU filters. Although the fundamental mechanisms controlling the formation and strengthening of these ash deposits have not been completely verified, a great deal of information has been compiled characterizing PFBC ash deposits. Based on these characterizations, this task developed and presented a model of deposit growth based on the formation of eutectic compounds in PFBC ash.

Several approaches to limiting the potential for bridging have been tried. Bridging was significantly reduced at Tidd by limiting the time that ash remained in the APF. At Karhula, various combinations of coals and sorbent materials were evaluated with one of the objectives being to minimize ash bridging. At the PSDF transport reactor, the temperature of the filter vessel has not been allowed to approach the levels believed to promote ash bridging. It is clear from the experiences at these facilities that understanding and optimizing ash characteristics is one of the keys to successful and optimized HGCU filter operation on PFBC systems.

In addition to bridging in HGCU filters, other key issues that are strongly dependent on the characteristics of the collected particles are pressure loss across the filter, potential for the compaction of filter cakes by the pressure drop applied across them, development of filter cakes that may be hard to remove during reverse-pulse cleaning, and reentrainment and recollection on the filter cake of previously collected particles following their removal by cleaning pulses.

For a given filter design, the permeability of the filter cake is the primary variable determining overall pressure loss across the filter. (Although inlet mass concentration, filtering face velocity, gas viscosity, and the permeability of clean ceramic filter elements also contribute to the overall pressure loss, these factors are set by the system design.) Given these design factors, the pressure loss through the filter cake is determined by the amount of cake on the filter surface (usually expressed in terms of its areal density), and the morphology of the filter cake. This morphology is a combination of the porosity of the cake structure, and the morphology of the particles composing the cake. As with the other factors set by the

system design, the morphology of the particles reaching the filter cake is determined by operating variables of the combustion or gasification system. Precollectors, such as cyclones upstream of the barrier filter, can also modify particle morphology in the filter cake by preferentially removing the larger entrained particles before they are allowed to enter the filter vessel.

Mathematical models of filtration, including the modified semi-empirical model refined under Task 1 of this contract describing the permeability of filter cakes composed of fine, irregular particles, demonstrate the sensitivity of flow resistance to cake porosity. Factors that can decrease the porosity of filter cakes in barrier filters include cake collapse caused by filtering pressure drop, alteration of particle morphology and rearrangement of the collected particles as a result of the formation of eutectic melts, and the filling of interparticle voids by the additional formation of sulfate salts on the surfaces of incompletely reacted sorbent particles.

Because the relationships between chemical constituents and particulate behavior are not yet established for gasification particulate, the effect on filtration behavior of the various chemical compounds present in gasification particulate samples are not yet known. Chemical reactions such as tar formation and chemical sintering between particles have the potential to create serious problems such as bridging in filters collecting gasification particulates. Although no direct evidence of tar formation in coal-based gasification systems was identified in this project, tar formation in some biomass gasifiers suggests that there may be conditions where tars could adversely affect the porosity and strength of coal gasifier char filter cakes.

Laboratory characterizations of gasifier and carbonizer chars have shown that these materials can have physical characteristics that can negatively affect filtration performance. Many of the gasification chars studied under this task comprised irregularly-shaped particles with very high specific surface areas ($> 100\ m^2/g$), and often with very fine size distributions (MMD $< 1\ \mu m$). (It is important to note that most of the char materials characterized in this report were generated from small, pilot-scale facilities, and that larger-scale gasifiers may ultimately produce char material without these negative characteristics.) As discussed in this report, chars with very high surface areas can generate filter cakes that have extremely low permeabilities. In addition, there is a potential for some filter cakes comprising gasifier char to compact, which would adversely affect permeability. Also, many of the gasification char samples studied under this task exhibited relatively low tensile strengths. The low tensile strengths measured for these samples may indicate that char particles dislodged from filter elements during pulse cleaning cycles may break up into very small agglomerates. If this type of breakup occurs, reentrainment of previously collected gasification residues may pose a significant problem. Continued observation of the behavior of gasifier char filter cakes in HGCU filters is needed to assess to what extent these phenomena (the formation of low permeability filter cakes, filter cake compaction, and particle reentrainment) occur.

This task has catalogued many characteristics of PFBC ashes and gasification chars, and has studied the fundamental ways in which these characteristics ultimately affect filter operation. In addition to this report, the interactive data bank issued as a deliverable to DOE/FETC under this task serves as an important tool for advancing these studies. (The reader of this

report is referred to the DOE/FETC Project Manager, Thomas P. Dorchak, for access to the interactive data bank.) The areas where the activities described in this report may continue and/or be enhanced are discussed in the following section.

7.1 OPPORTUNITIES FOR FUTURE WORK

In order to maximize the benefit of the characterization and analysis of particulate properties for HGCU technology, additional samples should be analyzed as they become available, operating data and observations from operating HGCU facilities should continue to be compiled, and critical analyses of these data must continue to be performed and communicated to the users of these filters. Tasks like the one described in this report, and especially the interactive data bank it produced, provide excellent means for achieving these continuing objectives.

One of the specific research opportunities that addresses the objectives stated above is the inclusion in the interactive data bank of data generated at the PSDF under Southern Company Services, Inc.'s Contract DE-FC21- 90MC25140 with DOE/FETC. PSDF personnel have indicated the desire to make available a significant amount of the ash characteristics and process parameters measured under the above-mentioned contract. The types of ash samples and sample analyses, as well as the process information, collected at the facility would greatly enhance the usefulness of the interactive data bank. The data bank was structured to accept additional data with relative ease. In some cases it is expected this additional PSDF data would be of a different type than the data bank already contains. In these cases, the structure of the data bank would have to be modified; however, this process should not be too difficult.

Also at the PSDF, the transport reactor will soon be operated in gasification mode. This mode of operation, as well as the eventual operation of Foster Wheeler's topped pressurized fluidized bed combustor at the PSDF will generate samples and operating data that will also greatly enhance the base of knowledge about HGCU operation at these types of advanced generation facilities. The inclusion of sample analyses and operating data from these facilities is a logical extension of the interactive data bank.

The same logic applies to including additional samples and information as they become available from the TRDU and Piñon Pine in the data bank. Other facilities should also be added to the data bank, including Tampa Electric Company's IGCC facility, and the advanced PFBC at Lakeland, Florida. Samples and operating data from HGCU facilities operating outside the United States should also be added to the data bank. In all cases, the data bank will be strengthened and its applicability enlarged by its continued growth.

To allow the data bank to be as broadly applied as possible, it may be advantageous to alter its presentation format from the CD-ROM format in which it was issued under this task, to a DOE/FETC intranet or world-wide-web internet application, probably accessed through DOE/FETC's web page. The options for these types of formats are currently being explored at DOE/FETC.

In addition to adding samples and data to the data bank, the interpretation of the significance of these data must continue to be developed. A deeper understanding of the formation of

PFBC ash deposits will hopefully allow these systems to optimize their efficiencies without endangering the integrity of their HGCU filters. Continued analyses of gasification chars will determine in what ways their unique characteristics will challenge HGCU filters.

8.0 REFERENCES

1. "Tidd Hot Gas Clean Up Final Report," American Electric Power Service Corporation, prepared for US DOE, Contract No. DE-FC21-89MC26042, October, 1995.

2. Lippert, T.E., et al, 1998, "Performance of the Westinghouse APF in Pilot Scale Test Facilities," Proceedings of the Advanced Coal-Based Power and Environmental Systems '98 Conference, DOE/FETC-98/1072.

3. Kozeny, J. *Ber. Wein. Akad.* **136a**, 271 (1927)

4. Carman, P. C. "Fluid flow through granular beds," *Trans. Inst. Chem. Engs.* **15**, 150 (1937).

5. Langmuir, I. "Report on Smokes and Filters," Section I. U.S. Office of Scientific Research and Development, **No. 865**, part IV (1942).

6. Davies, C.N., Air Filtration, Academic Press, New York, 1973, pp. 7-29.

7. Bush, P.V., T.R. Snyder, and R.L. Chang. Determination of Baghouse Performance from Coal and Ash Properties: Part I. J. Air Pollution Control Assn., Vol. 39, No. 2, Feb. 1989, pp. 228-237.

8. Lippert, T.E., et al, "Westinghouse Advanced Particle Filter System," Proceedings of the Advanced Coal-Based Power and Environmental Systems '97 Conference, DOE/FETC-97/1046.

9. Vimalchand, P., R.F. Leonard, and T.E. Pinkston, "Power Systems Development Facility: Operation of Transport reactor System with a Westinghouse Candle Filter," Proceedings of the Advanced Coal-Based Power and Environmental Systems '98 Conference, DOE/FETC-98/1072.

10. Leonard, R.F., P. Vimalchand, H.L. Hendrix, and T.E. Pinkston, "Power Systems Development Facility: Commissioning and Initial Operation of a Transport Reactor System with a Westinghouse Candle Filter," Proceedings of the Advanced Coal-Based Power and Environmental Systems '97 Conference, DOE/FETC-97/1046.

11. Davidson, M.D., et al, "Power Systems Development Facility: High Temperature, High Pressure Filter Systems Operations in a Combustion Gas," Proceedings of the Advanced Coal-Based Power and Environmental Systems '98 Conference, DOE/FETC-98/1072.

12. Raask, E., *Mineral Impurities in Coal Combustion: Behavior, Problems, and Remedial Measures.* Washington: Hemisphere Publishing Corporation, 1985.

13. Lippert, T.E., G.J. Bruck, and J. Isaksson, “Karhula Hot Gas Cleanup Test Results,” Proceedings of the Coal-Fired Power Systems 94 - Advances in IGCC and PFBC Review Meeting, Volume II, 1994, pp. 535-544.

14. Demuth, J.E. and H.G. Smith, “Piñon Pine Project Gasifier Start-Up,” Proceedings of the Advanced Coal-Based Power and Environmental Systems ’98 Conference, Federal Energy Technology Center, Morgantown, WV, July 21-23, 1998.

15. Swanson, M.L., R.O. Ness, M.D. Mann, and J.S. Haley, “Hot-Gas Filter Testing with the Transport Reactor Demonstration Unit,” Proceedings of the Advanced Coal-Fired Power Systems ‘95 Review Meeting, Vol. I, DOE/METC-95/1018 (DE95009732), June 1995, pp. 87–97.

16. Swanson, M.L. and M.D. Mann, “Advanced High-Temperature, High-Pressure Transport Gasifications,” Proceedings of the Advanced Coal-Based Power and Environmental Systems ’98 Conference, Federal Energy Technology Center, Morgantown, WV, July 21-23, 1998.

17. Pilpel, N., “Cohesive Pharmaceutical Powders,” Advan. Pharm. Sci. 3:173 (1971).

18. Bush, P.V., F.G. Pohl, W.B. Smith, and T.R. Snyder. Laboratory Determination of the Characteristic Drag of Various Fly Ashes Collected in Utility Baghouses. In: Proceedings, 80th APCA Annual Meeting and Exhibition, New York, 1987.

19. Levin, E.M., C.R. Robbins, and H.F. McMurdie, *Phase Diagrams for Ceramists.* Columbus: The American Ceramic Society, Inc., 1964.

20. Frankel, J.J., “Viscous flow of crystalline bodies under the action of surface tension,” *Jour. Phys. (Moscow)* 9: 385 (1945).

APPENDIX A TECHNIQUE FOR PRESERVING FILTER CAKES

Most of the filter cakes that have been observed on-site at HGCU facilities are quite fragile. Although relatively strong nodular deposits obtained at the Tidd PFBC were successfully encapsulated and preserved for analysis by the infiltration of low-viscosity epoxy, efforts to apply this epoxy to more fragile cakes have resulted in their destruction. Therefore a method was developed to strengthen these fragile cakes prior to the introduction of the low-viscosity epoxy. A method for hardening filter cakes with cynoacrylate "super" glue vapor was successfully demonstrated for a small simulated PFBC filter cake. The application of the glue vapor allowed the simulated filter cake to maintain its original structure, but with significantly increased strength. When the hardened sample was exposed to the low-viscosity epoxy, the epoxy easily impregnated the simulated cake. Based on the success of this bench-scale trial, a device was designed that could allow hardening of the bottom 12 to 16 inches of a 1.5 meter filter element and its attached filter cake. This device, which is shown schematically in the Figure A-1, was constructed and tested on filter cakes present on two filter elements removed from the Siemens Westinghouse FL0301 filter vessel at the PSDF.

The design of the device allowed a filter element to be suspended in an acrylic tube with its cake intact. A foam collar was positioned around the element to separate the upper portion of the element, which was not hardened, from the bottom portion of the element, which was hardened with cynoacrylate vapor. After purging the lower portion of the tube with dry gas, glue vapor was generated by passing dry nitrogen over an open container of liquid cynoacrylate glue maintained at about 250 °F. (A dry carrier gas was required because the presence of water cures the glue.) The vapor-laden gas was passed through the filter cake on the lower portion of the candle, where a portion of the vapor was adsorbed on the surfaces of the particles in the filter cake. Vapor which was not adsorbed by the cake was transported by the carrier gas through two water baths where it was cured into fine particles and collected. This collection was necessary to protect the pump from damage from the glue. The initial trials performed with this technique demonstrated that the glue cures almost immediately when it contacts the filter cake. This rapid curing is believed to result from the contact of the glue with hydrated water in the filter cake. The system shown in the attached figure also contained various flow controls and an overflow line for venting in case of failure of the pump or the source of dry carrier gas.

After strengthening the cake on the lower portion of a filter element, the entire lower portion of the element (candle and cake) was gradually impregnated with epoxy. This was done in relatively thin increments along the candle's length (about 2 inches thick), to allow for proper curing of the epoxy. Following encapsulation, sectioning, and polishing, fully encapsulated filter cake/filter element specimens were produced and provided to staff at the PSDF for analysis.

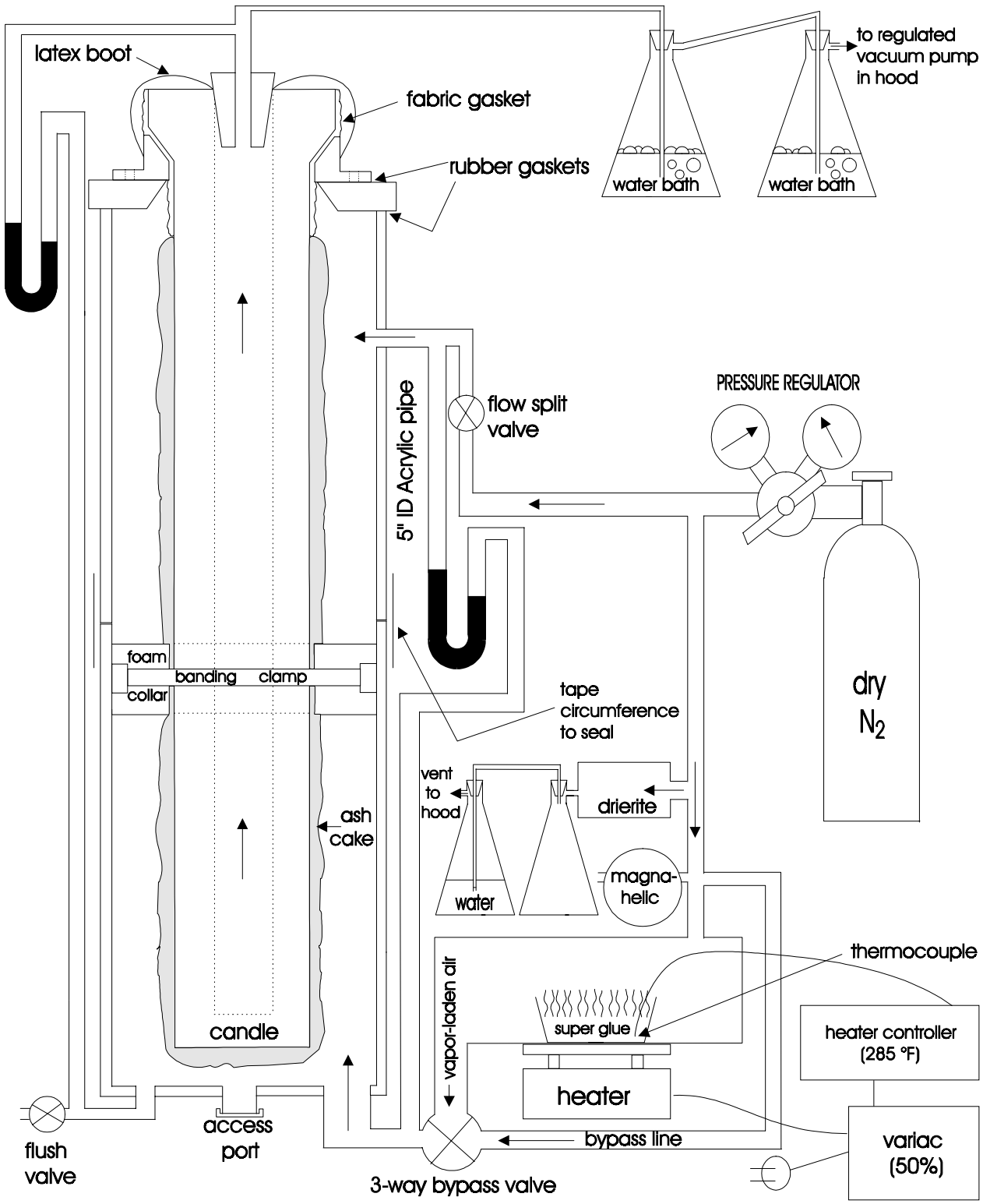

Figure A-1. Schematic diagram of a device for using cynoacrylate glue to strengthen filter cakes formed on a candle filter element in preparation for subsequent impregnation and encapsulation with low-viscosity epoxy.

APPENDIX B SAMPLE INFORMATION FORMS

SAMPLE INFORMATION
(Provided by Facility Operator)
Tracking ID # 4324

FACILITY

1	Name	Transport Reactor Demonstration Unit
2	Type of Gasifier	2.7 MM Btu/hr Pilot Plant
3	Plant Heat Rate (Btu/kWh)	
4	Plant Firing Rate (MWe)	
5	Maximum Continuous Rating (MWe)	
6	Site Altitude (ft)	850 ft

FUEL Wyodak P051

7	Type	Subbituminous
8	Source	Wyodak Seam from Belle Air Mine near Gillette, WY
9	Higher Heating Value (Btu/lb)	9360

10 Proximate analysis

	as received	dry basis
% moisture	~20	NA
% ash	4.68	5.85
% volatile	36.38	45.48
% fixed carbon	38.94	48.67
totals	100.00	100.00
Btu/lb.	9360	11705
% sulfur	0.35	0.44

11 Ultimate analysis

	as received	dry
% moisture	~20	NA
% carbon	55.25	69.06
% hydrogen	6.39	5.19
% nitrogen	0.67	0.84
% chlorine	ND	
% sulfur	0.35	0.44
% ash	4.68	5.85
% oxygen (diff.)	32.66	18.63
totals	100	100

12 Fly ash fraction (% wt.)

13 Chemical analysis of coal (% wt.)

Li_2O	Na_2O	K_2O	MgO	CaO	Fe_2O_3	Al_2O_3	SiO_2	TiO_2	P_2O_5	SO_3	LOI
	1.3	0.3	7.0	26.6	5.5	13.1	27.8	1.3	1.0	16.0	NA

14 Is sorbent added to fuel? yes

15 Type of sorbent Plum run dolomite from Greenfield formation @ 5 wt%

16 Chemical analysis of added sorbent (% wt.)

Li_2O	Na_2O	K_2O	MgO	CaO	Fe_2O_3	Al_2O_3	SiO_2	TiO_2	P_2O_5	SO_3	LOI
	0.3	0.3	27.5	66.6	1.3	1.0	2.7	0.0	0.0	0.3	43.1

PARTICULATE CONTROL DEVICE

17	Type	candle
18	Cleaning initiated on	30 in H_2O above baseline
19	Hopper pulling schedule (h)	0.5 hr
20	Normal operating temperature (°F)	1000
21	Normal operating pressure (psig)	120
22	Normal gas flow	20,100 scfm @ 1atm & 60 °F
23	Normal operating tubesheet pressure drop (in. H_2O)	20
24	Normal pressure drop prior to cleaning (in. H_2O)	100
25	Normal pressure drop following cleaning (in. H_2O)	80
26	Total active filtering surface (ft^2)	26.52

SAMPLE FOR ANALYSIS

27	Type of sample	filter hopper sample
28	Source of ash in plant layout	
29	Date 2/25/97 time 12:00 - 24:00	
30	Sample taken by Bill Sulkalski	
31	Description of operation prior to sample collection: no recirculation of dipleg solids (e.g. steady-state full load, boiler upset, ramping, etc.)	steady-state
32	How was sample obtained	scooped from hopper

ANALYSIS AND REPORTING

33	Sample sent to SRI by Mike Swanson	Phone 701-777-5239
34	Request for sample analysis initiated by Rich Dennis (DOE/FETC)	
35	Goal of laboratory analyses	
36	Specific tests requested	
37	Send report to	
38	Send copies of report to	
39	Special instructions	

SAMPLE INFORMATION
(Provided by Facility Operator)
Tracking ID # 4325

FACILITY

1	Name	Transport Reactor Demonstration Unit
2	Type of Gasifier	2.7 MM Btu/hr Pilot Plant
3	Plant Heat Rate (Btu/kWh)	
4	Plant Firing Rate (MWe)	
5	Maximum Continuous Rating (MWe)	
6	Site Altitude (ft)	850 ft

FUEL Wyodak P051

7	Type	Subbituminous
8	Source	Wyodak Seam from Belle Air Mine near Gillette, WY
9	Higher Heating Value (Btu/lb)	9360

10 Proximate analysis

	as received	dry basis
% moisture	~20	NA
% ash	4.68	5.85
% volatile	36.38	45.48
% fixed carbon	38.94	48.67
totals	100.00	100.00
Btu/lb.	9360	11705
% sulfur	0.35	0.44

11 Ultimate analysis

	as received	dry
% moisture	~20	NA
% carbon	55.25	69.06
% hydrogen	6.39	5.19
% nitrogen	0.67	0.84
% chlorine	ND	
% sulfur	0.35	0.44
% ash	4.68	5.85
% oxygen (diff.)	32.66	18.63
totals	100	100

12 Fly ash fraction (% wt.)

13 Chemical analysis of coal (% wt.)

Li_2O	Na_2O	K_2O	MgO	CaO	Fe_2O_3	Al_2O_3	SiO_2	TiO_2	P_2O_5	SO_3	LOI
	1.3	0.3	7.0	26.6	5.5	13.1	27.8	1.3	1.0	16.0	NA

14 Is sorbent added to fuel? yes

15 Type of sorbent Plum run dolomite from Greenfield formation @ 5 wt%

16 Chemical analysis of added sorbent (% wt.)

Li_2O	Na_2O	K_2O	MgO	CaO	Fe_2O_3	Al_2O_3	SiO_2	TiO_2	P_2O_5	SO_3	LOI
	0.3	0.3	27.5	66.6	1.3	1.0	2.7	0.0	0.0	0.3	43.1

PARTICULATE CONTROL DEVICE

17	Type	candle
18	Cleaning initiated on	30 in H_2O above baseline
19	Hopper pulling schedule (h)	0.5 hr
20	Normal operating temperature (°F)	1000
21	Normal operating pressure (psig)	120
22	Normal gas flow (acfm)	~ 20,100
23	Normal operating tubesheet pressure drop (in. H_2O)	20
24	Normal pressure drop prior to cleaning: 20-30 in H_2O above baseline (up to 100 in max)	
25	Normal pressure drop following cleaning (in. H_2O)	ranging from 30 up to 80
26	Total active filtering surface (ft^2)	26.52

SAMPLE FOR ANALYSIS

27	Type of sample	filter cake
28	Source of ash in plant layout	
29	Date 2/28/97 time end of test	
30	Sample taken by Mike Swanson	
31	Description of operation prior to sample collection: no recirculation of dipleg solids (e.g. steady-state full load, boiler upset, ramping, etc.)	steady-state until off-line
32	How was sample obtained	scraped off surface of candle

ANALYSIS AND REPORTING

33	Sample sent to SRI by Mike Swanson	Phone 701-777-5239
34	Request for sample analysis initiated by Rich Dennis (DOE/FETC)	
35	Goal of laboratory analyses	
36	Specific tests requested	
37	Send report to	
38	Send copies of report to	
39	Special instructions	

SAMPLE INFORMATION
(Provided by Facility Operator)
Tracking ID # 4326

FACILITY

1	Name	Transport Reactor Demonstration Unit
2	Type of Gasifier	2.7 MM Btu/hr Pilot Plant
3	Plant Heat Rate (Btu/kWh)	
4	Plant Firing Rate (MWe)	
5	Maximum Continuous Rating (MWe)	
6	Site Altitude (ft)	850 ft

FUEL Wyodak P056

7	Type	Subbituminous
8	Source	Wyodak Seam from Belle Air Mine near Gillette, WY
9	Higher Heating Value (Btu/lb)	9360

10 Proximate analysis

	as received	dry basis
% moisture	~20	NA
% ash	4.68	5.85
% volatile	36.38	45.48
% fixed carbon	38.94	48.67
totals	100.00	100.00
Btu/lb.	9360	11705
% sulfur	0.35	0.44

11 Ultimate analysis

	as received	dry
% moisture	~20	NA
% carbon	55.25	69.06
% hydrogen	6.39	5.19
% nitrogen	0.67	0.84
% chlorine	ND	
% sulfur	0.35	0.44
% ash	4.68	5.85
% oxygen (diff.)	32.66	18.63
totals	100	100

12 Fly ash fraction (% wt.)

13 Chemical analysis of coal (% wt.)

Li_2O	Na_2O	K_2O	MgO	CaO	Fe_2O_3	Al_2O_3	SiO_2	TiO_2	P_2O_5	SO_3	LOI
	1.3	0.3	7.0	26.6	5.5	13.1	27.8	1.3	1.0	16.0	NA

14 Is sorbent added to fuel? yes

15 Type of sorbent Plum run dolomite from Greenfield formation @ 5 wt%

16 Chemical analysis of added sorbent (% wt.)

Li_2O	Na_2O	K_2O	MgO	CaO	Fe_2O_3	Al_2O_3	SiO_2	TiO_2	P_2O_5	SO_3	LOI
	0.3	0.3	27.5	66.6	1.3	1.0	2.7	0.0	0.0	0.3	43.1

PARTICULATE CONTROL DEVICE

17	Type	candle filter
18	Cleaning initiated on	30 in H_2O above baseline
19	Hopper pulling schedule (h)	0.5 hr
20	Normal operating temperature (°F)	1000
21	Normal operating pressure (psig)	120
22	Normal gas flow	19,885 scfm @ 1atm & 60 °F
23	Normal operating tubesheet pressure drop (in. H_2O)	20
24	Normal pressure drop prior to cleaning (in. H_2O)	60
25	Normal pressure drop following cleaning (in. H_2O)	30
26	Total active filtering surface (ft^2)	26.52 (13 one-meter candles)

SAMPLE FOR ANALYSIS

27	Type of sample	filter hopper sample
28	Source of ash in plant layout	
29	Date 2/22/98 time 08:00 - 16:15	
30	Sample taken by Bill Sulkalski	
31	Description of operation prior to sample collection: with recirculation of dipleg solids (e.g. steady-state full load, boiler upset, ramping, etc.)	steady-state
32	How was sample obtained	scraped from barrel

ANALYSIS AND REPORTING

33	Sample sent to SRI by Mike Swanson	Phone 701-777-5239
34	Request for sample analysis initiated by Rich Dennis (DOE/FETC)	
35	Goal of laboratory analyses	
36	Specific tests requested	
37	Send report to	
38	Send copies of report to	
39	Special instructions	

SAMPLE INFORMATION
(Provided by Facility Operator)
Tracking ID # 4327

FACILITY

1	Name	Transport Reactor Demonstration Unit
2	Type of Gasifier	2.7 MM Btu/hr Pilot Plant
3	Plant Heat Rate (Btu/kWh)	
4	Plant Firing Rate (MWe)	
5	Maximum Continuous Rating (MWe)	
6	Site Altitude (ft)	850 ft

FUEL — Illinois #6

7	Type	Bituminous
8	Source	Seam 6 from Baldwin Mine, near Baldwin, IL
9	Higher Heating Value (Btu/lb)	12080

10 Proximate analysis

	as received	dry basis
% moisture	8.5	NA
% ash	10.7	11.7
% volatile	36.02	39.38
% fixed carbon	44.78	48.92
totals	100.00	100.00
Btu/lb.	11.289	12.341
% sulfur	3.24	3.55

11 Ultimate analysis

	as received	dry
% moisture	8.5	NA
% carbon	63.36	69.27
% hydrogen	5.55	5.03
% nitrogen	1.01	1.10
chlorine, µg/g	609	
% sulfur	3.24	3.55
% ash	10.7	11.7
% oxygen (diff.)	16.13	9.34
totals	100	100

12 Fly ash fraction (% wt.)

13 Chemical analysis of coal (% wt.)

Li_2O	Na_2O	K_2O	MgO	CaO	Fe_2O_3	Al_2O_3	SiO_2	TiO_2	P_2O_5	SO_3	LOI
ND	1.1	1.9	1.6	3.2	13.6	21.2	53.9	0.9	0.2	2.5	NA

14 Is sorbent added to fuel? yes

15 Type of sorbent Plum run dolomite from Greenfield formation @ 17 wt%

16 Chemical analysis of added sorbent (% wt.)

Li_2O	Na_2O	K_2O	MgO	CaO	Fe_2O_3	Al_2O_3	SiO_2	TiO_2	P_2O_5	SO_3	LOI
ND	0.3	0.3	27.5	66.6	1.3	1.0	2.7	0.0	0.0	0.3	43.1

PARTICULATE CONTROL DEVICE

17	Type	candle filter
18	Cleaning initiated on	30 in H_2O above baseline
19	Hopper pulling schedule (h)	0.33 hr
20	Normal operating temperature (°F)	1000
21	Normal operating pressure (psig)	120
22	Normal gas flow	16,300 scfh @ 1atm & 60 °F
23	Normal operating tubesheet pressure drop (in. H_2O)	20
24	Normal pressure drop prior to cleaning (in. H_2O)	20
25	Normal pressure drop following cleaning (in. H_2O)	40
26	Total active filtering surface (ft^2)	26.52 (13 one-meter candles)

SAMPLE FOR ANALYSIS

27	Type of sample	filter hopper sample
28	Source of ash in plant layout	
29	Date 2/25/98 time 06:40 - 10:00	
30	Sample taken by Bill Sulkalski	
31	Description of operation prior to sample collection: with recirculation of dipleg solids (e.g. steady-state full load, boiler upset, ramping, etc.)	steady-state
32	How was sample obtained	scooped from barrel

ANALYSIS AND REPORTING

33	Sample sent to SRI by Mike Swanson	Phone 701-777-5239
34	Request for sample analysis initiated by Rich Dennis (DOE/FETC)	
35	Goal of laboratory analyses	
36	Specific tests requested	
37	Send report to	
38	Send copies of report to	
39	Special instructions	

SAMPLE INFORMATION
(Provided by Facility Operator)
Tracking ID # 4328

FACILITY

1	Name	Transport Reactor Demonstration Unit
2	Type of Gasifier	2.7 MM Btu/hr Pilot Plant
3	Plant Heat Rate (Btu/kWh)	
4	Plant Firing Rate (MWe)	
5	Maximum Continuous Rating (MWe)	
6	Site Altitude (ft)	850 ft

FUEL SUFCo P057

7	Type	Bituminous
8	Source	Bituminous seam at SUFCo mine in Salina, UT
9	Higher Heating Value (Btu/lb)	11040

10 Proximate analysis

	as received	dry basis
% moisture	9.5	NA
% ash	7.56	8.35
% volatile	39.10	43.20
% fixed carbon	43.84	48.45
totals	100.00	100.00
Btu/lb.	11040	12200
% sulfur	0.33	0.36

11 Ultimate analysis

	as received	dry
% moisture	9.5	NA
% carbon	69.78	77.10
% hydrogen	5.23	4.61
% nitrogen	1.17	1.29
chlorine, µg/g	69	
% sulfur	0.33	0.36
% ash	7.56	8.35
% oxygen (diff.)	15.93	8.29
totals	100	100

12 Fly ash fraction (% wt.)

13 Chemical analysis of coal (% wt.)

Li_2O	Na_2O	K_2O	MgO	CaO	Fe_2O_3	Al_2O_3	SiO_2	TiO_2	P_2O_5	SO_3	LOI
ND	4.6	0.2	3.0	16.3	6.1	9.3	38.3	0.8	0.2	21.1	NA

14 Is sorbent added to fuel? yes

15 Type of sorbent Plum run dolomite from Greenfield formation @ 5 wt%

16 Chemical analysis of added sorbent (% wt.)

Li_2O	Na_2O	K_2O	MgO	CaO	Fe_2O_3	Al_2O_3	SiO_2	TiO_2	P_2O_5	SO_3	LOI
ND	0.3	0.3	27.5	66.6	1.3	1.0	2.7	0.0	0.0	0.3	43.1

PARTICULATE CONTROL DEVICE

17	Type	candle filter
18	Cleaning initiated on	30 in H_2O above baseline
19	Hopper pulling schedule (h)	0.5 hr
20	Normal operating temperature (°F)	1000
21	Normal operating pressure (psig)	120
22	Normal gas flow	20,100 acfm @ 1atm & 60 °F
23	Normal operating tubesheet pressure drop (in. H_2O)	20
24	Normal pressure drop prior to cleaning (in. H_2O)	60
25	Normal pressure drop following cleaning (in. H_2O)	25
26	Total active filtering surface (ft^2)	26.52 (13 one-meter candles)

SAMPLE FOR ANALYSIS

27	Type of sample	filter hopper sample
28	Source of ash in plant layout	
29	Date 4/4/98 time 14:00 - 18:00	
30	Sample taken by Bill Sulkalski	
31	Description of operation prior to sample collection (e.g. steady-state full load, boiler upset, ramping, etc.)	steady-state
32	How was sample obtained	scooped from barrel

ANALYSIS AND REPORTING

33 Sample sent to SRI by Mike Swanson Phone 701-777-5239
34 Request for sample analysis initiated by Rich Dennis (DOE/FETC)
35 Goal of laboratory analyses
36 Specific tests requested
37 Send report to

38 Send copies of report to

39 Special instructions

SAMPLE INFORMATION
(Provided by Facility Operator)
Tracking ID # 4329

FACILITY

1	Name	Transport Reactor Demonstration Unit
2	Type of Gasifier	2.7 MM Btu/hr Pilot Plant
3	Plant Heat Rate (Btu/kWh)	
4	Plant Firing Rate (MWe)	
5	Maximum Continuous Rating (MWe)	
6	Site Altitude (ft)	850 ft

FUEL SUFCo P057

7	Type	Bituminous
8	Source	Bituminous seam at SUFCo mine in Salina, UT
9	Higher Heating Value (Btu/lb)	11040

10 Proximate analysis

	as received	dry basis
% moisture	9.5	NA
% ash	7.56	8.35
% volatile	39.10	43.20
% fixed carbon	43.84	48.45
totals	100.00	100.00
Btu/lb.	11040	12200
% sulfur	0.33	0.36

11 Ultimate analysis

	as received	dry
% moisture	9.5	NA
% carbon	69.78	77.10
% hydrogen	5.23	4.61
% nitrogen	1.17	1.29
chlorine, µg/g	69	
% sulfur	0.33	0.36
% ash	7.56	8.35
% oxygen (diff.)	15.93	8.29
totals	100	100

12 Fly ash fraction (% wt.)

13 Chemical analysis of coal (% wt.)

Li_2O	Na_2O	K_2O	MgO	CaO	Fe_2O_3	Al_2O_3	SiO_2	TiO_2	P_2O_5	SO_3	LOI
ND	4.6	0.2	3.0	16.3	6.1	9.3	38.3	0.8	0.2	21.1	NA

14 Is sorbent added to fuel? yes

15 Type of sorbent Plum run dolomite from Greenfield formation @ 5 wt%

16 Chemical analysis of added sorbent (% wt.)

Li_2O	Na_2O	K_2O	MgO	CaO	Fe_2O_3	Al_2O_3	SiO_2	TiO_2	P_2O_5	SO_3	LOI
ND	0.3	0.3	27.5	66.6	1.3	1.0	2.7	0.0	0.0	0.3	43.1

PARTICULATE CONTROL DEVICE

17	Type	candle filter
18	Cleaning initiated on	30 in H_2O above baseline
19	Hopper pulling schedule (h)	0.5 hr
20	Normal operating temperature (°F)	1000
21	Normal operating pressure (psig)	120
22	Normal gas flow	20,100 acfm @ 1atm & 60 °F
23	Normal operating tubesheet pressure drop (in. H_2O)	20
24	Normal pressure drop prior to cleaning (in. H_2O)	20
25	Normal pressure drop following cleaning (in. H_2O)	50
26	Total active filtering surface (ft^2)	26.52 (13 one-meter candles)

SAMPLE FOR ANALYSIS

27	Type of sample	filter hopper sample
28	Source of ash in plant layout	
29	Date 4/7/98 time 08:50 - 12:00	
30	Sample taken by Bill Sulkalski	
31	Description of operation prior to sample collection (e.g. steady-state full load, boiler upset, ramping, etc.)	steady-state
32	How was sample obtained	scooped from barrel

ANALYSIS AND REPORTING

33 Sample sent to SRI by Mike Swanson Phone 701-777-5239
34 Request for sample analysis initiated by Rich Dennis (DOE/FETC)
35 Goal of laboratory analyses
36 Specific tests requested
37 Send report to

38 Send copies of report to

39 Special instructions

SAMPLE INFORMATION
(Provided by Facility Operator)
Tracking ID # 4330

FACILITY

1	Name	Transport Reactor Demonstration Unit
2	Type of Gasifier	2.7 MM Btu/hr Pilot Plant
3	Plant Heat Rate (Btu/kWh)	
4	Plant Firing Rate (MWe)	
5	Maximum Continuous Rating (MWe)	
6	Site Altitude (ft)	850 ft

FUEL Pet Coke P058

7	Type	Pet Coke
8	Source	Hunt Oil Refinery in Tuscaloosa, AL
9	Higher Heating Value (Btu/lb)	15150

10 Proximate analysis

	as received	dry basis
% moisture	0.90	NA
% ash	0.98	0.99
% volatile	9.62	9.71
% fixed carbon	88.50	89.30
totals	100.00	100.00
Btu/lb.	15150	15300
% sulfur	5.44	5.49

11 Ultimate analysis

	as received	dry
% moisture	0.90	NA
% carbon	89.83	90.65
% hydrogen	3.96	3.89
% nitrogen	1.68	1.70
chlorine, µg/g	ND	
% sulfur	5.44	5.49
% ash	0.98	0.99
% oxygen (diff.)	-1.89	-2.72
totals	100	100

12 Fly ash fraction (% wt.)

13 Chemical analysis of coal (% wt.)

Li_2O	Na_2O	K_2O	MgO	CaO	Fe_2O_3	Al_2O_3	SiO_2	TiO_2	P_2O_5	SO_3	LOI
ND	1.0	0.2	5.1	11.9	7.6	4.8	18.9	0.0	0.1	13.8	NA

14 Is sorbent added to fuel? yes

15 Type of sorbent Plum run dolomite from Greenfield formation @ 20 wt%

16 Chemical analysis of added sorbent (% wt.)

Li_2O	Na_2O	K_2O	MgO	CaO	Fe_2O_3	Al_2O_3	SiO_2	TiO_2	P_2O_5	SO_3	LOI
ND	0.3	0.3	27.5	66.6	1.3	1.0	2.7	0.0	0.0	0.3	43.1

PARTICULATE CONTROL DEVICE

17	Type	candle filter
18	Cleaning initiated on	2 hour intervals
19	Hopper pulling schedule (h)	2 hr
20	Normal operating temperature (°F)	1050
21	Normal operating pressure (psig)	110
22	Normal gas flow	13950 acfh @ 1atm & 60 °F
23	Normal operating tubesheet pressure drop (in. H_2O)	20
24	Normal pressure drop prior to cleaning (in. H_2O)	27
25	Normal pressure drop following cleaning (in. H_2O)	24
26	Total active filtering surface (ft^2)	26.52 (13 one-meter candles)

SAMPLE FOR ANALYSIS

27	Type of sample	filter hopper sample
28	Source of ash in plant layout	
29	Date 5/5-8/98 time	
30	Sample taken by Bill Sulkalski	
31	Description of operation prior to sample collection (e.g. steady-state full load, boiler upset, ramping, etc.)	steady-state
32	How was sample obtained	scooped from barrel

ANALYSIS AND REPORTING

33 Sample sent to SRI by Mike Swanson Phone 701-777-5239
34 Request for sample analysis initiated by Rich Dennis (DOE/FETC)
35 Goal of laboratory analyses
36 Specific tests requested
37 Send report to

38 Send copies of report to

39 Special instructions

PARTICULATE HOT GAS STREAM CLEANUP TECHNICAL ISSUES

Task 1 ASSESSMENT OF ASH CHARACTERISTICS

FINAL REPORT
October 1994 - September 1999

SRI-ENV-99-8484-T1F

Contract No. DE-AC21-94MC31160

September 30, 1999

Approved by

Duane H. Pontius, Principal Investigator